

**Range-Resolved Cross-Wind Remote Sensing Using a Polychromatic
AlGaAs Semiconductor Laser**

Feng Chen

B.S., Physics, Anhui University, China, 1985

M.S., Laser Remote Sensing, Anhui Institute of Optics & Fine Mechanics,
Academia Sinica, China, 1988

M.S., Electrical Engineering, Oregon Graduate Institute of Science & Technology, 1993

A dissertation submitted to the faculty of the
Oregon Graduate Institute of Science & Technology
in partial fulfillment of the
requirements for the degree
Doctor of Philosophy
in
Electrical Engineering

January, 1996

The dissertation "*Range-Resolved Cross-Wind Remote Sensing Using a Polychromatic AlGaAs Semiconductor Laser*" by Feng Chen has been examined and approved by the following Examination Committee:

J. Fred Holmes, Dissertation Advisor
Professor

V. S. Rao Gudimetla
Assistant Professor

Tony Bell
Associate Professor

Aslam Khalil
Professor
Portland State University

Acknowledgements

I would like to thank my advisor, Dr. J. Fred. Holmes for giving me the opportunity to work on this research project; for his help and encouragement throughout the work; for his profound knowledge and great personality. I would also like to acknowledge Drs. Holmes, Gudimetla, Bell, and Khalil for serving in my dissertation examination committee.

I would like to take this opportunity to thank John Hunt for his guidance and contributions to this research project; for his strict disciplines of being a good engineer. I appreciate my fellow students Dr. Badih Rask and Chunyan Zhou for the help and friendship and for good suggestions they made to the development of the project.

Finally I wish to thank my wife Yang Niu for her love and support, for her great contribution to the experiments.

Table of Contents

	Page
ACKNOWLEDGEMENTS	iii
TABLE OF CONTENTS	iv
LIST OF FIGURES	vi
LIST OF TABLES	ix
ABSTRACT	x
Chapter 1 INTRODUCTION	1
Chapter 2 THEORETICAL BACKGROUND OF LASER REMOTE SENSING SYSTEM	6
2.1 The Intensity Correlation Function for a Polychromatic Source	7
2.2 Time-Delayed Covariance of the Received Intensity	13
2.3 Wind Sensing Techniques	17
Chapter 3 NUMERICAL ANALYSIS OF VARIANCE AND COVARIANCE.	22
3.1 Some Simplifications for Numerical Analysis	23
3.2 TDC and Autocovariance for the Point Detectors.	31
3.3 Aperture Averaging Effect on TDC and Autocovariance.	38
Chapter 4 SYSTEM DESIGN AND EXPERIMENT SETUP	47
4.1 The Optics of the “White Light” System	50
4.1.1 The Transmitter	50
4.1.2 The Receiver Telescope.	51
4.1.3 Intensity vs. Range for “White Light” System	55
4.1 Signal Processing Schemes and Signal to Noise Ratio.	60
4.2.1 Coding Schemes.	61

4.2.2	Signal Noise Ratio and Simulation Results	66
4.3	Signal to Noise Ratio for the “White Light” System	75
4.4	Electronics	79
4.5	Experiment Setup	85
Chapter 5	EXPERIMENTAL RESULTS	87
5.1	Experiment Procedure and Results of Autocovariance and TDC	91
5.2	Experiment on Aperture Averaging Effect	105
5.3	More Wind Measurements	113
5.4	New Receiver and Processing Design	122
Chapter 6	CONCLUSIONS AND FUTURE WORK	131
	References	136
	Appendix A	142
	Appendix B	145
	Appendix C	153
	Appendix D	163
	Appendix E	188
	Vita	192

List of Figures

	Page
2.1 Configuration of the path geometry for a lidar system.	7
2.2 Techniques for wind remote sensing.	18
3.1 Effect of the simplification on the exponential term of r with strong turbulence..	25
3.2 Effect of the simplification on the exponential term of r with weak turbulence. .	26
3.3 Comparison of $\exp(4C_\chi)$ and $\exp\left(-\frac{\rho^4}{4a}\right)$	27
3.4 Comparison of $\exp(4C_\chi)$ and $\exp\left(-\frac{\rho^4}{4a}\right)$	28
3.5 TDC for the point detectors with $C_n^2 = 1.0e - 14$, P=25mm.....	32
3.6 TDC for the point detectors with $C_n^2 = 1.0e - 16$, P=25mm.....	33
3.7 TDC for point detectors, with $C_n^2 = 1.0e - 16$, P=5mm.	34
3.8 TDC for point detectors, with $C_n^2 = 1.0e - 14$, P=5mm.	35
3.9 Auto-covariance of point detectors, $C_n^2 = 1.0e - 14$	36
3.10 Auto-covariance of point detector, $C_n^2 = 1.0e - 16$	37
3.11 TDC of two half-moons with radius r=5mm.	41
3.12 TDC of two half-moons with radius r=25mm.	42
3.13 Auto-covariance of half-moon shaped receiver, radius r=5mm.	43
3.14 Auto-covariance of half-moon shaped receiver, radius r=25mm.	44

3.15	TDC of rectangular shaped receiver with width of 20 mm.	45
3.16	The autocovariance of rectangular shaped receiver of width of 20 mm.	46
4.1	Configuration of “White Light” system.	49
4.2	Schematic of the telescope.	52
4.3	Simplified diagram of the transmitter and receiver system (not in scale).	53
4.4	Theoretical intensity profile for a coaxial system.	58
4.5	Received signal profile for “White Light” system.	59
4.6	Schematic of pseudo-random code generator.	62
4.7	Simulated results of cross-correlation functions of a_i and a'_i	65
4.8	Recovered signal for different modulation codes, no background noise.	73
4.9	Recovered signal for different modulation codes, severe background noise is presented.	74
4.10	Pseudo Random Generator and control logic for the receiver.	81
4.11	Detector and preamplifier.	82
4.12	Two channel receiver.	83
4.13	Timing diagrams of the “White Light” system.	84
5.1	Cross wind measurements with both “White Light” and Campbell unit.	89
5.2	Intensity vs. range of the return signal off hard target at 250 meters.	93
5.3	Two channel lidar signal from hard target at 250 meters.	94
5.4	Autocovariance of two channel signals from a hard target at 250 meters.	95
5.5	Time delayed cross covariance of intensities.	96
5.6	Processed results. (a) TDC from different ranges; (b) calculated cross wind speed.	97
5.7	TDC off hard target at 800 meters. 3 inches receiver is used.	101

5.8	Auto-covariances of two channel intensities from hard target at 800 meters.	102
5.9	TDC with hard target at 800 meters and receiving aperture of 5.5 inches.	103
5.10	Autocovariance with hard target at 800 meters and receiving aperture of 5.5 inches.	104
5.11	Two different receiving apertures: (a) two half-moons; (b) two rectangles.	105
5.12	Aperture averaging effect on time delayed covariance for two half-moon receivers.	107
5.13	Autocovariance of both experiment and numerical analysis of two half-moon receivers.	108
5.14	Aperture averaging effect on time delayed covariance for two rectangular receivers.	110
5.15	TDC's of both numerical analysis and experiment of two rectangular receivers.	111
5.16	Autocovariance of both experiment and numerical analysis with rectangular receivers.	112
5.17	The TDC of experiment with two rectangular receivers of width=20 mm.	114
5.18	Cross wind measurements by both "White Light" and Campbell unit.	115
5.19	The TDC of experiment with rectangular receiver of width=20 mm, double pulse A/D trigger was used.	117
5.20	Cross wind measurements by both "White Light" and Campbell unit, double pulse A/D trigger was used.	118
5.21	Intensity vs. range profiles from aerosols produced by "White Light" system.	120
5.22	Two channels signals from aerosols at about 300 meters.	121

5.23	Diagram of receiver optics, where a 50/50 beam splitter and two knife edges are used.	123
5.24	Equivalent receiver area for the receiver system shown in figure (5.23).	124
5.25	Cross covariance with autocovariance, bigger common area was used.	126
5.26	Cross covariance with autocovariance, smaller common area was used.	127
5.27	Cross covariance with autocovariance subtracted from figure (5.26).	128
5.28	Cross covariance with autocovariance subtracted from figure (5.25).	129
5.29	Cross covariances before and after autocovariance is subtracted.	130

List of Tables

	page
4.1	List of components in “White Light” system. 86

ABSTRACT

Range-Resolved Cross-Wind Remote Sensing Using a Polychromatic AlGaAs Semiconductor Laser

Feng Chen

Oregon Graduate Institute of Science & Technology

Supervising Professor: Dr. J. Fred Holmes

Laser generated speckle and its interaction with turbulence have been studied for more than twenty years and have been utilized in atmospheric wind sensing. When a diffuse target or randomly distributed aerosols generated speckle pattern propagates back to the receiver, a scintillation pattern is created due to the speckle turbulence interaction. If a cross wind is present, the scintillation pattern will move with time across the field-of-view of the receiver. As a result, the average cross wind velocity can be obtained using the time-delayed statistics of the speckle field at the receiver.

Previously developed statistics of the polychromatic laser speckle field were adopted. Some development and simplifications were made on the autocovariance and Time-Delayed covariance(TDC) so that numerical analysis can be implemented for a

finite receiving area. Numerical calculations were performed on the SUN work station using the Gauss Quadrature approximation. The aperture averaging effect which was simulated, corresponded to that actually observed from the experimental results.

Pseudo-random code modulation made it possible to run the transmitter CW and still have range resolving capability. Semiconductor lasers have the advantage that modulation can be applied to the laser directly as a driving current. Small and reliable laser diodes and optical fibers made it possible to build a reliable and compact lidar system with potential practical applications such as wind shear detection for airplane safety. A coaxial lidar was built with an 8-inch receiving telescope. An AlGaAs laser diode with pigtailed 5 μ m single mode fiber was used as a transmitter. A single mode, multi-frequency laser working at 830 nm with a CW power of 50 mW was transmitted for better aerosol back-scattering. Highly sensitive photomultiplier tubes were used as detectors and an integration detection scheme was employed. Different receiver systems were also designed and tested for the purpose of increasing the TDC and detectability.

Experiments were conducted over a variety of atmospheric conditions and receiver configurations. The aperture averaging effect was observed from the experimental results and comparisons were made with the numerical predictions. Large amounts of data were taken to produce cross wind speed estimates using the Peak Shift method. Time series of cross wind speed measurements were also produced and compared with the results of other equipment. The results of a new receiver and processing scheme are presented. Suggestions for improvements and future work are also discussed.

Chapter 1

Introduction

Optical remote sensing of atmospheric parameters using the effects produced by the atmosphere on optical propagation started in late 1960's.¹⁻⁵ The measurements of the spatial averaged turbulence strength (represented by the refractive index structure function C_n^2) and wind velocity are some of the great applications of laser remote sensing. Early version of laser remote sensing systems for atmospheric wind and turbulence using double-ended configuration have been demonstrated during the early 1970's⁶⁻⁹ and has been proven to be reliable over the years. However, the use of these sensors are limited to applications where both ends of the path are accessible, because it requires a laser source at one end and a receiver at the other end. More research work have devoted to the development of single ended laser remote sensors since late 1970's for such applications as the study of global weather changes, environmental monitoring and control, and even wind shear detecting and warning for aviation safety.¹⁰⁻¹⁴

When a coherent laser source illuminates a diffuse target, a speckle pattern will be generated.¹⁵⁻¹⁶ The effect of turbulence on the target-generated speckle pattern can be utilized in single-end optical remote sensing of atmospheric cross winds. The speckle pattern is perturbed by the atmosphere as it propagates back to the transmitter end. This creates a scintillation pattern at the receiver which will move across the field of the receiver

in the presence of a cross wind. As a result, the average vector crosswind along a horizontal path perpendicular to the direction of the outgoing laser beam can be obtained by using the time delayed statistics of the speckle field at the receiver.

Pulsed laser systems that utilize the speckle-turbulence interaction and direct detection have been developed by some researchers and their results indicated the potential of the speckle-turbulence technique.¹⁷⁻²¹ The range resolved wind profile can also be obtained using a pulsed system. But such systems are inadequate due to the limit of laser technology such as pulse repetition rate restrictions and processing techniques. Furthermore, a pulsed laser remote sensing system requires a complicated and expensive transmitter and a complex electronic receiver which suffers from the additional problems of beam alignment and stability.

Coherent heterodyne detection combined with the effect of speckle-turbulence has the advantage of good signal to noise ratio and high sensitivity.²² An optimum SNR can be reached by controlling the local oscillator signal level. Furthermore, the crosswind obtained using speckle turbulence interaction can also be a by-product of a coherent heterodyne detection doppler lidar remote sensing system. A doppler lidar system uses the aerosols in the atmosphere to backscatter some of the transmitter energy from a pulsed laser back to the receiver where the doppler shift is used to measure the magnitude of the wind velocity along the line of the sight. Because non-uniformities of the turbulence do not effect the doppler shift, the doppler systems are very well suited for global measurement from the earth's orbit.^{23,24} However, the disadvantages of large and complicated pulse system are still a big issue which prevents building a reliable system for practical applications.

Pseudo random code (PRC) modulation has been around for quiet a long time. It makes it possible to run the transmitter as CW and still be capable of having range information. The simplicity of the design of both the optical control system and electronics make it very attractive to the laser wind remote sensing applications. It has been very active in the research and development of compact and reliable CW laser remote sensing systems using both heterodyne and direct detection schemes.²⁵⁻²⁷ A coherent lidar using PRC modulation in conjunction with heterodyne detection was developed in the Remote Sensing Group at Oregon Graduate institute to measure the three dimensional wind speed by doppler techniques and statistics of speckle-turbulence interaction effect.²⁸ Some good results obtained demonstrate the feasibility of future uses.

Some disadvantages have to be mentioned related to heterodyne detection. A good phase match between local oscillator and backscattering beam has to be reached in order to obtain the optimum detection. Relatively longer wavelength lasers have to be chosen as transmitter for better alignment and detection but lower interaction with aerosols is observed. In addition, the complexity of optical modulation may be a problem. All these issues make the use of higher frequency lasers at near infrared with PRC modulation and direct detection very attractive.

With the development of the communication and semiconductor laser technology, high power, small and reliable diode lasers are available with the ease of applying PRC modulation directly to laser diodes as a driving current. Pseudo random code modulated semiconductor laser and direct detection was first used to detect chemicals in the atmosphere and later used for atmospheric water vapor in differential absorption lidar.^{29,30}

Range resolution and successful measurements were also reported.³¹⁻³⁵

A single transverse, multi-longitudinal mode at wavelength around 830 nm AlGaAs laser with about 100mW CW power was used as transmitter for this thesis project. The primary goal of this project is to build a low power, CW, compact and reliable laser system to measure range resolved atmospheric cross wind using interactions between aerosols-created speckles and turbulence. Optical direct detection and a pseudo random code of code length of 511 us are used. Integration of code length is used to increase the signal to noise ratio. Fibers can be directly pigtailed to the laser diode and used for delivering the received light. This also make it possible to have a reliable and compact system.

Early theoretical work on speckle propagation in the turbulent atmosphere was accomplished by Holmes et al.³⁶ A monochromatic laser source was used and the extended Huygens Fresnel principle was utilized to make it possible to express the second order statistics analytically. A diffuse hard target was used for both coherent heterodyne detection and direct detection system. Later this work was generalized by Holmes et al.³⁷ to include the effect of the log-amplitude fluctuations and feasibility of remote sensing of cross wind was determined. In his thesis dissertation, V. S. Gudimetla extended the work to the polychromatic source and partially coherent laser source generated speckle pattern propagation in turbulent atmosphere was studied in detail.³⁸

In this thesis, the theory about polychromatic laser speckle propagation is adopted and several wind sensing techniques are introduced. Extension is made from a point detector to a finite receiving area. Simplifications are made to the formulations of the second order statistics, so numerical analysis is possible. In chapter 3, Gauss Quadrature

approximation subroutines in the NAG library are used for numerical analysis of autocovariance and time delayed covariance. Different sizes and shapes of receiver are considered and aperture averaging effect is studied in detail.

A great deal of effort was devoted to the construction and development of the direct detection lidar "White Light" system used in gathering data. In chapter 3, the experimental set-up is outlined and the optics and electronics are described. The detected signal is calculated and the signal to noise ratio is analyzed. Different coding schemes are introduced and signal to noise ratios are simulated. The parameters of components used for the system are also listed in table(4.1).

The experimental results are presented in chapter 5. The received intensities off of a hard target, processed autocovariance, TDC and cross wind speed are presented. The aperture averaging effect is experimentally tested. Different shapes and sizes of receiver are used in the experiment and the results are compared with the numerical predictions. Practically optimum receivers are chosen for cross wind measurements and the time series of cross wind measurements are compared with the cross wind measurements from a Campbell Scientific Crosswind Sensor. Some results of aerosol measurement are presented and some problems are discussed. New receiver and processing schemes are introduced to increase the TDC and the performance of the system.

In chapter 6, the conclusions for the theoretical and experimental work in this thesis are given and future extensions of this work are also discussed.

Some computer simulation programs, A/D programs and signal processing programs are listed in the appendices.

Chapter 2

Theoretical Background of Laser Remote Sensing Systems

The atmosphere is constantly moving. Solar radiation, heat transportation and wind are the main contributors to random motion. Energy is consumed by the random spatial and temporal fluctuations of parameters such as pressure, temperature and velocity. This phenomena of the atmosphere, called turbulence is characterized by its rotational, three-dimensional, nonlinear, diffusive and stochastic process. Turbulence not only exists in the atmosphere, it can be found in any material with a fluid nature. Studies on turbulence characteristics can be found in many books and papers.³⁹⁻⁴¹

One of the most important aspects about atmospheric turbulence is its interaction with electromagnetic waves.⁴²⁻⁴⁵ Because of the random characteristics of turbulence, distortion is introduced to the electromagnetic field, which is seen in optical and microwave communications, laser ranging, etc. A lot of effort has been made on adaptive system to eliminate the error of phase and intensity introduced by turbulence. On the other hand, it is possible to measure atmospheric properties using the interaction between electromagnetic waves and turbulence provided that the statistic properties of turbulence are known. Laser wind remote sensing of atmospheric winds is one of the great applications of this. It should be pointed out that there are two categories of optical wind remote sensing radar: coherent and incoherent. A heterodyne detection scheme is used for coherent system, direct detection scheme is used for incoherent system.

2.1 The Intensity Correlation Function for a Polychromatic Source

The fluctuations of refractive index of atmosphere change effect electromagnetic wave. To study the statistics of turbulence, one generally starts with the refractive index given by

$$n(r) = 1 + n_1(r) \quad (2.1)$$

here $n_1(r)$ is the fluctuating part and $n_1 \ll 1$. Applying this to the Helmholtz equation, gives

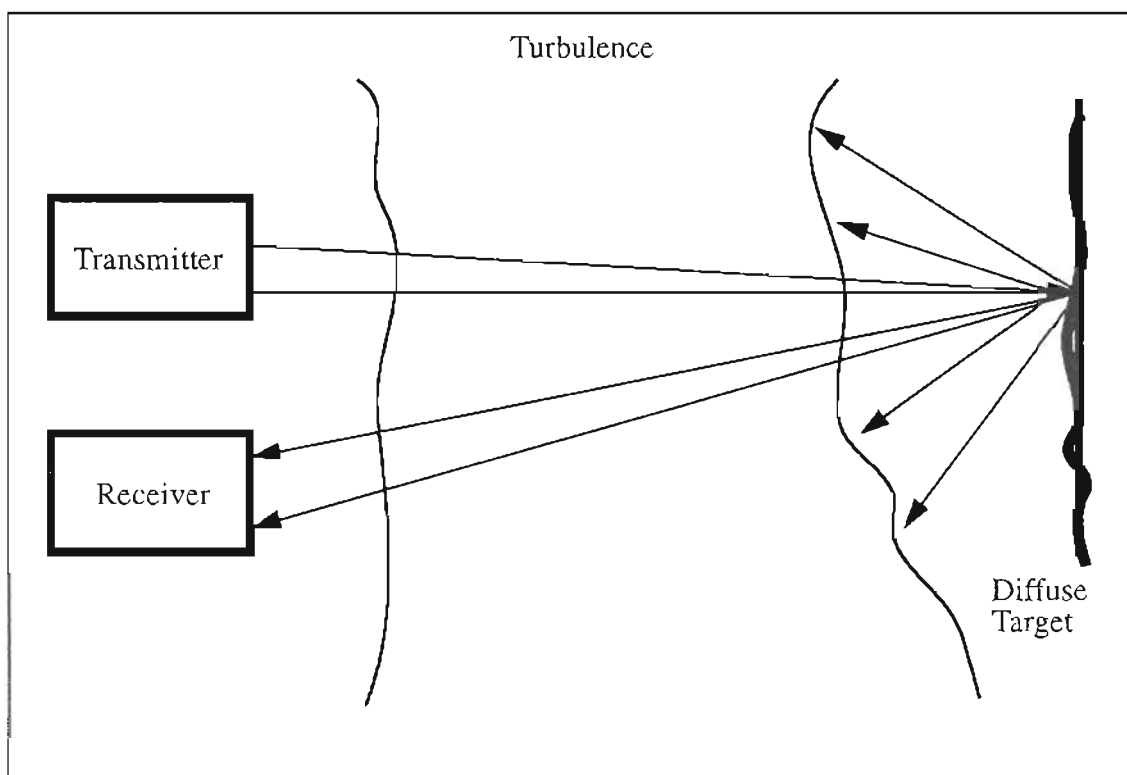


Figure 2.1 Configuration of the path geometry for a lidar system.

$$\left(\nabla^2 + k^2 (1 + n_1(r))^2 \right) U_1 = 0 \quad (2.2)$$

where k is wave number, U_1 is electrical field.

One of the most important statistical parameters in optical remote sensing is the correlation function of the received intensities from two space points. Cross-wind speed is obtained by processing the cross-correlation function of the intensities. The general form of the correlation function of the received intensities at two space time points in the receiver plane is defined as

$$B_I(P_1, t_1; P_2, t_2) = \langle I(p_1, t_1) I(p_2, t_2) \rangle \quad (2.3)$$

where $I(p_i, t_i)$ is the intensity at a point p_i at time t_i in the receiver plane. This function is evaluated by determining the intensities at two space time points and taking an ensemble average over both space and time as well as over an ensemble of rough surface and atmospheres. From this general form, other important parameters can be obtained. By choosing $p_1 = p_2$, Eq. (2.3) gives auto-correlation; $t_1 = t_2$ gives the covariance; $p_1 = p_2$ and $t_1 = t_2$ give the variance.

The derivation of the general form of correlation of intensities for a coherent laser source was performed under the assumptions of a diffuse target and independent paths of outgoing and incoming laser beam.⁴⁶⁻⁴⁹ More complicated form for a polychromatic laser source can be found in Rao Gudimetla's Ph.D. dissertation.³⁸ Fig. (2.1) is the path geom-

etry for the problem under consideration. The transmitter and receiver are located at one end of the path and the laser beam propagates through the turbulent atmosphere and scattered back by the diffused target or from the aerosols. It is assumed that the transmitter consists of a number of discrete frequencies given by k_j , $i = 1, 2, \dots, N$ and that the receiver bandwidth is very much smaller than any difference frequency present in the transmitter ($\Delta\omega \ll \omega_i - \omega_j$) but large enough to recover all the amplitude fluctuations due to the turbulent atmosphere. Let \mathfrak{r} , \mathfrak{p} and \mathfrak{r} denote the transverse coordinates in the receiver, target and transmitter planes, respectively, which are perpendicular to the line of sight path for coaxial system or biaxial system with small distance between transmitter and receiver. It is known that the intensity fluctuations in the turbulent atmosphere at different frequencies are perfectly correlated for small bandwidths of the transmitter.^{50,51} Widely separated frequencies are needed in order to see intensity fluctuations at different frequencies decorrelated.

For a laser beam with TEM00 wave at several frequencies, the electric field distribution at the transmitter is given by

$$U_0(\mathfrak{r}) = \sum_{j=1}^N U_0(\mathfrak{r}, k_j) = \sum_{j=1}^N U_{0j} \exp \left\{ \frac{-r^2}{2\alpha_0^2} + \frac{-ik_j r^2}{2F} \right\} \quad (2.4)$$

where $U(\mathfrak{r}, k_j)$ corresponds to the field distribution at the frequency k_j , and α_0 and F are the characteristic beam radius and focal length respectively. The field at the target plane before backscattering can be written, using the extended Huygens Fresnel principle, as

$$\begin{aligned}
U'(\vec{p}) &= \sum_{j=1}^N U'(\vec{p}, k_j) = \sum_{j=1}^N \left(\frac{k_j U_{0j}}{i2\pi L} \right) \exp \left\{ ik_j \left(L + \frac{\rho^2}{2L} \right) \right\} \\
&\times \int \exp \left\{ -\frac{r^2}{2\alpha_0^2} - ir^2 \frac{k_j}{2L} \left(1 - \frac{L}{F} \right) - ik_j \frac{(\vec{r} \cdot \vec{p})}{L} + \psi_1(\rho, r, k_j) \right\} d\vec{r} \quad (2.5)
\end{aligned}$$

where the random function $\psi_1(\dots)$ represents the effect of the turbulent atmosphere on the propagation of the spherical wave from a point \vec{r} in the transmitter plane to a point \vec{p} in the target plane, k is the wave number and L is the path length.

Similarly, the electric field at the receiver can be written in terms of the fields

$U(\vec{p}, k_j)$ at the target after scattering as

$$\begin{aligned}
U(\vec{p}) &= \sum_{j=1}^N \left(\frac{k_j}{i2\pi L} \right) \exp \left(ik_j \left(L + \frac{\rho^2}{2L} \right) \right) \int d\vec{p}' U(\vec{p}', k_j) \exp \left(\frac{ik_j}{2L} \left(\rho'^2 - 2\vec{p}' \cdot \vec{p} \right) \right) \\
&\times \exp(\psi_2(\vec{p}', \vec{p}, k_j)) \quad (2.6)
\end{aligned}$$

where $\psi_2(\vec{p}', \vec{p}, k_j)$ represents the effect of the turbulence on the wave from the target to the receiver plane.

The field before and after scattering from the target are related by the scattering properties of the target. The complex random function is given as

$$\psi = \chi + i\phi \quad (2.7)$$

where χ represents the log-amplitude perturbation of the spherical wave due to the atmo-

spheric turbulence and ϕ , the phase perturbation. Two other functions are two frequency structure function

$$D_{\Psi} = 0.132\pi^2 L \int_0^1 dt C_n^2(t) \int_0^{\infty} du u^{-8/3} \left[k_1^2 + k_2^2 - 2k_1 k_2 \cos \left\{ \left(u^2 t (1-t) \frac{L}{2} \right) \left(\frac{1}{k_1} - \frac{1}{k_2} \right) \right\} \right] \\ \times J_0 \left\{ u |t(p_2 - p_1) + (1-t)(p_2 - p_1) - V(t_2 - t_1)| \right\} \quad (2.8)$$

and log-amplitude covariance function

$$C_{\chi} = 0.132\pi^2 L \int_0^1 dt C_n^2(t) \int_0^{\infty} du u^{-8/3} \sin \left[u^2 t (1-t) \frac{L}{2k_1} \right] \times \\ \sin \left[u^2 t (1-t) \frac{L}{2k_2} \right] J_0 \left\{ u |t(\check{p}_2 - \check{p}_1) + (1-t)(\check{p}_2 - \check{p}_1) - \check{V}(t_2 - t_1)| \right\} \quad (2.9)$$

The dummy variable t represents the distance from the source to the field point normalized by the total path L . \check{V} is the vector wind, J_0 is the 0th order Bessel function, $C_n(t)$ is the strength of turbulence. Since the target is perfectly diffuse, it can be assumed that at the target the fields due to any particular frequency are gaussian (spatially incoherent). If the coherence length of the source is larger than the surface correlation length, the fields before and after scattering can be related as

$$\langle U(\check{p}_1, 0, k_i) U^*(\check{p}_2, 0, k_i) U(\check{p}_3, \tau, k_j) U^*(\check{p}_4, \tau, k_j) \rangle \\ = \left(\frac{4\pi}{k^2} \right)^2 \langle I(\check{p}_1, 0) \rangle \langle I(\check{p}_3, \tau) \rangle \delta(\check{p}_1 - \check{p}_2) \delta(\check{p}_3 - \check{p}_4)$$

$$\begin{aligned}
& + \left(\frac{4\pi}{k} \right)^2 \langle U(\check{\rho}_4, 0) U^*(\check{\rho}_4, \tau) \rangle \langle U(\check{\rho}_2, \tau) U(\check{\rho}_1, 0) \rangle \delta(\check{\rho}_1 - \check{\rho}_4) \delta(\check{\rho}_3 - \check{\rho}_2) \quad \text{if } i = j \\
& = \left(\frac{4\pi}{k_i k_j} \right)^2 \langle I(\check{\rho}_1, 0, k_i) \rangle \langle I(\check{\rho}_3, \tau, k_j) \rangle \delta(\check{\rho}_1 - \check{\rho}_2) \delta(\check{\rho}_3 - \check{\rho}_4) \quad \text{if } i \neq j \quad (2.10)
\end{aligned}$$

Then the correlation of the received intensity is given by

$$B(\check{\rho}, \tau) = B_{I1}(\check{\rho}, \tau) + B_{I2}(\check{\rho}, \tau) \quad (2.11)$$

The final expressions of B_{I1} and B_{I2} are

$$\begin{aligned}
B_{I1} &= \left(\frac{\alpha_0^4}{2\pi L^4} \right) \sum \sum U_{0i}^2 U_{0j}^2 \int d\check{\rho} \int r dr J_0(\rho r) \\
&\quad \exp \left\{ -\frac{r^2 L^2}{4\alpha_0^2} \left(\frac{1}{k_i^2} + \frac{1}{k_j^2} \right) - \left(\frac{rL}{k_i \rho_{0i}} \right)^{5/3} - \left(\frac{rL}{k_j \rho_{0j}} \right)^{5/3} \right\} \\
&\quad \exp \left(-r^2 \left(\frac{\alpha_0^2}{2} \right) \left(1 - \frac{L}{F} \right)^2 \right) \exp \{ 4C_\chi(\check{\rho}, \check{\rho}, \tau, k_i, k_j) \} \quad (2.12)
\end{aligned}$$

and

$$\begin{aligned}
B_{I2} &= \sum U_{0i}^4 \left(\frac{\alpha_0^4}{4\pi^2} \right) \int d\check{\rho}_3 \int d\check{\rho} \exp \{ -r_3^2 L^2 / (2k^2 \alpha_0^2) - D_\Psi(0, -L\check{\rho}_3/k_i - \tau) \} \\
&\quad \times \exp \left\{ \left(-\frac{r_3^2}{2} \right) \alpha_0^2 \left(1 - \frac{L}{F} \right)^2 \right\} \exp \left(i \frac{k_i}{L} \check{\rho} \cdot \check{\rho} \check{\rho} \cdot \check{\rho}_3 \right) H_2(\check{\rho}, \check{\rho}, \tau) \quad (2.13)
\end{aligned}$$

where

$$\begin{aligned}
 H_2(\hat{\rho}, \hat{\rho}, \tau) &= \exp \left\{ -D_\psi(0, \hat{\rho}, 0) - D_\psi(\hat{\rho}, 0, \tau) + \left(\frac{1}{2}\right) D_\psi(\hat{\rho}, -\hat{\rho}, \tau) \right\} \\
 &\times \exp \left\{ \left(\frac{1}{2}\right) D_\psi(\hat{\rho}, \hat{\rho}, \tau) + 2C_\chi(\hat{\rho}, -\hat{\rho}, \tau) + 2C_\chi(\hat{\rho}, \hat{\rho}, \tau) \right\} \quad (2.14)
 \end{aligned}$$

2.2 Time-Delayed Covariance of the Received Intensity

The time-delayed covariance (TDC) of the received intensity is a measure of the correlation between the intensity fluctuations at two points in space and time. Cross-wind is directly related to the TDC. By definition, TDC is given by

$$\begin{aligned}
 C_I(\hat{\rho}_1, t_1, \hat{\rho}_2, t_2) &= \langle I(\hat{\rho}_1, t_1) I(\hat{\rho}_2, t_2) \rangle - \langle I \rangle^2 \\
 &= B_{I1}(\hat{\rho}, \tau) + B_{I2}(\hat{\rho}, \tau) - \langle I \rangle^2 \quad (2.15)
 \end{aligned}$$

In general eq.(2.12)-eq.(2.15) must be used to calculate B_{I1} and B_{I2} to get the final TDC.

This requires knowledge of the average intensity of each uncorrelated speckle pattern at zero turbulence level. However for many practical problems, the span of wavenumbers is small enough that the midpoint value of k can be used in those equations. This restriction is not severe because the atmospheric fluctuations are strongly correlated even for widely separated wavenumbers.

Since the average value of the intensity at each frequency is given as

$$\langle I_i \rangle = U_{0i} \left(\frac{\alpha_0^2}{L^2} \right) \quad (2.16)$$

The covariance can be written as

$$C_{I1} = AINT_1 \sum_i \sum_j \langle I_i \rangle \langle I_j \rangle = AINT_1 \langle I \rangle^2$$

$$C_{I2} = AINT_2 \sum_i \langle I_i \rangle^2 \quad (2.17)$$

where

$$AINT_1 = \frac{1}{2\pi} \int d\vec{\rho} \int \vec{\rho} d\vec{\rho} J_0(\rho r) \exp \left\{ - \left(\frac{r^2 L^2}{4\alpha_0^2} \right) \cdot \frac{2}{k^2} - 2 \left(\frac{rL}{k\rho_0} \right)^{5/3} - r^2 \left(\frac{\alpha_0^2}{2} \right) \left(1 - \frac{L}{F} \right)^2 \right\}$$

$$\times \exp \{ 4C_\chi(\vec{\rho}, \vec{\rho}, \tau) \}$$

$$AINT_2 = \frac{k^2}{4\pi^2 L^2} \int d\vec{r}_2 \int d\vec{\rho} \exp \left[- \frac{r_2^2}{2\alpha_0^2} - D_\psi(0, -r_2, -\tau) - r_2^2 k \alpha_0^2 \left(1 - \frac{L}{F} \right)^2 \right]$$

$$\times \exp \left[\frac{ik}{L} \vec{\rho} \cdot (\vec{\rho} + \vec{r}_2) \right] H_2(\vec{\rho}, \vec{\rho}, \tau, k) \quad (2.18)$$

It should be mentioned here that the substitution has been made

$$\mathfrak{r} = \frac{k}{L} \mathfrak{r}_1 \quad (2.19)$$

where \mathfrak{r}_1 is real coordinate.

By choosing appropriate parameters, we can get variance and covariance. Letting $\tau = 0$ and $\mathfrak{p} = 0$, the TDC becomes the variance

$$\sigma_I^2 = \langle I \rangle AINT_1|_{\tau=0, \mathfrak{p}=0} + \sum_i \langle I_i \rangle^2 AINT_2|_{\tau=0, \mathfrak{p}=0} - \langle I \rangle^2 \quad (2.20)$$

in which

$$\begin{aligned} AINT_1|_{\tau=0, \mathfrak{p}=0} &= \frac{1}{2\pi} \int d\mathfrak{p} \int r dr J_0(\rho r) \exp \left\{ - \left(\frac{r^2 L^2}{4\alpha_0^2} \right) \frac{2}{k^2} - 2 \left(\frac{rL}{k\rho} \right)^{5/3} \right\} \\ &\quad \times \exp \left\{ -r^2 \left(\frac{\alpha_0^2}{2} \right) \left(1 - \frac{L}{F} \right)^2 \right\} \exp \{ 4C_\chi(0, \mathfrak{p}, 0) \} \\ C_\chi(0, \mathfrak{p}, 0) &= 0.132\pi^2 k^2 L \int_0^1 dt C_n^2(t) \int_0^\infty du u^{-8/3} \sin^2 \left[u^2 t(1-t) \frac{L}{2k} \right] J_0 \{ u | (1-t) \mathfrak{p} | \} \\ AINT_2|_{\tau=0, \mathfrak{p}=0} &= \frac{k^2}{4\pi^2 L^2} \int d\mathfrak{r}_2 \int d\mathfrak{p} \exp \left[- \frac{r_2^2}{2\alpha_0^2} - D_\psi(0, -\mathfrak{r}_2, 0) \right] \\ &\quad \times \exp \left[-r_0^2 k \frac{\alpha_0^2}{2L} \left(1 - \frac{L}{F} \right)^2 \right] \exp \left[\frac{ik}{L} \mathfrak{p} \cdot \mathfrak{r}_2 \right] H_2(0, \mathfrak{p}, 0, k) \end{aligned} \quad (2.21)$$

It is convenient to normalize the TDC by the average intensity,

$$C_{IN} = AINT_1 + \frac{\sum_i \langle I_i \rangle^2}{\langle I \rangle^2} AINT_2 - 1 \quad (2.22)$$

When there is no turbulence, $AINT_1$ and $AINT_2$ are unity, so Eq. (2.21) becomes

$$C_{IN} = \frac{\sum \langle I_i \rangle^2}{\langle I \rangle^2} = [VSCR]^2 \quad (2.23)$$

VSCR is called the Vacuum Speckle Contrast Ratio which represents the degree of speckle contrast reduction.

For a ‘‘White Light’’ source which has single transverse mode but with many longitudinal modes, the speckle contrast ratio is very small. Therefore, B_{f2} can be neglected. Consequently, a simplified normalized TDC can be written for polychromatic source

$$C_{In} = AINT_1 - 1 \quad (2.24)$$

In some cases of interest, the TDC is normalized by the variance

$$\begin{aligned} C_{IN}' &= \left(AINT_1 \langle I \rangle^2 - I^2 \right) / \sigma_I^2 = (AINT_1 - 1) \langle I \rangle^2 / \sigma_I^2 \\ &= (AINT_1 - 1) / \sigma_{IN}^2 = C_{IN} / \sigma_{IN}^2 \end{aligned} \quad (2.25)$$

Since the TDC depends on the cross-wind, the following chapter will focus on the numerical analysis of the two-point TDC and aperture averaging effects on the TDC when the receivers have finite area instead of simple point. The reason for using finite receiving area is to increase level of backscattering signal.

The next section discusses, wind sensing techniques. The complete analytical solution of the cross wind speed from the TDC and the autocovariance is obtained using point detector and “frozen turbulence” assumptions. Polychromatic laser source can be treated as single central frequency plus the effect of VSCR effect when frequency differences are small. For finite receiving areas, the approximation is to treat them as point detectors with an effective detector spacing. More accurate results can be obtained if aperture averaging effect is included using numerical methods.

2.3 Wind Sensing Techniques

There are several well-know processing techniques that should be useful in determining the wind speed from the received signal. Some of the techniques are illustrated in Fig.2.2. The briggs method measures the time delay τ_B at which the autocovariance and TDC curves cross. The delay to peak method measures the time delay τ_p where the TDC peaks. The width of the autocovariance method measures the time delay τ_w , at which the autocovariance curve decreases to 67% of the peak value. The slope method measures the slope of the TDC at zero time delay. To process the signals for the wind, the relationships

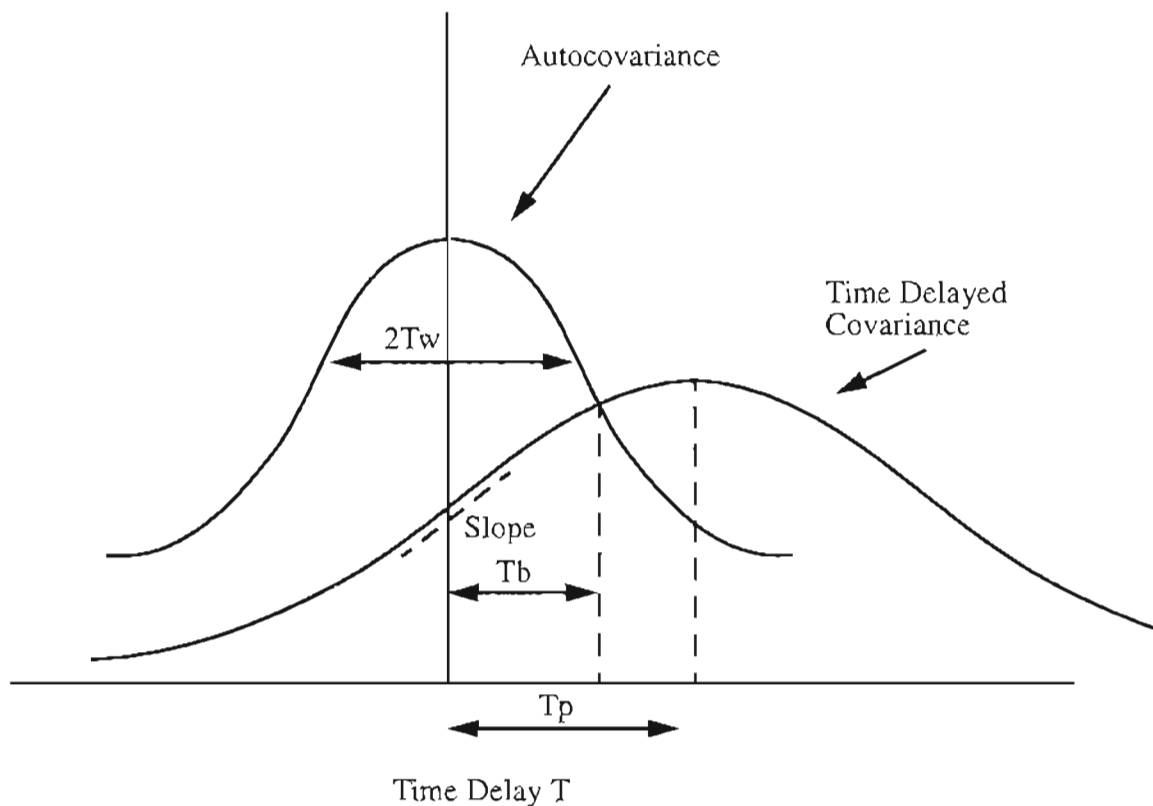


Figure 2.2 Techniques for wind remote sensing.

between the time delays, slope, and the wind must be derived from the previous equations. It was found that the delay to peak and Braggs techniques yield the wind directly, whereas the width of the autocovariance and slope techniques either require a knowledge of ρ_0 , the transverse phase coherent length, or must be used in conjunction with one of the other techniques to determine the wind and ρ_0 .

The time delayed covariance function for point detector of polychromatic laser source

can be simplified and written as⁵⁶

$$C_f(p, \tau) = AINT_1 - 1 = \frac{1}{2\pi} \int d\bar{\rho} \int r dr J_0(\rho r) \exp \left[-\frac{r^2 L^2}{2\alpha_2^2 k^2} - 2 \left(\frac{rL}{k\rho} \right)^{5/3} - r^2 \frac{\alpha_0}{2} \left(1 - \frac{L}{F} \right)^2 \right] \\ \times \exp \left\{ 4 \times 0.132 \pi^2 k^2 L C_n^2 \int dt H(a_1, b) \right\} - 1 \quad (2.26)$$

where

$$H(a_1, b) = H \left\{ \left[\frac{t(1-t)L}{2k} \right]^{1/2}, \quad |t\bar{\rho} + (1-t)\bar{\rho} - \bar{V}\tau| \right\} = -\frac{3b^{5/3} \Gamma^2(1/3)}{20\pi^{1/2} \Gamma(11/6)} \cos\left(\frac{\pi}{6}\right) + \\ \frac{3a_1^{5/3} \Gamma(1/6)}{5(2)^{1/6}} \left\{ \frac{\exp[i(\pi/12)]}{2i} F_1 \left(-\frac{5}{6}, 1, -\frac{ib^2}{8a_1^2} \right) - \frac{\exp[-i(\pi/12)]}{2i} F_1 \left(-\left(\frac{5}{6}, 1, \frac{ib^2}{8a_1^2} \right) \right) \right\} \quad (2.27)$$

and

$$a_1^2 = \frac{t(1-t)L}{2k}, \quad b = |t\bar{\rho} + \bar{\rho}(1-t) - \bar{V}\tau| \quad (2.28)$$

The slope of the Eq. (2.26) is given by

$$S_f = \left. \frac{\partial}{\partial \tau} C_f(p, \tau) \right|_{\tau=0} \quad (2.29)$$

When the wind and the turbulence are uniform along the path, Eq. (2.29) reduces to

$$S_I = \text{const} \cdot C_I(p, 0) \frac{\rho_0^{2/3}}{\rho_0^{5/3}} V_p \quad (2.30)$$

where V_p is the wind component along p and can be obtained when ρ_0 is known. This implies that slope method must be used in conjunction with one of the other methods in order to be useful.

The method that is usually used in conjunction with the slope method is the width of the autocovariance. In this method, the time delay, τ_w , at which the autocovariance falls to 67% of its peak value is measured. The slope of the autocovariance curve is a maximum at this time delay. With $p = 0$ and $\tau = \tau_w$, for uniform wind and turbulence.

Eq.(2.26) gives

$$V = \frac{0.1395\rho_0}{\tau_w} \quad (2.31)$$

This method is best utilized with the slope method in determination of both the wind speed and turbulence coherence length (ρ_0) which is related to the strength of the turbulence.

The time delay corresponding to the peak is obtained by differentiating Eq. (2.26) with respect to τ and setting the result equation to zero.

$$S_I = \frac{\partial}{\partial \tau} C_I(p, \tau) = 0 \quad (2.32)$$

For the case where \hat{V} and \hat{p} are colinear and \hat{V} is uniform along the path, Eq. (2.32) can be solved analytically, giving $\tau_p = \frac{p}{2V}$, or $V = \frac{p}{2\tau_p}$. For the case where \hat{V} and \hat{p} are orthogonal, the solution to Eq. (2.32) is $\tau_p = 0$. This means that there is no shift of the peak of TDC function. The accuracy of this method is defined by the time resolution of the TDC which is sampling period and spacing between the detectors.

The other methods are Briggs method which is often used in the line of sight case of wind measurements and Z-Log Ratio method. Detailed discussion and simulation of the application and accuracy can be found in Dr. Farzin Amzajerdian's dissertation.

Chapter 3

Numerical Analysis of Variance and Covariance

The analytical expressions of the second order statistics of polychromatic LIDAR signals are very complicated as it was seen in the previous chapter. Numerical analysis is necessary to realize and visualize the behavior of the autocovariance and time delayed covariance and compare them with experimental results. It is computer time consuming to analysis numerically these formulations developed in the previous chapter because series expansions and multidimensional integrals are involved. Previous work on this matter was done by Rao Gudimetla with some good results but it was incomplete to some extent because of the constraint of computer facilities at that time. In this chapter, with some simplification on the formulation, numerical analysis was done on SUN-workstation for both a point detector and a finite receiving aperture. Gauss Quadrature integration subroutines in the NAG library were used for numerical integrations. A Newton trapezoidal method was also used for comparison. The aperture averaging effect⁵²⁻⁵⁵ was observed and good results have been reached. Comparison of numerical results with experimental results will be presented in chapter 5 and as it will be seen that good agreement was found. It is also very important to notice where the experimental system stands by looking at these results, so improvements can be made.

3.1 Some Simplifications for Numerical Analysis

As it is mentioned in the previous chapter, for a “White Light” system, the second term, $AINT_2$ in the TDC is so small that it can be neglected. Much of the effort has been put on the numerical analysis of the TDC behavior of two point detectors and the finite area receivers. The aperture average effect is observed. Some simplifications are needed in order to effectively evaluate the time delayed covariance. For the point detector case, the integration is three fold; for two finite receiving area, it becomes four fold; for the aerosol case, the integrals grow up to five fold. The new computer technology makes the numerical analysis possible in a reasonable amount of time.

The complete expression of $AINT_1$ is

$$AINT_1 = \frac{1}{2\pi} \int d\bar{\rho} \int r dr J_0(\rho r) \exp \left[-\frac{r^2 L^2}{2\alpha_2^2 k^2} - 2 \left(\frac{rL}{k\rho} \right)^{5/3} - r^2 \frac{\alpha_0}{2} \left(1 - \frac{L}{F} \right)^2 \right] \\ \times \exp \left\{ 4 \times 0.132 \pi^2 k^2 L C_n^2 \int dt H(a_1, b) \right\} \quad (3.1)$$

where

$$H(a_1, b) = H \left\{ \left[\frac{t(1-t)L}{2k} \right]^{1/2}, |t\bar{\rho} + (1-t)\bar{\rho} - \bar{V}\tau| \right\} = -\frac{3b^{5/3} \Gamma^2(1/3)}{20\pi^{1/2} \Gamma(11/6)} \cos\left(\frac{\pi}{6}\right) + \\ \frac{3a_1^{5/3} \Gamma(1/6)}{5(2)^{1/6}} \left\{ \frac{\exp[i(\pi/12)]}{2i} F_1 \left(-\frac{5}{6}, 1, -\frac{ib^2}{8a_1^2} \right) - \frac{\exp[-i(\pi/12)]}{2i} F_1 \left(-\left(\frac{5}{6}, 1, \frac{ib^2}{8a_1^2} \right) \right) \right\} \quad (3.2)$$

and

$$a_1^2 = \frac{t(1-t)L}{2k}, \quad b = |\mathfrak{P}t + \mathfrak{P}(1-t) - \mathfrak{V}\tau| \quad (3.3)$$

To accomplish the integral, the integration over \mathfrak{P} is first performed. A simplification is made, that,

$$\left(\frac{rL}{k\rho_0}\right)^{5/3} \rightarrow \left(\frac{rL}{k\rho_0}\right)^2$$

so the integration can be completed analytically.

$$\begin{aligned} AINT_1 &= \frac{1}{2\pi} \int d\mathfrak{P} \int r dr J_0(\rho r) \exp[-ar^2] \exp(4C_\chi) \\ &= \frac{1}{2\pi} \left(\frac{1}{2a}\right) \int \exp\left[-\frac{\rho^2}{4a}\right] d\mathfrak{P} \exp(4C_\chi) \end{aligned} \quad (3.4)$$

where

$$a = \frac{L^2}{2\alpha_0^2 k^2} + 2\left(\frac{L}{k\rho_0}\right)^2 + \frac{\alpha_0^2}{2} \left(1 - \frac{L}{F}\right)^2 \quad (3.5)$$

Some analysis must be done on the effect of the simplification. The following figures show the exponential term as a function of \mathfrak{P} with and without the simplification at different turbulence strength. It is seen that the effect becomes substantial only when $C_n^2 \geq 10^{-13}$, which is very high. It must be noticed that it is not because the square is a good approximation of 5/3. The real reason is that this term comes from phase structure

function which is induced by phase fluctuations. The effect of the phase fluctuation is closely related to the coherence of the laser source. As the coherence decreases, the contribution of the phase fluctuation to the covariance decreases. A more accurate analysis is to use Bessel expansions instead of approximations. Detailed derivations was done by Dr. Rask. In his thesis work,²⁸ Bessel expansion was used for the complete integration. Little difference was found even with 5/3 term dropped which is another simple approximation.

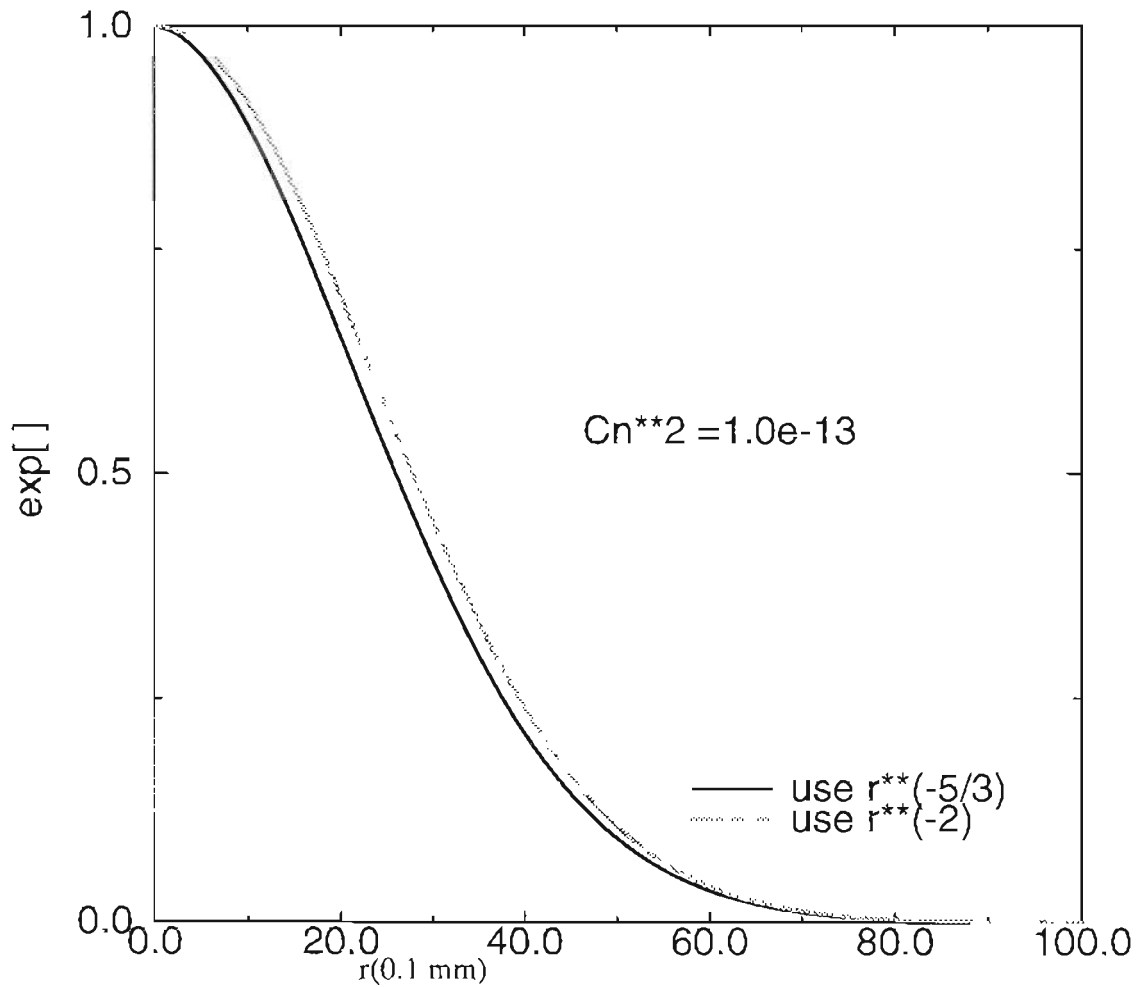


Figure 3.1 Effect of the simplification on the exponential term of r with strong turbulence.

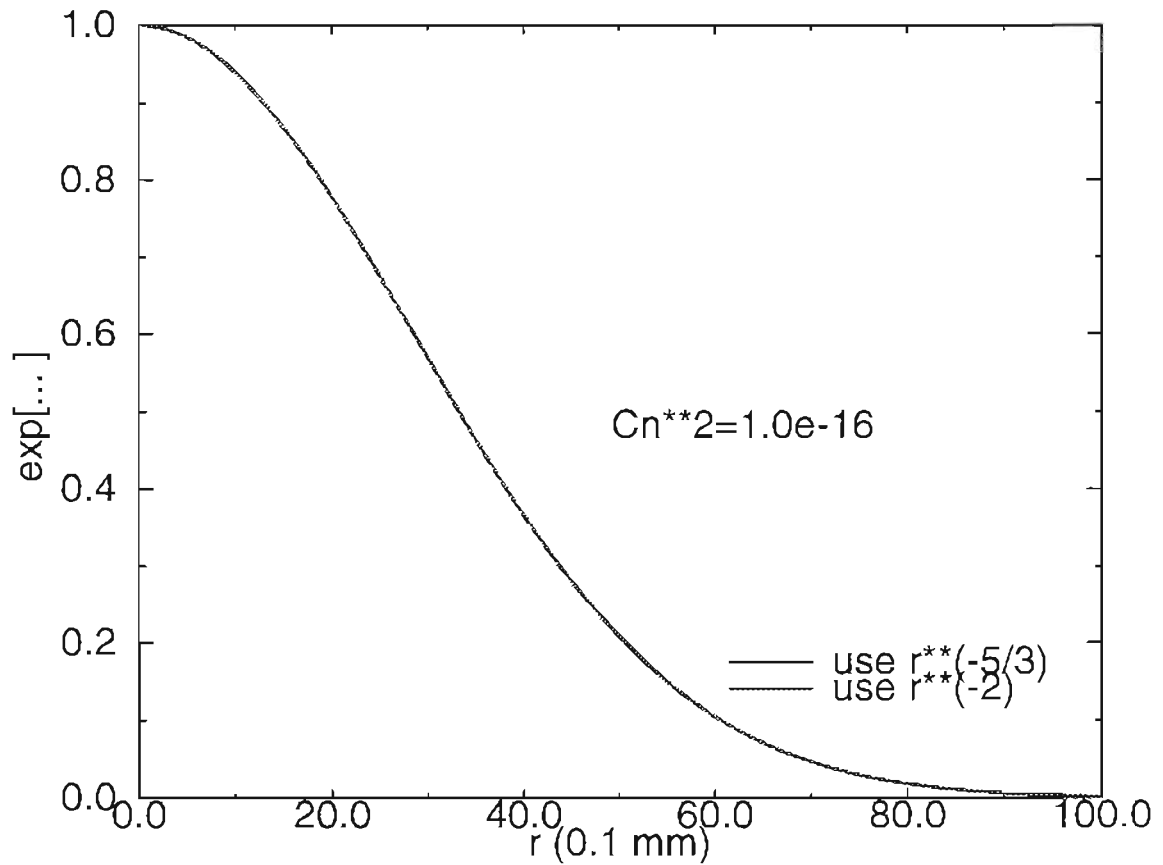


Figure 3.2 Effect of the simplification on the exponential term of r with weak turbulence.

The integration over \vec{p} can be made by using another approximation. Compare

$\exp\left(-\rho^2 / (4a)\right)$ and $\exp(4C_\chi)$ for different C_n^2 , L , F , it is found that the former term

drops much faster the latter term as it can be seen in Fig.(2.4) and Fig.(2.5). Only when the

turbulence strength is extremely high, $\exp(4C_\chi)$ will decrease at a rate comparable to

$\exp\left(-\rho^2/(4a)\right)$. So it is reasonable to treat $\exp(4C_\chi)$ as constant and take it out of the integral to complete the integration. So the final expression of $AINT_1$ becomes

$$AINT_1 = \frac{1}{2\pi} \int_0^{2\pi} \sin\theta \exp(4C_\chi) d\theta \quad (3.6)$$

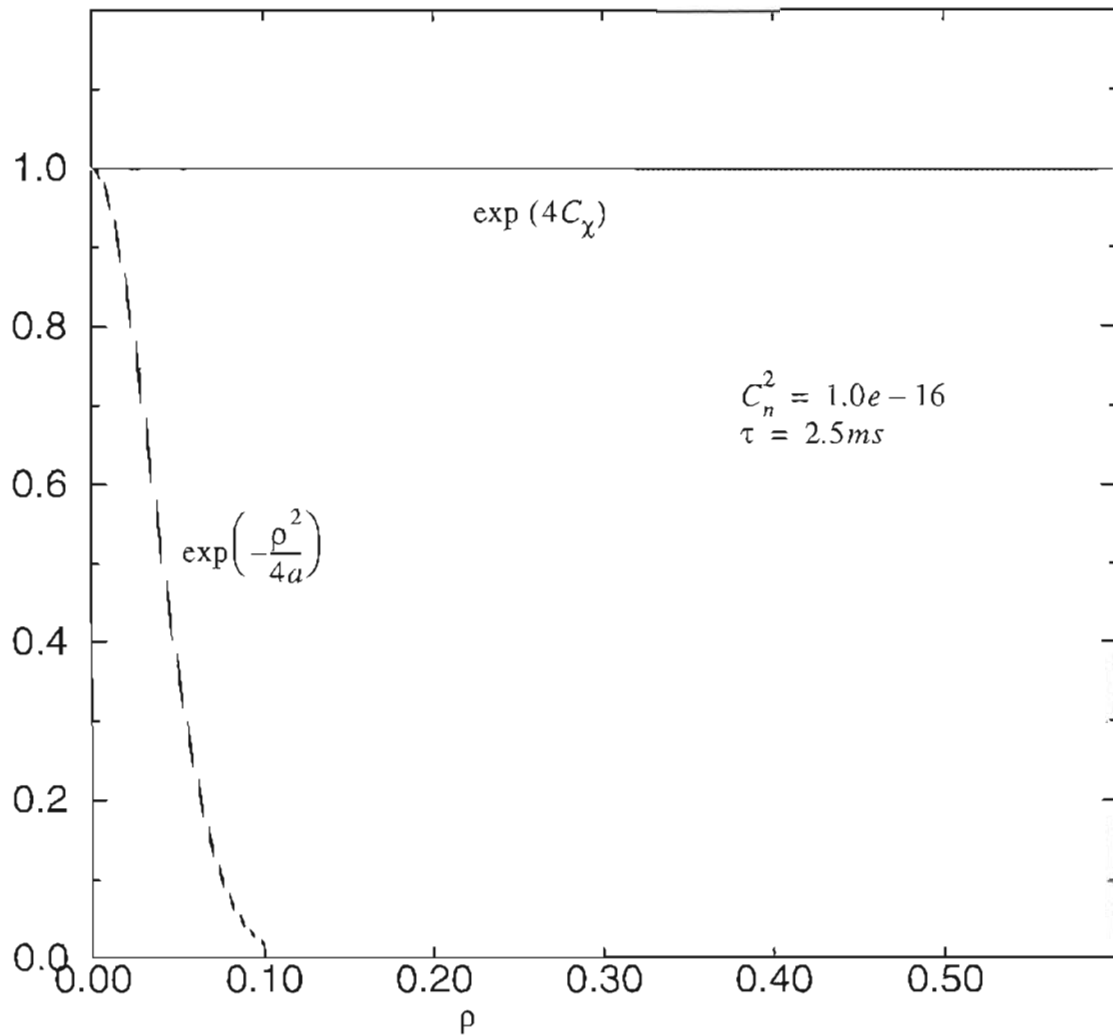


Figure 3.3 Comparison of $\exp(4C_\chi)$ and $\exp\left(-\frac{\rho^2}{4a}\right)$.

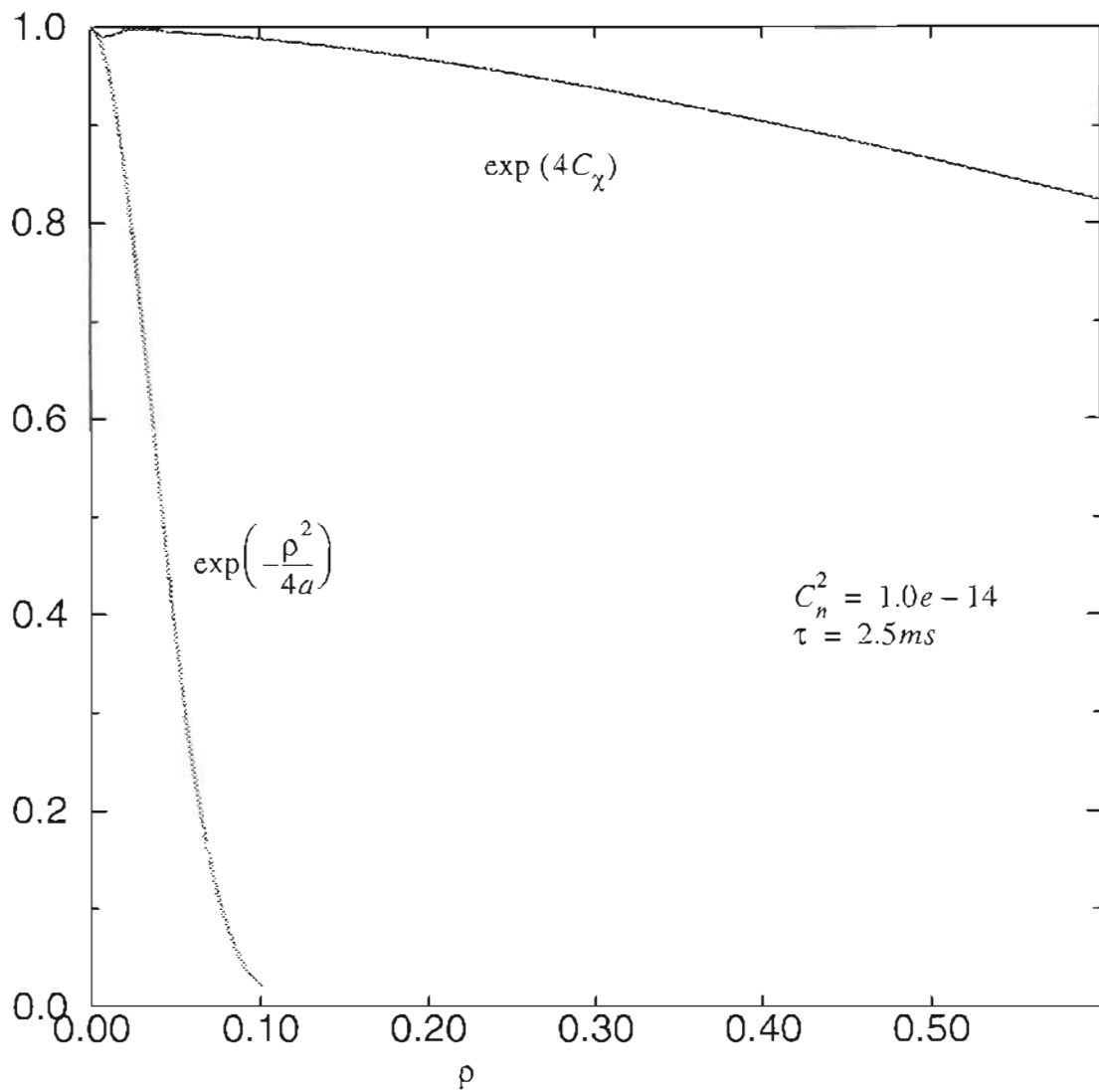


Figure 3.4 Comparison of $\exp(4C_\chi)$ and $\exp\left(-\frac{\rho^2}{4a}\right)$.

The Confluent Hypergeometric functions in Eq.(3.2) can be written as⁶¹

$$M(a;c;x) = 1 + \frac{a}{c}x + \frac{a(a+1)}{c(c+1)}\frac{x^2}{2!} + \dots, \quad c \neq 0, -1, -2, \dots$$

$$= \sum_{n=0}^{\infty} \frac{(a)_n x^n}{(c)_n n!} \quad (3.7)$$

when x is small. Since the confluent hypergeometric series converges slowly for large values of x , the Asymptotic series should be used in Eq(2.26) when $x > 4\pi$.⁵⁶

$$M(a, c, Z) = \frac{\Gamma(c)}{\Gamma(c-a)} e^{\pm i\pi a} Z^{-a} \sum_{n=0}^{R-1} (a)_n \frac{(1+a-c)_n}{n!} (-Z)^{-n} \\ + \frac{\Gamma(c)}{\Gamma(a)} e^z Z^{a-c} \sum_{n=0}^{s-1} \frac{(c-a)_n}{n!} (1-a) Z^{-n} \quad (3.8)$$

The + sign is used when $-\frac{1}{2}\pi < \arg Z < \frac{3}{2}\pi$, and the - sign is used when $-\frac{3}{2}\pi < \arg Z \leq -\frac{1}{2}\pi$.

With above expansions, following the procedure in Appendix A, the confluent hypergeometric function term can be written as

$$\frac{\exp(i(\pi/12))}{2i} F_1\left(-\frac{5}{6}; 1; \frac{ib^2}{8a_1^2}\right) - \frac{\exp(-i(\pi/12))}{2i} F_1\left(-\frac{5}{6}; 1; \frac{ib^2}{8a_1^2}\right) = \\ \cos(\beta) \left[-\frac{ay}{c} + \frac{a(a+1)(a+2)y^3}{c(c+1)(c+2)3!} - \frac{a(a+1)(a+2)(a+3)(a+4)y^5}{c(c+1)(c+2)(c+3)(c+4)5!} + \dots \right] \\ + \sin(\beta) \left[1 - \frac{a(a+1)y^2}{c(c+1)3!} - \left(\frac{a(a+1)(a+2)(a+3)y^4}{c(c+1)(c+2)(c+3)4!} + \dots \right) \right] \quad (3.9)$$

where $\beta = \pi/2$, $a = 5/6$, $c = 1$, $y = b^2/(8a_1^2)$.

When asymptotic expansions are used, the final expression is

$$\begin{aligned} & \frac{\exp(i(\pi/12))}{2i} F_1\left(-\frac{5}{6}; 1; \frac{ib^2}{8a_1^2}\right) - \frac{\exp(-i(\pi/12))}{2i} F_1\left(-\frac{5}{6}; 1; \frac{ib^2}{8a_1^2}\right) = \\ & \frac{1}{\Gamma(1-a)} \sum \frac{a_n^2}{n!} y^{-(n+a)} \sin\left(\beta - (a+n)\frac{\pi}{2}\right) + \\ & \frac{1}{\Gamma(a)} \sum \frac{(1-a)_n^2}{n!} y^{-(n+1-a)} \sin\left[\beta - y + (n+1-a)\frac{\pi}{2}\right] \end{aligned} \quad (3.10)$$

It was found that about nine terms are accurate enough for the normal expansions, about 11 terms are needed for the asymptotic case. Numerical analysis was done on Sun-workstations. Gauss Quadrature integration subroutines in the NAG library are used for the numerical integrations. Gauss Quadrature integration subroutines can do the multidimensional integration up to 11th fold under some constraints. A Newton trapezoidal method was also used for comparison. It was found that Gauss Quadrature runs and converges much faster than the Newton method. The autocorrelation and TDC for the point detector case are simulated for different wind speeds and turbulence strengths. It has been shown that the formulation for a focused beam and collimated beam are the same. Other parameters such as the wavelength or the output beam size are chosen according to the parameters of the incoherent LIDAR system designed.

3.2 TDC and Autocovariance for the Point Detectors

Numerical analysis for the point detectors was done using program in Appendix B. The results presented in this section were obtained with wavelength of 830 nm which is used for the “White Light” system. In the following figures dashed line at $\tau = 0$ is plotted as a reference of lag time of TDC function. With the same detector spacing and turbulence strength but different wind speeds, the time shift of the peak of the TDC function decreases as the cross wind speed increases. This intuitively makes sense because wind speed is proportional to the detector distance and inversely proportional to the peak shift time. The TDC function is wide for smaller wind speeds as it is shown in figure (3.5). The TDC function is normalized by the average intensity, so the magnitude of the TDC is higher when turbulence is stronger but with similar shape as can be seen in figure (3.5) and (3.6). It is the coherence of the turbulence induced variance which contributes to the correlation. In some cases, it may be useful to normalize the TDC by variance instead of the average intensity. Figure (3.7) shows the TDC functions with different detector spacing which should be compared to figure (3.5). A short lag time has been observed with short detector spacing when the cross wind speed is the same. Figure (3.7) and (3.8) is another comparison with different turbulence strengths. Figure (3.9), and (3.10) are simulated results of the autocovariance. Different wind speeds and turbulence were used. As it is shown, the autocovariance has a smaller width when the cross wind speed is higher because the correlation time is smaller. All the simulations used a distance of 800 meters. It should be noted that the path length also has a contribution to the magnitude of the autocovariance and the TDC before they start to saturate.

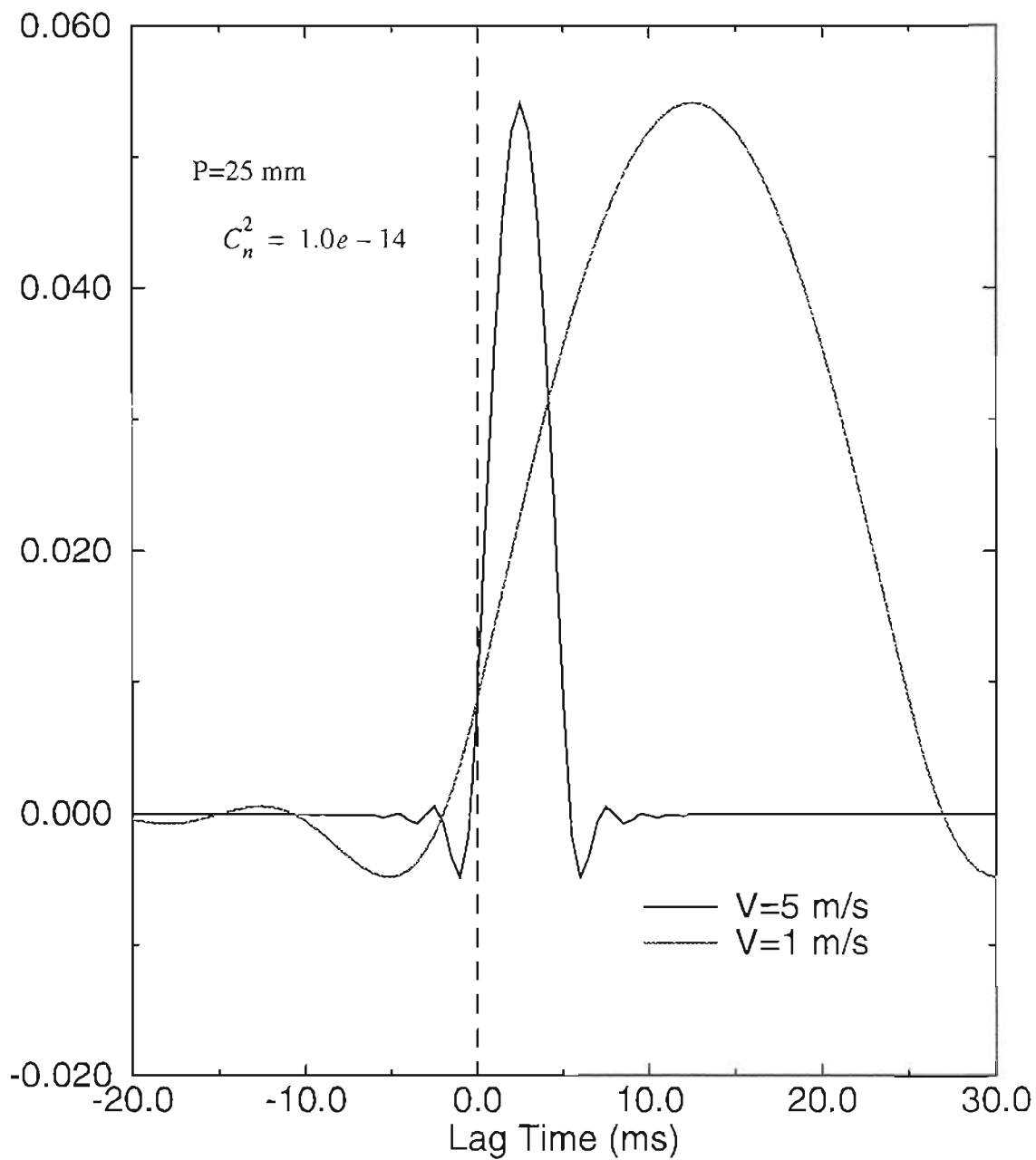


Figure 3.5 TDC for the point detectors with $C_n^2 = 1.0e-14$, $P=25$ mm.

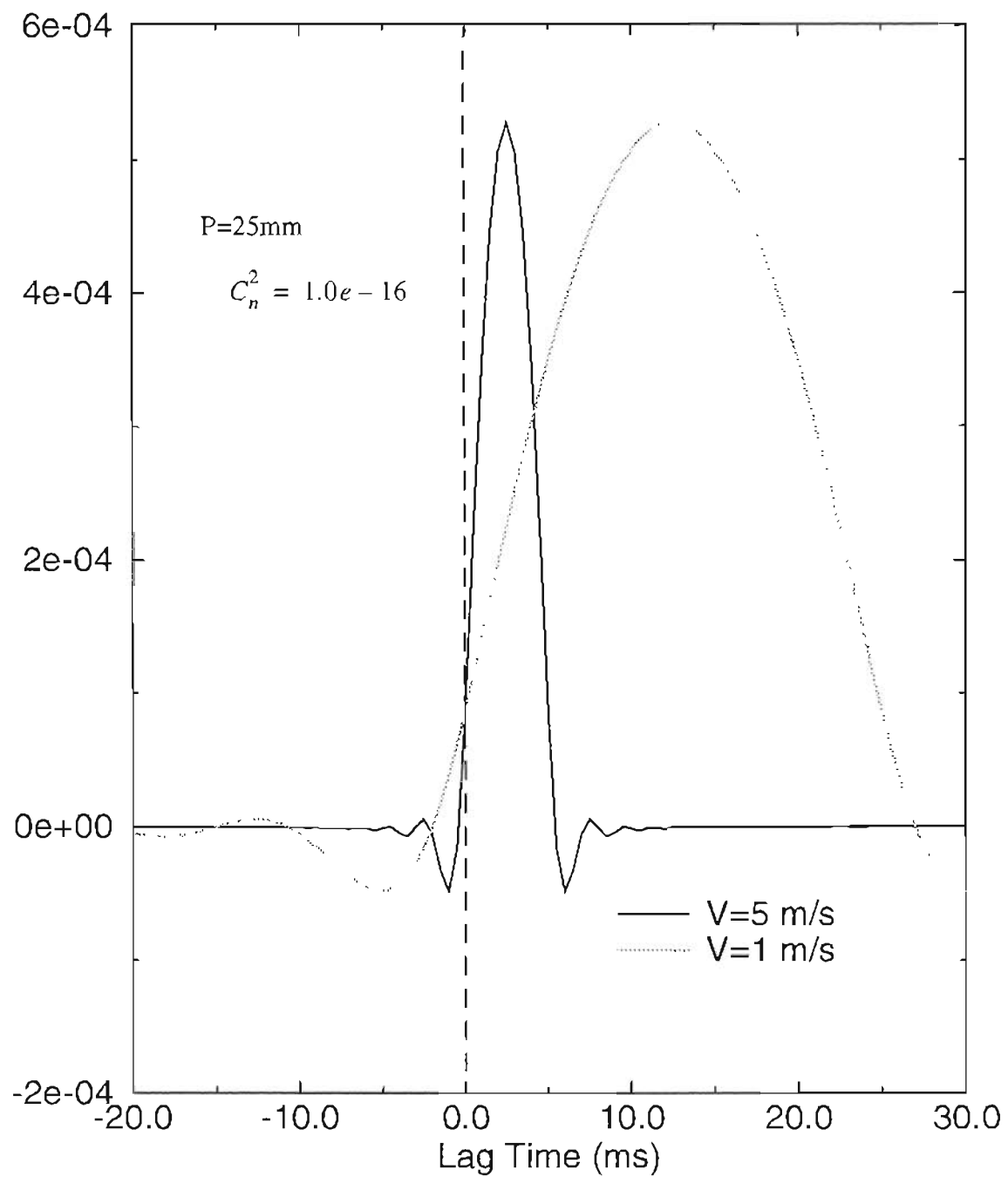


Figure 3.6 TDC for the point detectors with $C_n^2 = 1.0e-16$, $P=25\text{mm}$.

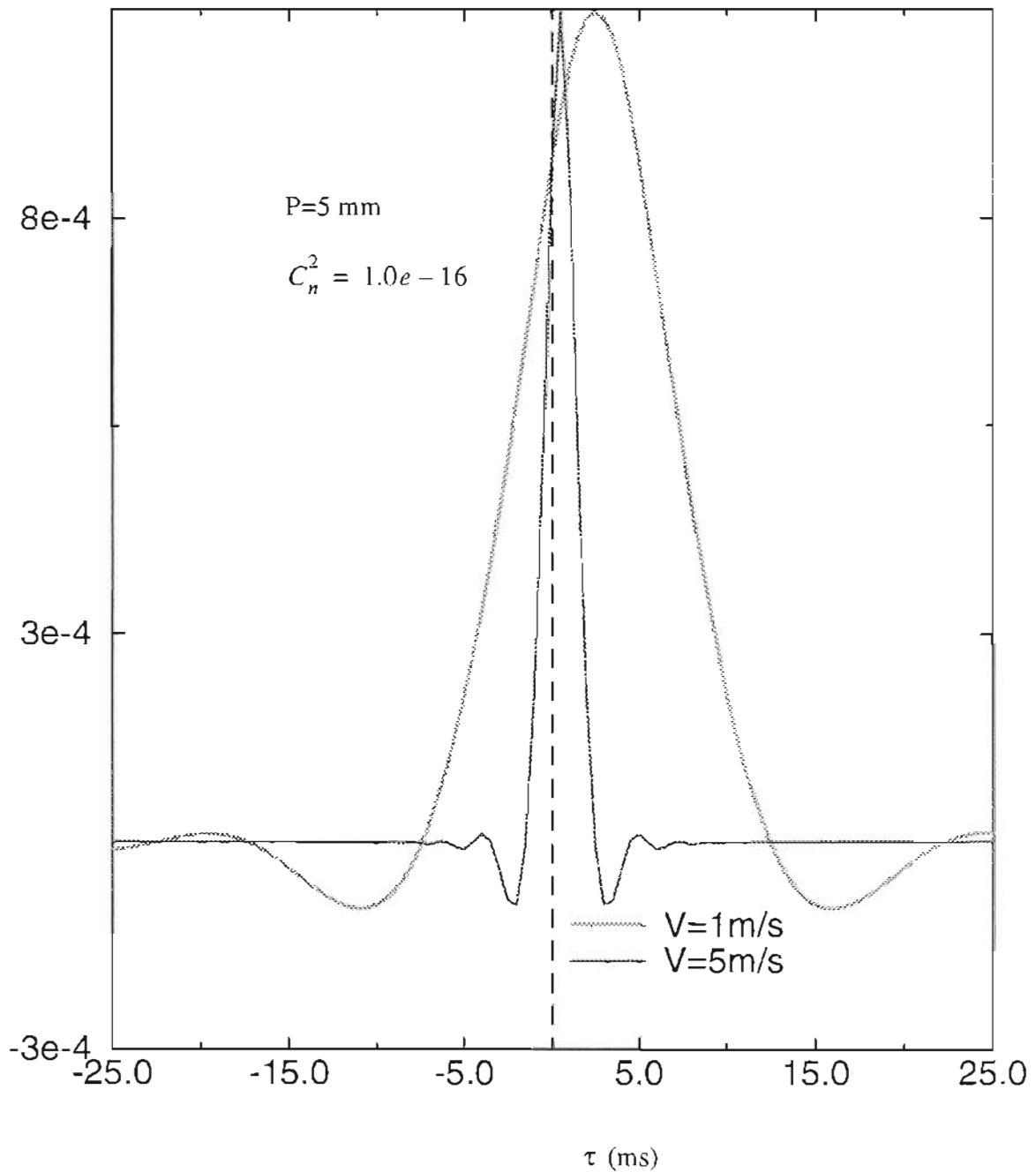


Figure 3.7 TDC for point detectors, with $C_n^2 = 1.0e-16$, $P=5\text{mm}$.

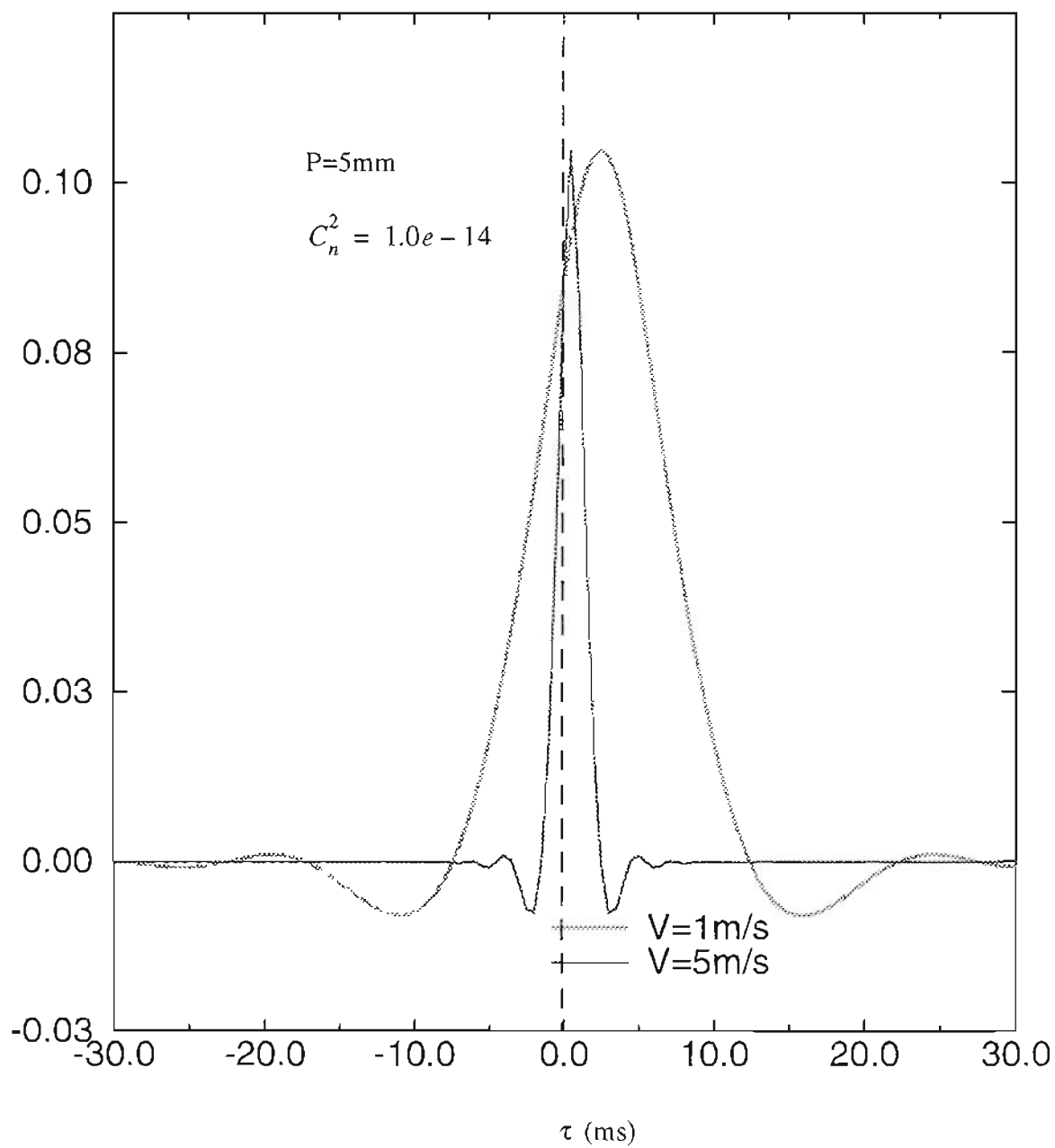


Figure 3.8 TDC for point detectors, with $C_n^2 = 1.0e - 14$, P=5mm.

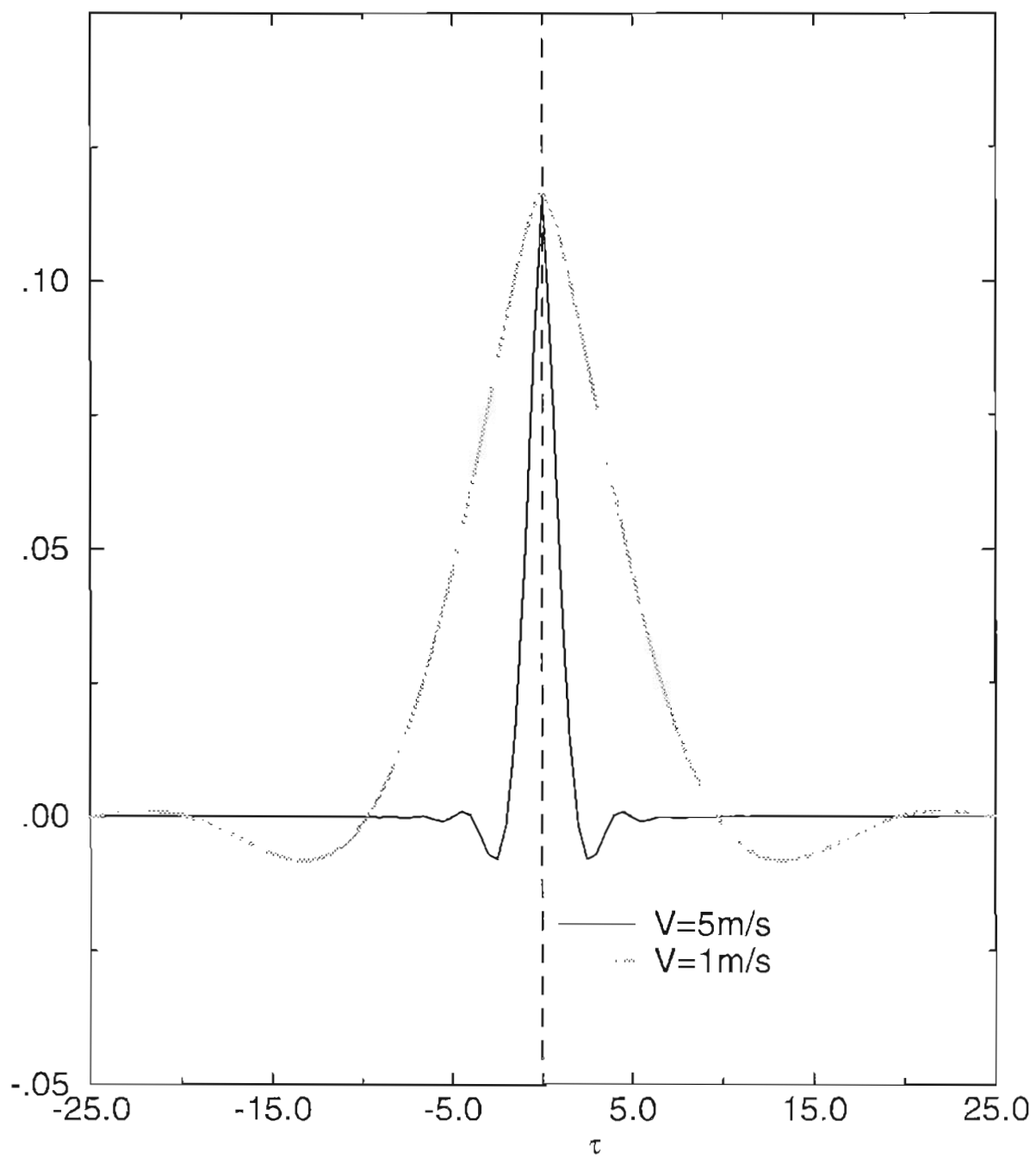


Figure 3.9 Auto-covariance of point detectors, $C_n^2 = 1.0e - 14$.

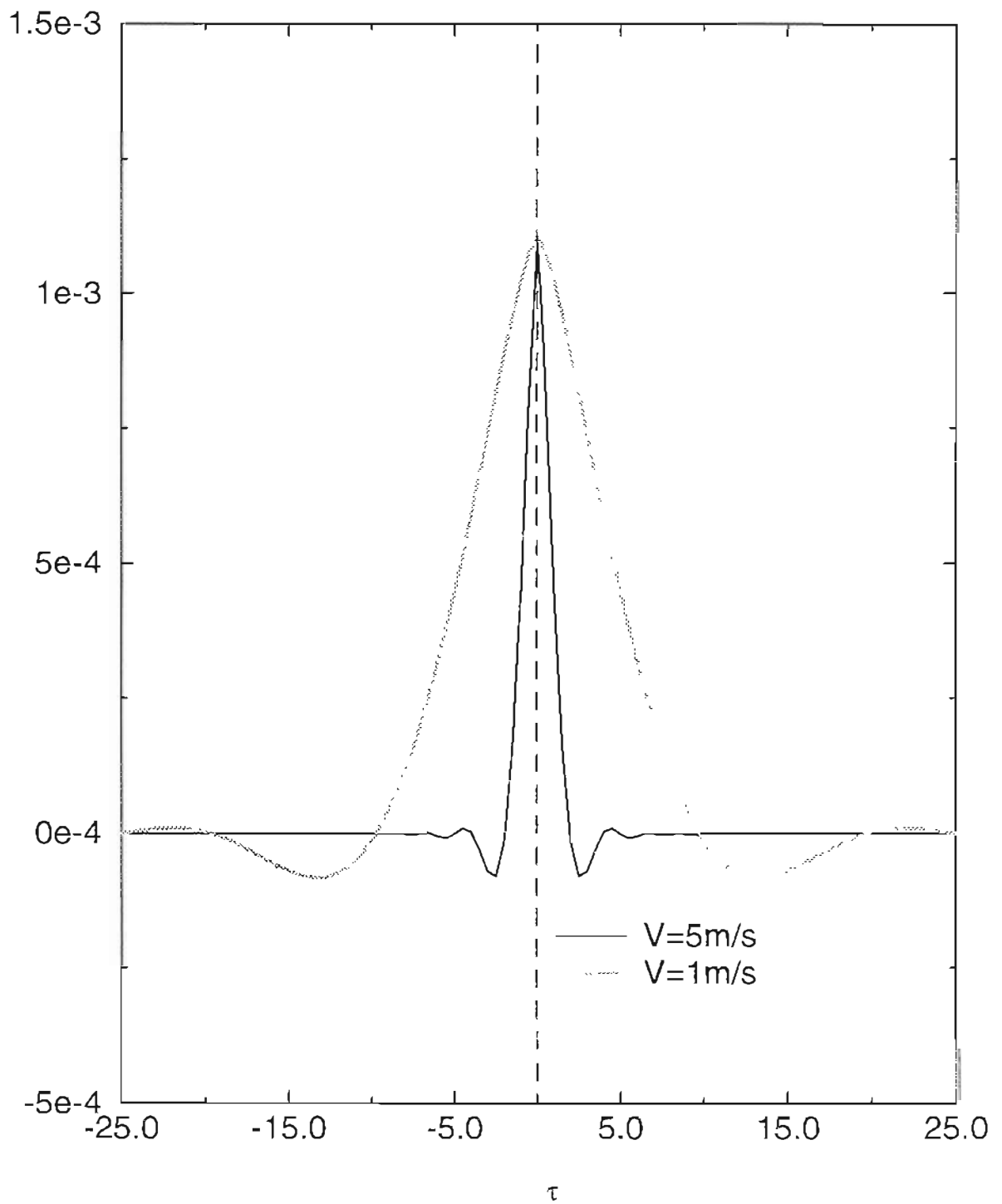


Figure 3.10 Auto-covariance of point detector, $C_n^2 = 1.0e - 16$.

3.3 Aperture Averaging Effect on TDC and Auto-covariance

All the previous theoretical development was based on the assumptions of point detectors, and uniform turbulence along the propagation path. It is an ideal situation to have a point detector, but it helps to gain insight into the phenomenon and characterize the physical behavior in an accurate and easy fashion. Because of the small coherence length of atmospheric turbulence, a very small detector area is preferred for accurate and sensitive detection. But in a real LIDAR system, finite receiving area is almost always used in order to increase the level of detected signals. However, increasing the area of the receiving aperture introduces aperture averaging. Aperture averaging is a complex operation on the received signal, which is closely related to the small coherence length of the atmospheric turbulence. Aperture averaging comes into effect in two ways as receiving area increases:

- 1) As area increases, the distance between any two points in the receiver plane also increases. As can be seen in the point detector case, the cross-covariance decreases, so the total cross-covariance decreases.
- 2) The signal in one receiver should add up coherently if the receiving area is much smaller than the atmospheric coherent length. As the area becomes bigger, the incoherent part of the signal begins to add up in random fashion, resulting in an averaging effect which reduces the information. It is very important to understand this phenomenon, to lead to a correct design of a LIDAR system.

The theory about the point detector can be directly applied to the finite receiving area case. However caution must be used for the incoherent, direct detection system. Because direct detection systems detect the signal power, instead of the electric field, the signal presented is spatially averaged intensities. Cross-correlation of intensities happens after the

fields are spatial averaged. Applying surface integrals on the receiver plane to the right side of Eq.(2.3), and taking them inside the assemble average. The high frequency terms created by two different laser wavelengths are block out because of the limited bandwidth of the receiver. The averaging effect happens before correlation is calculated.

Gauss Quadrature is used for the multi-dimensional integrals. The programs are listed in Appendix C. Different receiver sizes are used correspond to the actual apertures used in the experiment. The accuracy of the numerical calculation depends on the number N chosen for Gauss Quadrature estimation. But the CPU time increases as 2 to the N th power. Therefore, limited accuracy must be accepted to get the results in reasonable amount of computer time. It was found that for the hard target case, a four fold Gauss Quadrature is needed to get one point on the TDC or autocovariance curve. If same number of N is used for each dimensional Gauss Quadrature estimation, $N=16$ gives about 6 minute for each point. About 10 hours are needed for a plot of 100 points.

The result of two half-moons of radius 5 mm is shown in figure (3.11). Other parameters chosen for the simulation are as written in the figure. When the radius of the receiver is small, the TDC behaves like the point detector case. As the radius increases, the magnitude of TDC decreases and the shape becomes asymmetric because the aperture averaging effect becomes more severe. This result can be seen in figure (3.12). This phenomena is verified by experimental results. Figure (2.13) and (3.14) are autocovariance for two half-moons of different sizes. The aperture averaging effect makes the autocovariance decrease as the size of receiver increases.

Two rectangles next to each other are also used as receivers. Numerical analysis was

conducted to study the aperture averaging effect. Figure (3.15) and (3.16) are the TDC function and autocovariance function of rectangular receiver with total width of 40 mm. Similar results as of two half-moons are obtained. Many simulations were done for different widths of rectangle and different radii in order to develop a curve, so practically optimum size of receiver can be found. More simulation results will be presented in chapter 5 where experimental results are used for comparison. It should be noted that good agreement was found between experiment and simulated curve of peak TDC value vs. aperture size. Excellent agreement was also found between experiment and simulated results of autocovariance as it will be seen in chapter 5.

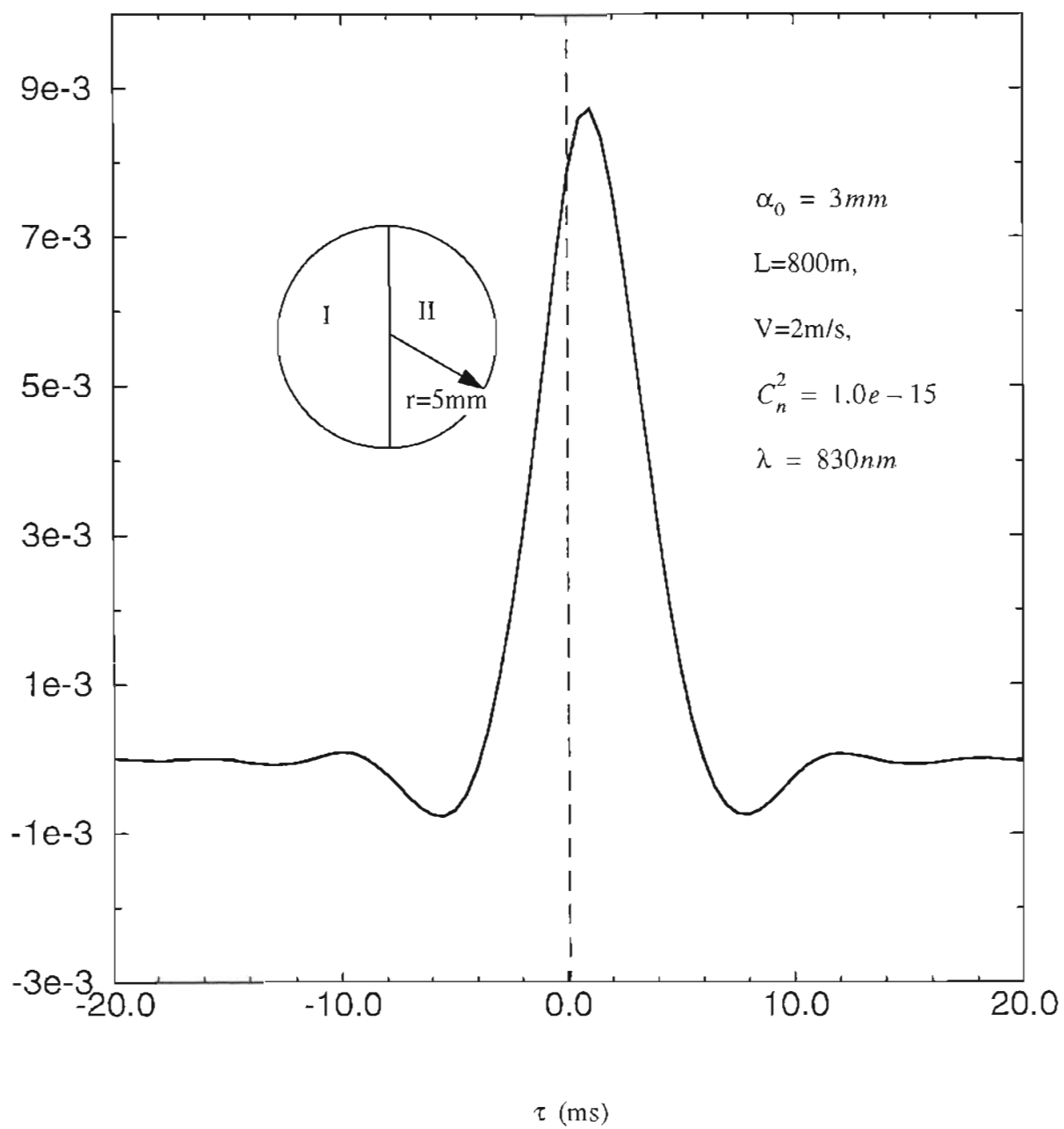


Figure 3.11 TDC of two half-moons with radius $r=5\text{mm}$.

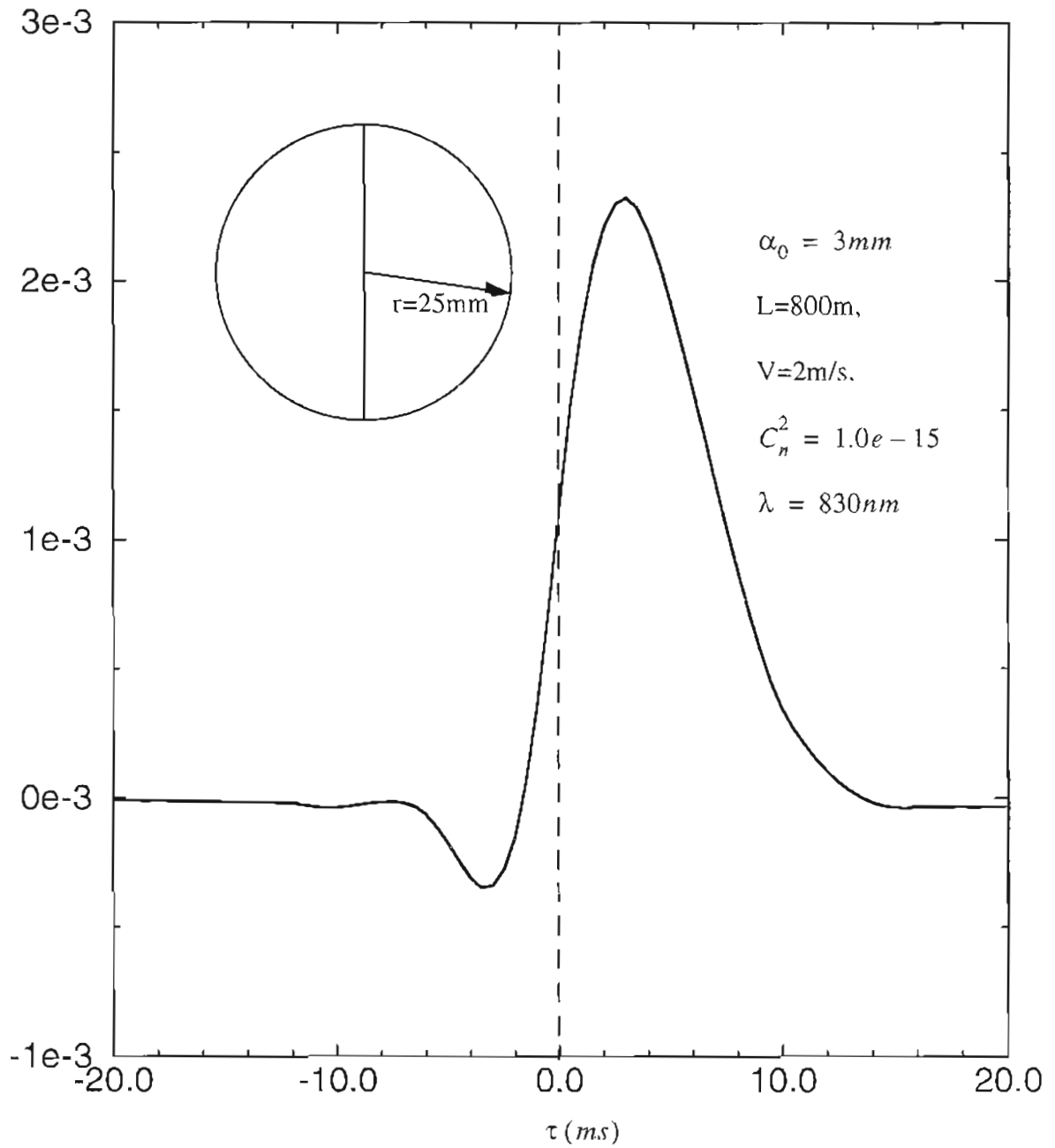


Figure 3.12 TDC of two half-moons with radius $r=25\text{mm}$.

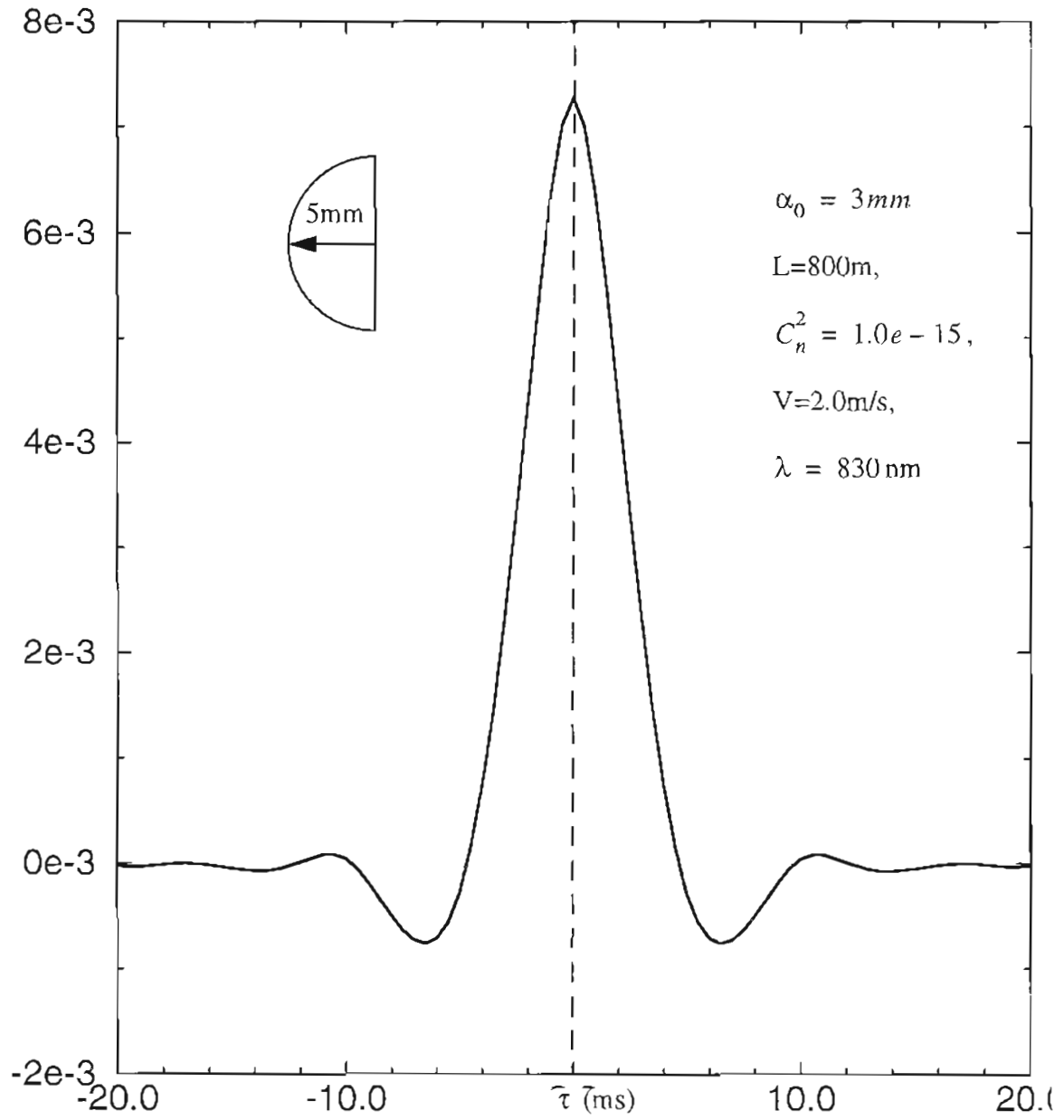


Figure 3.13 Auto-covariance of half-moon shaped receiver, radius $r=5\text{mm}$.

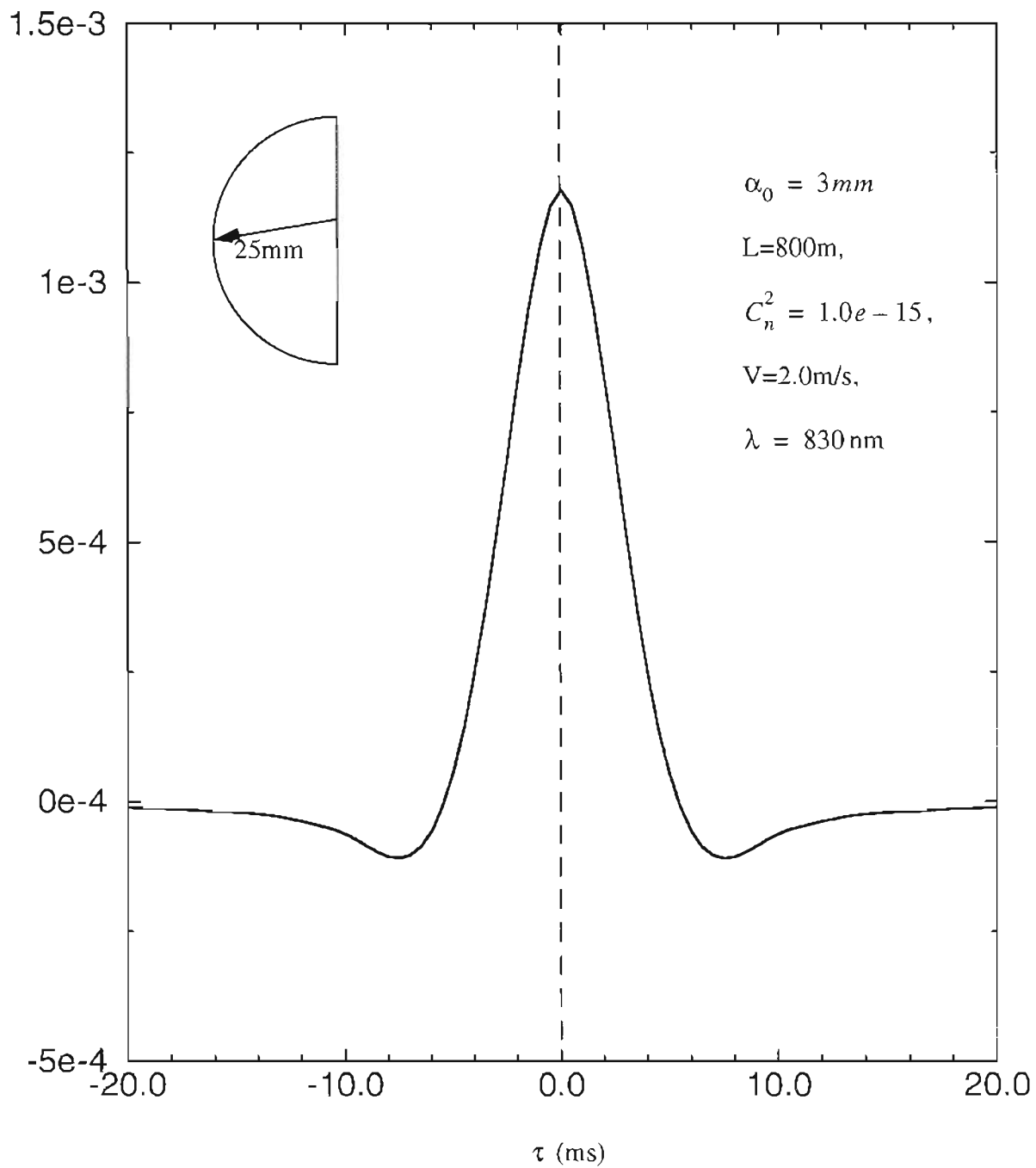


Figure 3.14 Auto-covariance of half-moon shaped receiver, radius $r=25\text{mm}$.

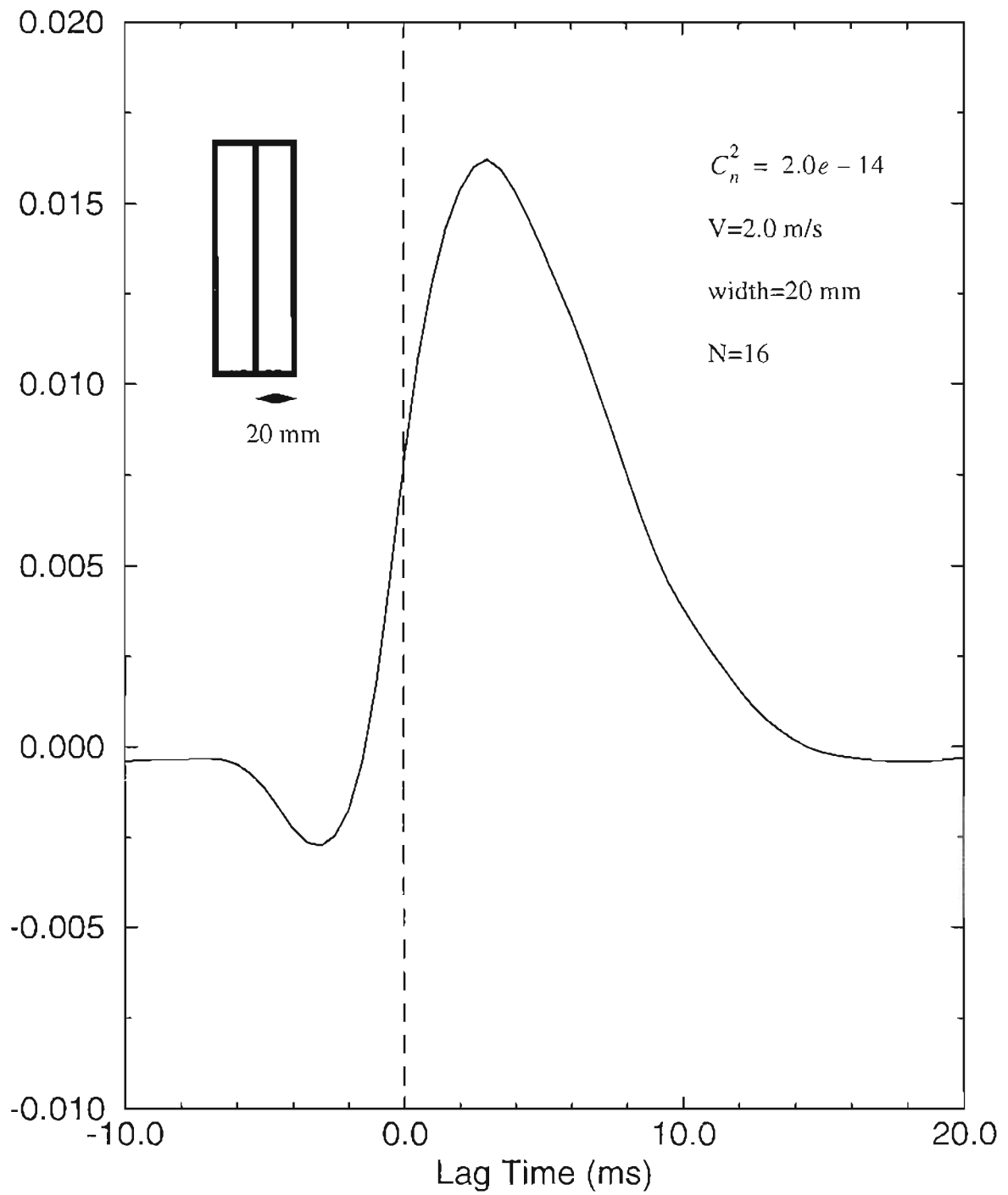


Figure 3.15 TDC of rectangular shaped receiver with width of 20 mm.

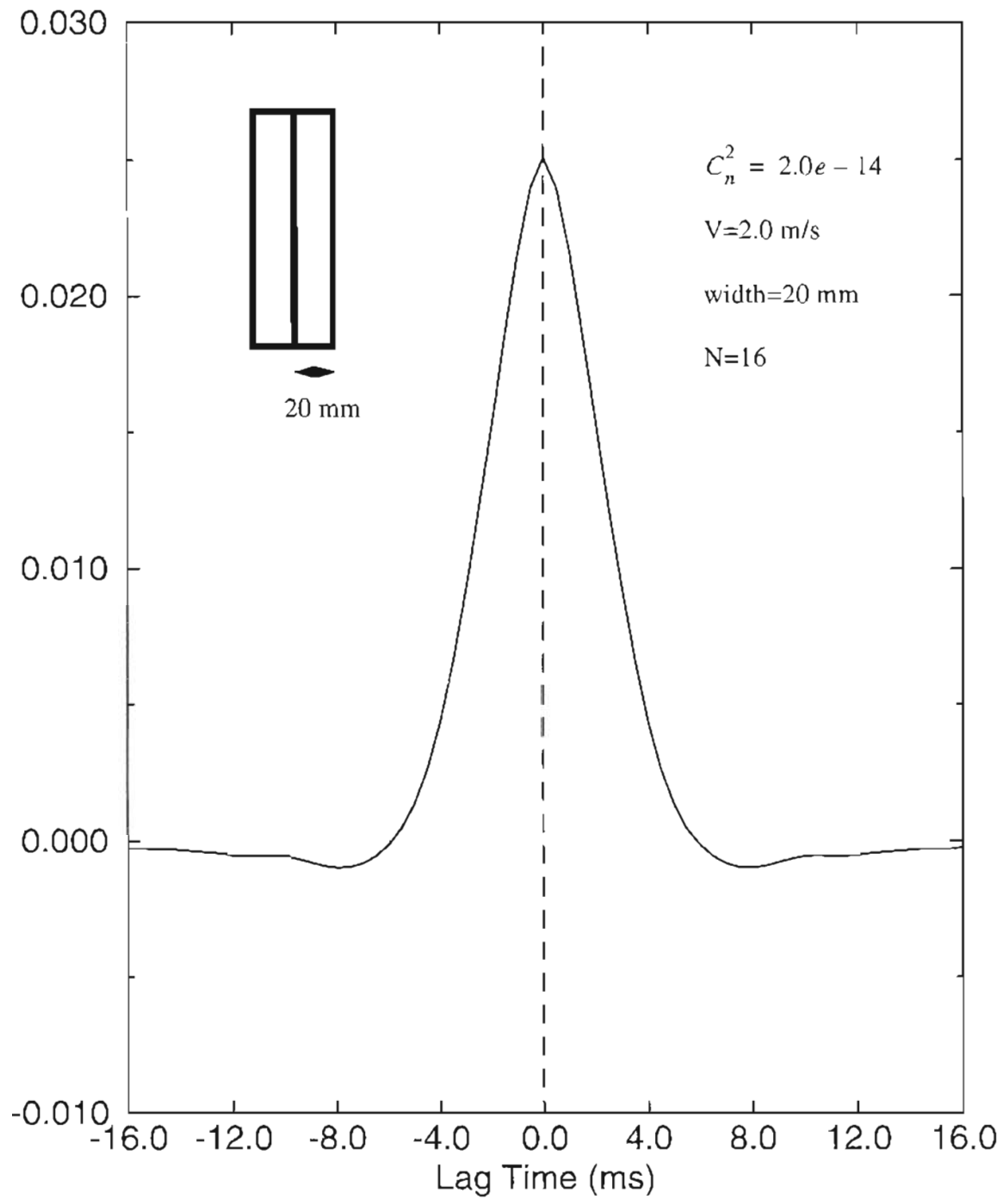


Figure 3.16 The autocovariance of rectangular shaped receiver of width of 20 mm.

Chapter 4

System Design and Experiment Setup

As was mentioned in Chapter 1, many lidar systems have been developed in the past two decades for different measurement applications. Different detection schemes and signal processing schemes have also been developed along the way as more laser sources and detector devices have been developed. Coherent doppler lidars have been widely used to measure the radial wind and recently it has also been successfully used to measure the cross wind²⁸. However, coherent lidars using heterodyne detection are usually large. In addition, modulation could be another problem of the big gas lasers such as a CO₂ laser used for coherent lidar. Because good phase overlap is essential for heterodyne detection, it is necessary to have a stable optical table and more room to make it possible. Since in some applications, the compactness and reliability are very important, it is useful to develop lidar systems using new laser sources and detection and processing schemes to meet these requirements.

Semiconductor lasers are very good candidates. They are small and reliable and with a thermal electric cooler (TEC), can run very stably over a long time period. There is a wide frequency range to be chosen for different applications. High frequency modulation can be applied directly to the driving current of the laser diode which can be used in optical communications. Power up to 100mW running CW makes it possible to measure the

signal off of aerosols without eye safety being an issue. Single mode or multi-mode optical fibers can be pig-tailed to the diode laser so that the design of the transmitter is simplified. Since direct detection is used, receiving optics can be very simple as well. Optical fibers can be used for delivering the signal to the detector. High sensitivity Photo Multiplier Tubes are the best choices for detectors because of their high gains.

Pseudo random code (PRC) modulation has been around for quiet a long time. It makes it possible to run the transmitter CW and still be capable of having range information. Some analysis is done in this chapter on the improvement of signal to noise ratio for different coding schemes. By implementing hardware for the demodulation and integration, a very low sampling rate is needed and storage space can also be saved. The specific range of interest is selected by choosing the delay time of the local PRC' which can be controlled by the PC through the A/D board.

Data processing can be done on the PC or the SUN workstation. Permanent storage may also be needed to store data for future use. It is possible to use a single DSP chip to generate the PRC code and do multi-channel signal processing. Therefore, real time wind speed can be obtained and displayed if needed. The use of DPS chips for the processing can greatly reduce the complexity of the hardware design and make the system even more compact.

As it is shown in figure (4.1), the "White Light" system includes a 8-inch telescope, a diode laser with controller and cooler, some optics for both transmitter and receiver, optical fibers, detectors, electronics, A/D board and a PC. Detailed parameters of these components are listed in table (4.1).

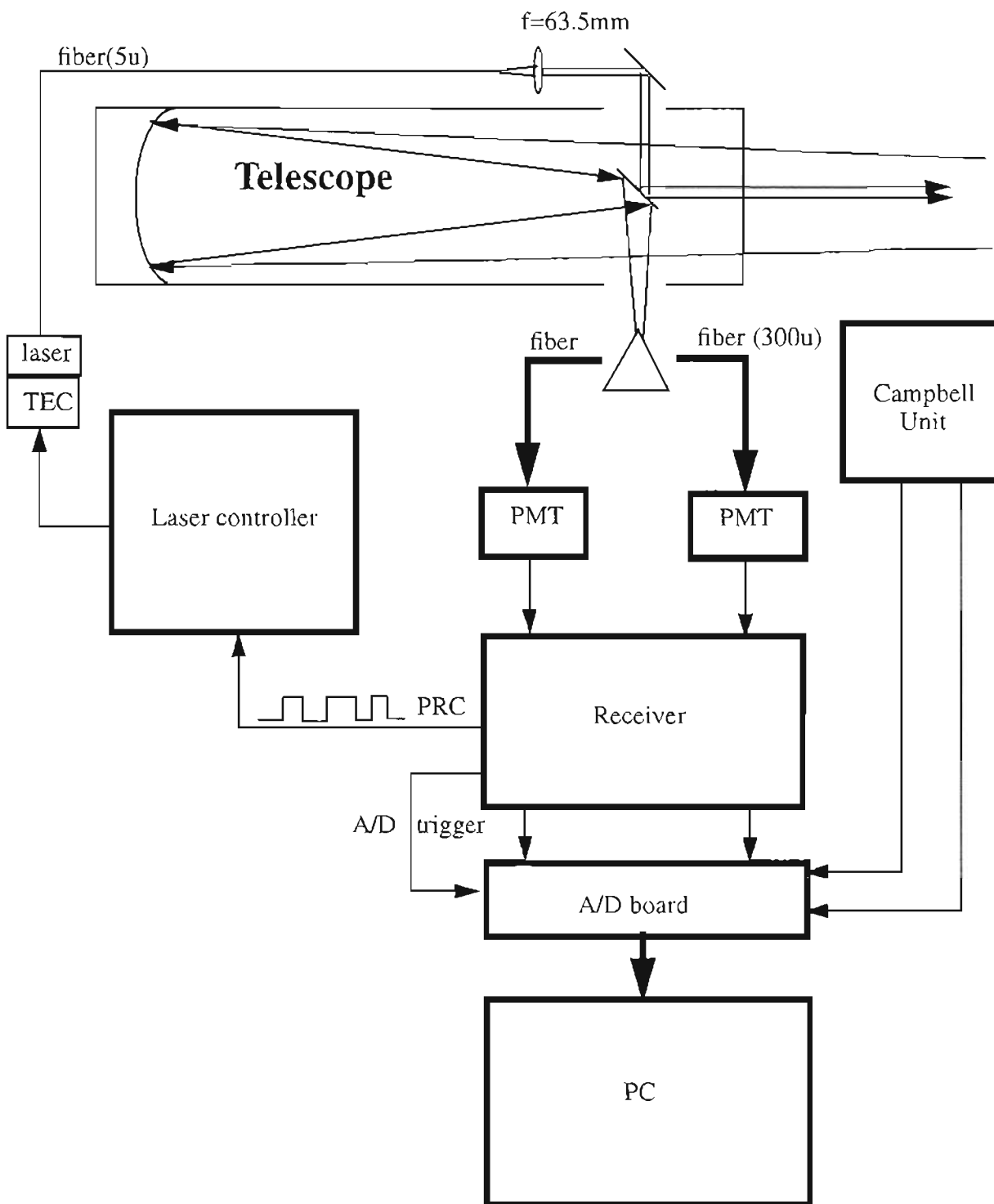


Figure 4.1 Configuration of "White Light" system.

4.1 The Optics of the “White Light” System

4.1.1 The Transmitter

A pigtailed semiconductor laser diode is used as the transmitter. It has a single transverse mode and multi longitudinal modes running around 830nm. The pigtailed fiber is a Sum single mode fiber with Numerical Aperture(NA) of 0.11. The intensity distribution is Gaussian. The waist size at the fiber end can be calculated using the V number defined as

$$V = \frac{2\pi a \sqrt{n_1^2 - n^2}}{\lambda} \quad (4.1)$$

where $a=5/2=2.5\mu m$, is the radius of the single mode fiber, and $\lambda = 830nm$ is the wavelength of the laser. Applying these numbers gives $V=2.08$.

The waist size is calculated to be⁵⁷

$$\omega_0 = \left(0.65 + 1.619V^{-3/2} + 2.879V^{-6} \right) a = 1.225a = 3.1\mu m \quad (4.2)$$

The beam divergence angle at the fiber end is

$$\theta_1 = \frac{\lambda}{\pi\omega_0} = \frac{830nm}{\pi \times 3.1\mu m} = 8.5 \times 10^{-2} rad \quad (4.3)$$

The output beam size α_0 depends on the focal length F of the output lens,

$$\alpha_0 = F \times \theta_1 \quad (4.4)$$

The output beam divergence is

$$\theta_2 = \frac{\lambda}{\pi \alpha_0} = \frac{830nm}{\pi \times 8.5 \times 10^{-2} F} \quad (4.5)$$

The beam divergence must be chosen much smaller than the field of view of the receiving telescope. Choosing $\theta_2 \leq 50 \mu rad$ is reasonable, then the focal length F becomes

$$F = \frac{830 \times 10^{-6} mm}{5 \times 10^{-5} \times \pi \times 8.5 \times 10^{-2}} = 62.2 mm \quad (4.6)$$

The output beam size is $\alpha_0 = \theta_1 \cdot F = 5.3 mm$. The lens diameter D can be calculated using 3X rule $D = 3\omega_0 = 15.9 mm$. So the standard 1 inch diameter lens can be used as transmitter lens.

4.1.2 The Receiving Telescope

An eight inch telescope is used as the receiver. With two mirrors on the diagonal at the optical axis, a coaxial system is constructed. The laser is brought up to the top of the telescope, and the fiber output end is put at the focal point of the transmitter lens. The collimated laser beam is mirrored down onto the diagonal mirror by a 45° mirror on the top of the telescope and the laser is transmitted out on the optical axis by the diagonal mirror. The backscattering optical signal is collected and focused by the 8 inch mirror, directed out and then split into two parts. Multi-mode fibers with various sizes can be put on the

telescope, at the focal point of the receiver. The receiving fibers bring the optical signal to the detector box. The telescope has three dimensional freedom so it can point to any direction without adjusting the optics on the telescope. The receiving fiber holders that sit on the stages have three dimensional freedom for the convenience of alignment. Because the transmitter laser is in the infrared, another visible laser (635nm) is put on the top of the telescope for alignment and also as a warning for human beings.

As it can be seen from Fig.4.2, the diagonal mirror will block some of the receiving area, so the effective receiver is smaller than 8 inches. But the benefit from the diagonal mirror is that it can completely block the near field backscattering to some distance depending on the field of view of the receiver. This will effectively reduce the unnecessary dynamic range of the receiver electronics.

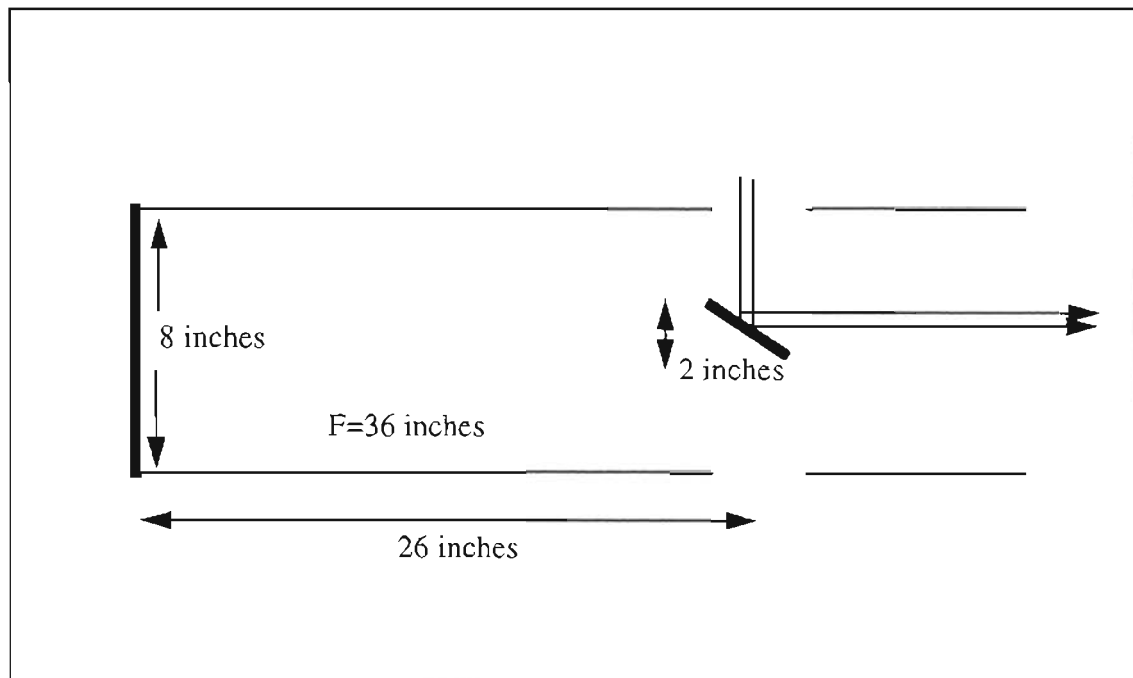


Figure 4.2 Schematic of the telescope.

Because the spider blocks some of the near field, as can be seen in Fig.4.3, the received signal is not proportional to $1/r^2$. It is important to characterize the received signal vs. range to help design the receiver electronics and explain the experiment results. As is explained in Fig.4.3, when $L < Z_b$, the signal is completely blocked; when $Z_b < L < Z_{pb}$, part of the signal will be blocked, part of the signal can get into the receiver but under the constraint of the field of view; when the distance is in the range of $Z_{pb} < L < D_1$, there is no blocking, but there is still field of view limitation; when $D_1 < L < D_2$, part of the signal is still under the field of view constraint, part of the signal will reach the receiver without the

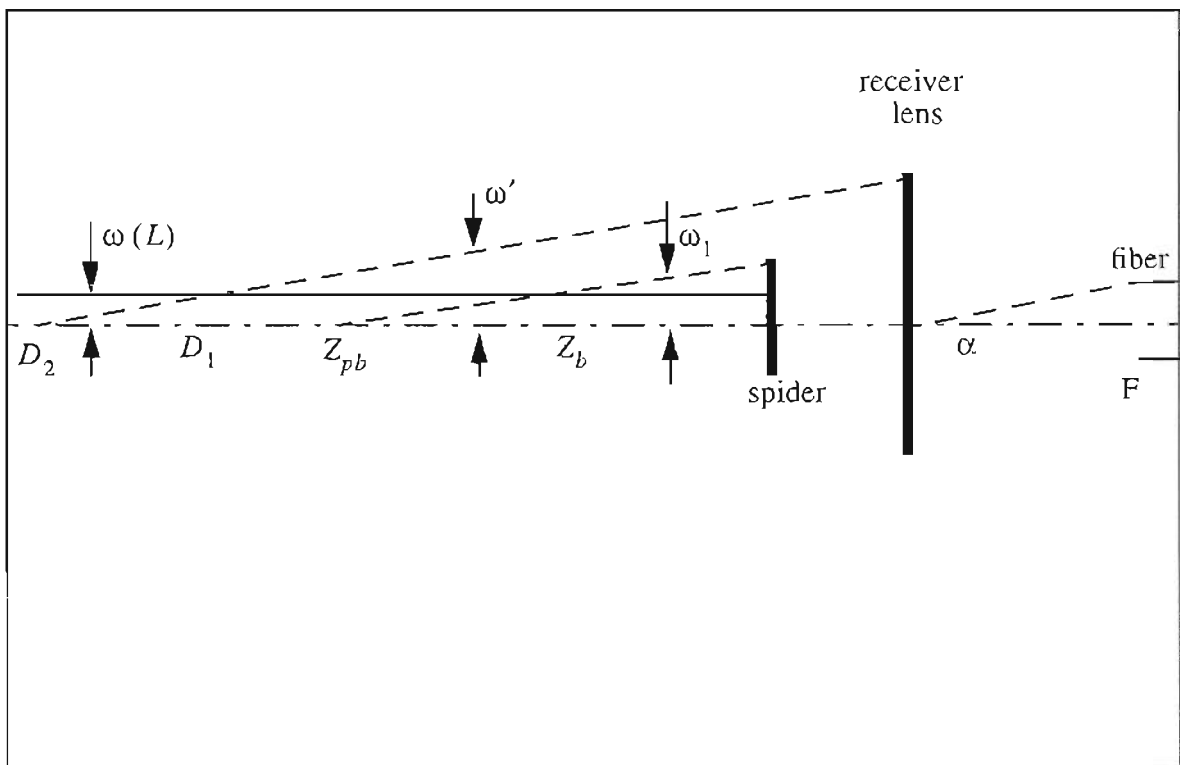


Figure 4.3 Simplified diagram of the transmitter and receiver system (not in scale).

field of view constraint; beyond D_2 , there is no field of view constraint because all the rays can reach the receiver will have the angle of arrival smaller than the FOV.

In Fig.4.3, α is the field of view defined by the size of the fiber. Usually, 100um to 1mm fiber can be used. With the picture of Fig.4.3 in mind, it is easy to estimate all these distances if the size of fiber, size and focal length of the telescope, and the beam size and divergence angle of the laser are known. The following equations will be used for the calculation:

$$(R_d - \omega(Z_b)) / Z_b = \alpha / 2$$

$$(R_l - \omega(D_1)) / D_1 = \alpha / 2$$

$$R_d / Z_{pb} = \alpha / 2$$

$$R_l / D_2 = \alpha / 2 \tag{4.7}$$

where R_l and R_d are the radius of telescope and spider respectively. For the “White Light”, if 100um fiber is used then,

$$Z_b = 201meters \quad Z_{pb} = 508meters$$

$$D_1 = 861.4meters \quad D_2 = 1828.8meters \tag{4.8}$$

With these numbers available, it is possible to calculate the received intensity from different ranges, considering that the laser beam has a Gaussian distribution.

4.1.3 Intensity vs. Range for “White Light” System

For a Gaussian beam with waist of ω , the energy in the circle of radius, a , is

$$P(a) = P_t \left(1 - \exp\left(-2a^2/\omega^2\right) \right) \quad (4.9)$$

where P_t is transmitted power, so

$$dP(a) = P_t \frac{4a}{\omega^2} \exp\left(-2\frac{a^2}{\omega^2}\right) da \quad (4.10)$$

In the range $L < Z_b$, the received power from that range is zero, $P(L) = 0$.

In the range $Z_b < L < Z_{pb}$, the received power from a small range of ΔL at distance L is

$$\begin{aligned} P(L) &= \int_{\omega_1}^{\omega} dP(a) \beta \Delta L \frac{\pi}{L^2} \left(\left(L \frac{\alpha}{2} + a \right)^2 - R_d^2 \right) \\ &= P_t \beta \Delta L \pi \int_{\omega_1}^{\omega} 4 \frac{a}{\omega^2} \exp\left(-2\frac{a^2}{\omega^2}\right) \frac{1}{L^2} \left(\left(L \frac{\alpha}{2} + a \right)^2 - R_d^2 \right) da \\ &= C \int_{\omega_1}^{\omega} \left(\frac{\alpha}{2} \right)^2 \frac{4a}{\omega^2} \exp\left(-\frac{2a^2}{\omega^2}\right) da + C \int_{\omega_1}^{\omega} \alpha \frac{4a^2}{L} \frac{1}{\omega^2} \exp\left(-\frac{2a^2}{\omega^2}\right) da \\ &\quad + C \int_{\omega_1}^{\omega} \frac{4a^3}{\omega^2} \frac{1}{L^2} \exp\left(-\frac{2a^2}{\omega^2}\right) da - C \int_{\omega_1}^{\omega} \frac{4a R_d^2}{\omega^2 L^2} \exp\left(-\frac{2a^2}{\omega^2}\right) da \end{aligned} \quad (4.11)$$

where $C = P_t \times \beta \times \Delta L \times \pi$, and β is the backscattering coefficient of the aerosols.

Completing the integration, then

$$\begin{aligned}
\frac{P(L)}{C} &= \left(\frac{\alpha}{2}\right)^2 \left(\exp\left(\left(-\frac{2\omega_1^2}{\omega^2}\right) - \exp(-2)\right) \right) + \frac{\alpha}{2} \left(\omega_1 \exp\left(-\frac{2\omega_1^2}{\omega^2}\right) - \omega \exp(-2) \right) \\
&+ \omega \frac{\alpha}{L} \left(\frac{\pi}{2} \left(\exp\left(-\frac{2\omega_1^2}{\omega^2}\right) - \exp(-2) \right) \right)^{1/2} + \frac{(\omega_1^2 + \omega^2/2)}{L^2} \exp\left(-2\frac{\omega_1^2}{\omega}\right) \\
&- \frac{3\omega^2}{2L^2} \exp(-2) - \frac{R_d}{L^2} \left(\exp\left(-2\frac{\omega_1^2}{\omega^2}\right) - \exp(-2) \right)
\end{aligned} \tag{4.12}$$

In the range of $Z_{pb} < L < D_1$, P(L) is

$$\begin{aligned}
\frac{P(L)}{C} &= \int_0^{\omega} \frac{4a}{\omega^2} \exp\left(-\frac{2a^2}{\omega^2}\right) \frac{1}{L^2} \left(\left(L\frac{\alpha}{2} + a \right)^2 - R_d^2 \right) da \\
&= \left(\frac{\alpha}{2}\right)^2 (1 - \exp(-2)) - \frac{\alpha}{L} \omega \exp(-2) + \frac{\alpha}{L} \omega \left(\frac{\pi}{2} (1 - \exp(-2)) \right)^{1/2} \\
&+ \frac{\omega}{2L^2} - \frac{3}{2L^2} \omega^2 \exp(-2) - R_d (1 - \exp(-2))
\end{aligned} \tag{4.13}$$

In the range of $D_1 < L < D_2$, P(L) can be written as

$$\frac{P(L)}{C} = \int_0^{\omega'} \frac{4a}{\omega^2} \exp\left(-\frac{2a^2}{\omega^2}\right) \frac{1}{L^2} \left(\left(L\frac{\alpha}{2} + a \right)^2 - R_d^2 \right) da + \int_{\omega'}^{\omega} \frac{4a^2}{\omega} \frac{1}{L} (R_l^2 - R_d^2) \exp\left(-\frac{2a^2}{\omega^2}\right) da$$

$$\begin{aligned}
&= \left(\frac{\alpha}{2}\right)^2 \left(1 - \exp\left(-\frac{2\omega'^2}{\omega^2}\right)\right) - \frac{\alpha}{L} \omega' \exp\left(-\frac{2\omega'^2}{\omega^2}\right) + \frac{\alpha\omega}{L} \left(\frac{\pi}{2} \left(1 - \exp\left(-\frac{\omega'^2}{\omega^2}\right)\right)\right)^{1/2} \\
&\quad - \frac{1}{L^2} \omega'^2 \exp\left(-\frac{2\omega'^2}{\omega^2}\right) + \frac{\omega^2}{2L^2} \left(1 - \exp\left(-\frac{2\omega'^2}{\omega^2}\right)\right) - \frac{R_d}{L^2} \left(1 - \exp\left(-\frac{2\omega'^2}{\omega^2}\right)\right) \\
&\quad + \frac{(R_l^2 + R_d^2)}{L^2} \left(\exp\left(-\frac{2\omega'^2}{\omega^2}\right) - \exp(-2)\right) \tag{4.14}
\end{aligned}$$

Beyond D_2 , $1/r^2$ begins to take over. The intensity is

$$\begin{aligned}
P(L) &= \int_0^{\omega} dP(a) \beta \Delta L \frac{\pi}{L^2} (R_l^2 + R_d^2) \\
\frac{P(L)}{C} &= \frac{(R_l^2 + R_d^2)}{L^2} (1 - \exp(-2)) \tag{4.15}
\end{aligned}$$

The intensity vs. range is calculated and plotted in figure (4.4) for the receiving fiber of 100 μ m. The curve of $1/r^2$ is also plotted for comparison. The received intensity is normalized by C which is $P_l \beta \pi \Delta L$. As it can be seen, the contribution from different range starts at zero, then stays nearly constant for about 300 m then drops off as $1/r^2$. The dynamic range is greatly reduced, so it is possible to design a receiver with higher sensitivity for very weak signals from further distances.

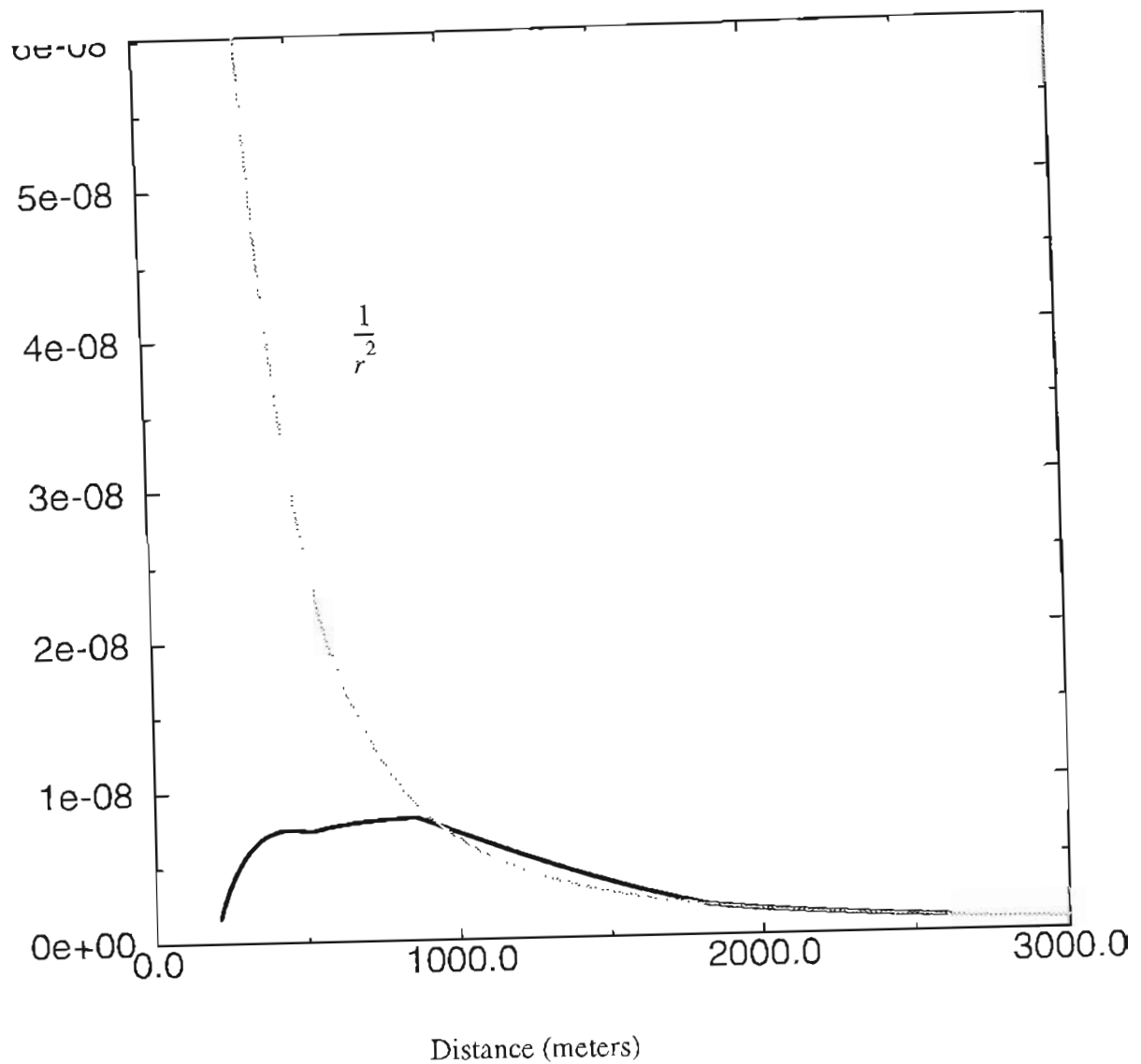


Figure 4.4 Theoretical intensity profile for a coaxial system.

To recover the signal from different ranges, pseudo random code (PRC) modulation is used. The multiplication of the delayed bipolar pseudo random code (PRC') is equivalent to the convolution of signal from different ranges and correlation of PRC and PRC'. So the *actual signal vs. range for the "White Light" is*

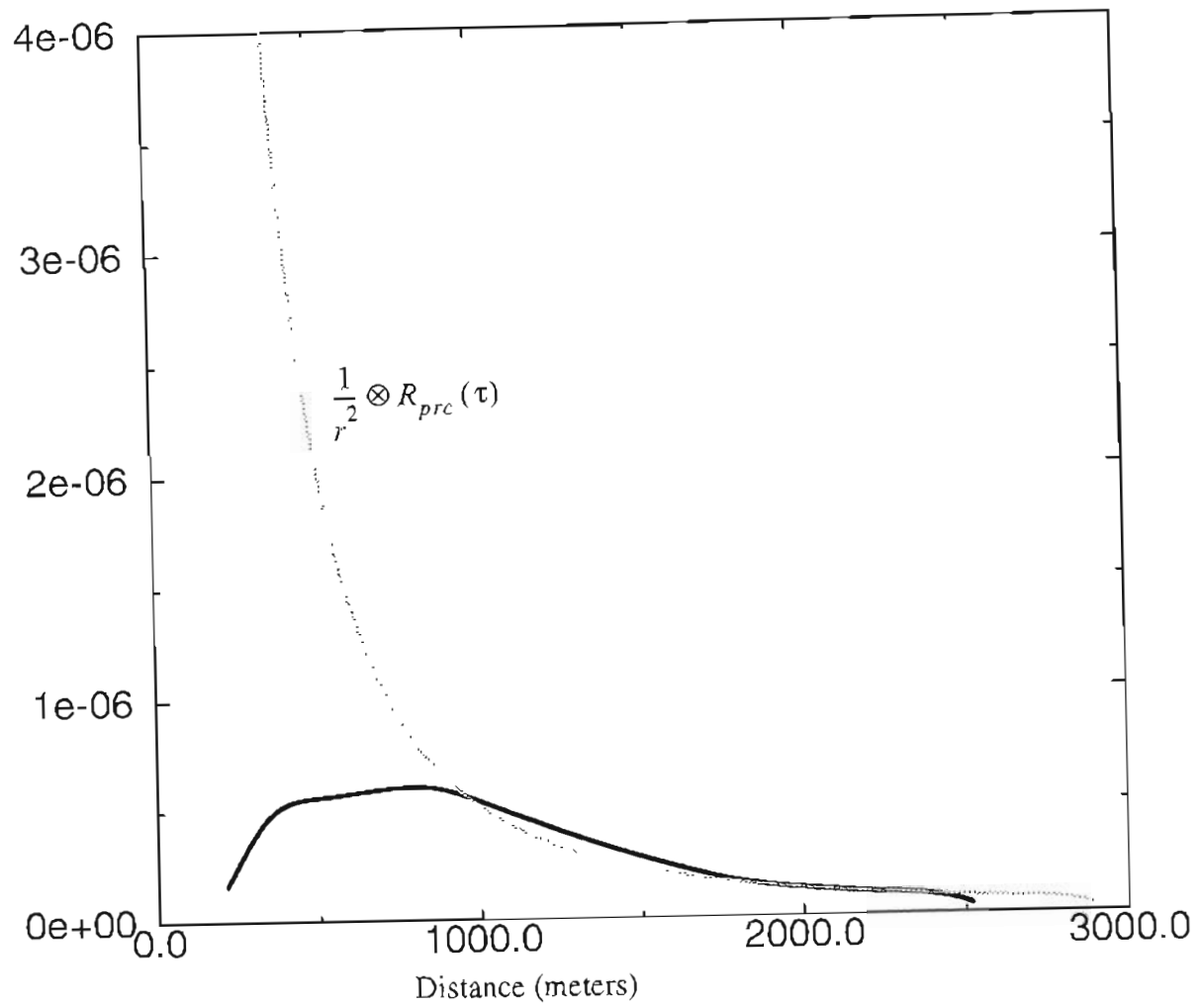


Figure 4.5 Received signal profile for “White Light” system.

$$P_r(L) = P(L) \otimes R_{prc}(\tau) \quad (4.16)$$

As it will be seen in the following sections, the correlation function of PRC and PRC' is a symmetrical triangle with a basic pulse width of, $1\mu s$ for “white Light” system which corresponds to a range bin of 150 meters at each sides. The final result is plotted in figure (4.5).

avoided. Their results showed that the DC part of the background is removed and they also claimed that new sequences also improve the signal to noise ratio.

Simulations have been performed to generate different sequences and to simulate the modulation and processing schemes. Range resolved signals are recovered from the background noise and signal shot noise. In these simulations, it is assumed that shot noise dominates the received signal which is true in almost all lidar systems. Different signal to noise ratios are assumed to compare these three different sequences. The results are also compared with the results of reference. Some consistencies are found, but the big advantage of the A1 and A2-sequences over the M-sequence they claimed, great improvement of SNR over accumulation time, is not observed.

Signal to noise ratio for different atmospheric conditions and different back-scattering sources are calculated to help the design of the receiver electronics and to determine the possibility of measuring backscattering signal from aerosols. Numbers of samples needed are also estimated from the signal to noise calculation.

4.2.1 Coding Schemes

To construct a pseudo-random sequence of length $n = 2^m - 1$ (M-sequence), one needs a primitive polynomial, $h(x)$, of degree m .⁵⁸ As an example of degree $m=4$, $h(x)$ is

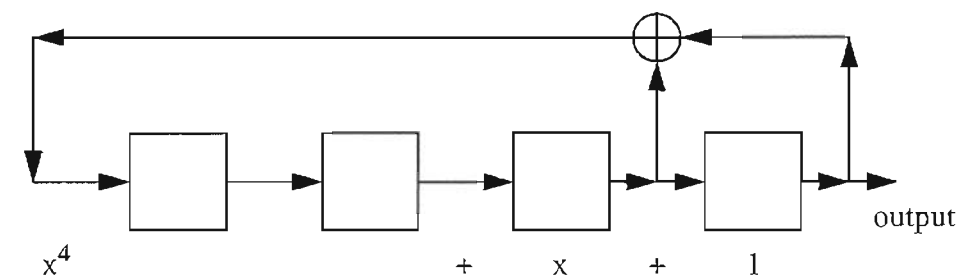
$$h(x) = x^4 + x + 1 \quad (4.17)$$

This polynomial specifies a feed back shift register as in Fig.4.6. The symbol \oplus repre-

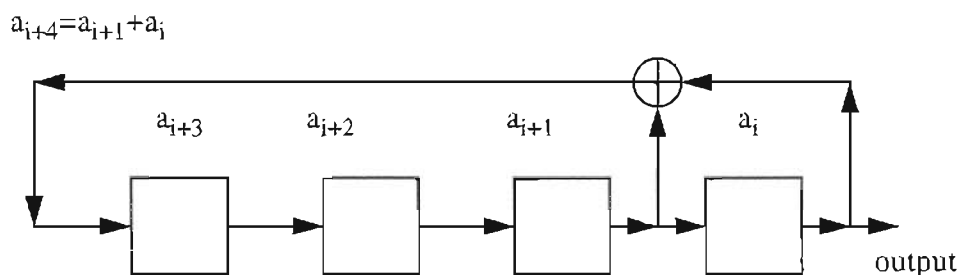
sents a mod-2 adder or exclusive-or gate, defined by $0+0=1+1=0$, $0+1=1+0=1$.

Each of the little boxes in Fig.4.6 represents a memory element or flip-flop, containing a 0 or 1. Using shift registers and delay elements we can generate M-sequence of length up to $2^{40} - 1$ using a polynomial $h(x)$ given in reference 58.

The sequence, a_i , which represent (0,1) code is used to modulate the laser, $a_i' = 2a_i - 1$, represent (-1,1) code which is to take phase-shift cross-correlation with the detected signal. The delayed code, a_i' , and the multiplication and integration can be done



(a). Feedback shift register corresponding to x^4+x+1 .



(b). The shift register specifies a recurrence relation.

Figure 4.6 Schematic of pseudo-random code generator.

by hardware or by computer, in order to recover the signal from different ranges (lidar profile). The advantages of doing the integrated detection by hardware are that the signal to noise ratio is greatly increased by integration, the sampling rate is greatly decreased, so high speed A/D is not needed and, since the # of data samples is decreased, large computer memory is not needed for signal processing

As mentioned earlier, the M-sequence has the property that the number of ones in a sequence always exceeds the number of zeros by one. To remove this extra one, new sequences are proposed for RM-CW lidar. These new sequences (A1 and A2-sequence) are based on the M-sequence in the way that the A1-sequence has sequence length of $2N$, the A2-sequence has period length of $4N$, where N represents the period length of the M-sequence. The A1-sequence is

$$a_{1i}' = (-1)^i a_i' \quad i = 0, 1, \dots, 2N - 1. \quad (4.18)$$

Similarly, the A2-sequence is given by

$$a_{2i}' = \begin{cases} a_i' & i = 4m, 4m + 1 \\ -a_i' & i = 4m + 2, 4m + 3 \end{cases} \quad m = 0, 1, \dots, N - 1. \quad (4.19)$$

Signal recovering can be seen explicitly from the cross-correlation of (0,1) codes and (-1,1) codes. For the M-sequence

$$R_{aa'}(k) = \begin{cases} (N+1)/2N & k = 0 \\ 0 & k \neq 0 \end{cases}, \quad (4.20)$$

For the A1-sequence

$$R_{a_1 a_1'}(k) = \begin{cases} 1/2 & k = 0 \\ 1/2N & k = 2n-1 \\ -1/2N & k = 2n \\ -1/2 & k = N \end{cases} \quad n = 1, 2, \dots, (N-1)/2, \quad (4.21)$$

and for the A2-sequence

$$R_{a_2 a_2'}(k) = \begin{cases} 1/2 & k = 0 \\ 1/2N & k = 4n-2 \\ 0 & k = 2n-1 \\ -1/2N & k = 4n \\ -1/2 & k = 2N \end{cases} \quad n = 1, 2, \dots, (N-1)/2. \quad (4.22)$$

These three cross-correlation functions are plotted in figure (4.7).

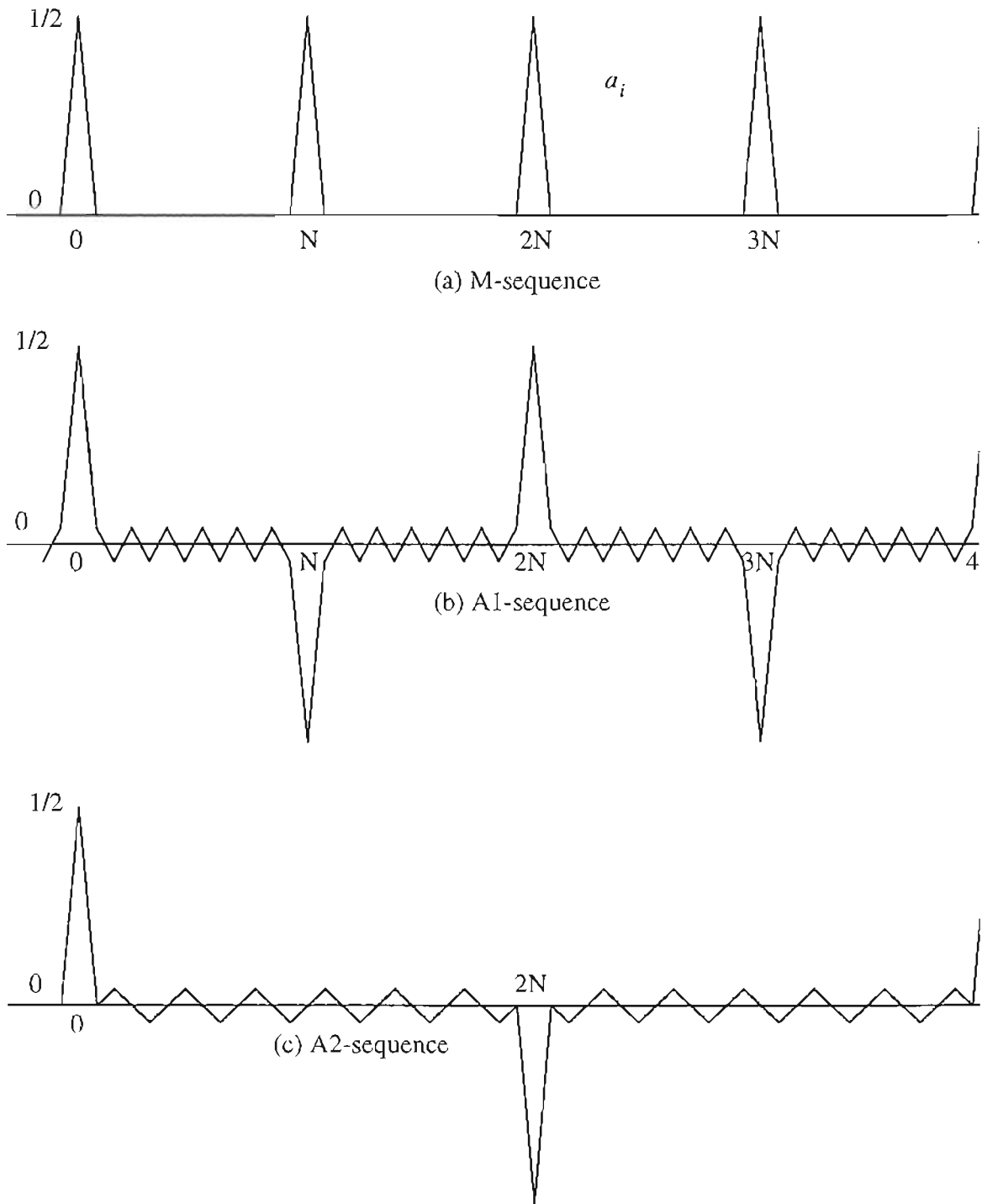


Figure 4.7 Simulated results of cross-correlation functions of a_i and a'_i .

4.2.2 Signal to Noise Ratio and Simulation Results

The backscattering optical signal at the receiver is the summation of the contributions of aerosol scattering all over the path, plus the background noise,

$$S_i(t) = \int_0^{\infty} P_0 a\left(t - \frac{2R}{C}\right) G(R) A(R) P_f(R, t) dR + n(t), \quad (4.23)$$

where P_0 is the output laser power, R is the distance to the scattering particles, a is the modulation code, C is the speed of light, $G(R)$ is the geometric factor which is defined by the optical system, $A(R)$ is atmospheric attenuation factor which is defined by

$$A(R) = \exp\left[\int_0^R \alpha(r) dr\right].$$

For the short distance we are interested and simplicity, we

assume $\alpha = 0$ which gives $A(R) = 1$ which yields no attenuation in the path.

$P_f(R, t)$ is the aerosol distribution profile in which we are interested, n is the background radiation that the telescope receives.

The gain of the system is omitted here without losing consistency. In deriving the following equations, single aerosol scattering is assumed. In case of heavy background light and weak signals, the background shot noise dominates, therefore the electronic noise and signal shot noise can be neglected.

Correlation detection is used to recover the signal related to the profile,

$$S_o(t_j) = \int_{t_{j-1}}^{t_j} S_i(t) a'(t-t') dt, \quad (4.24)$$

where $a'(t-t')$ is the delayed version of the M-sequence converted to a bipolar (-1,1) code.

Use Eq.(4.23), Eq.(4.24) becomes

$$S_o(t_j) = \int_0^{\infty} P_0 G(R) dR \int_{t_{j-1}}^{t_j} P_f(R, t) a\left(t - \frac{2R}{C}\right) a'(t-t') dt + \int_{t_{j-1}}^{t_j} n a'(t-t') dt \quad (4.25)$$

The integration time $\Delta t = t_j - t_{j-1}$ is the period of the pseudo random code which is on the order of milliseconds. During this time $p_f(R, t)$ is assumed constant. Eq. (4.25) becomes.

$$\begin{aligned} S_o(t_j) &= P_0 \int_0^{\infty} G(R) P_f(R, t) \int_{t_{j-1}}^{t_j} a\left(t - \frac{2R}{C}\right) a'(t-t') dt + \int_{t_{j-1}}^{t_j} n a'(t-t') dt \\ &= MTP_0 \int_0^{\infty} G(R) P_f(R, t) R_{aa'}\left(t' - \frac{2R}{C}\right) dR + \int_{t_{j-1}}^{t_j} n a'(t-t') dt \end{aligned} \quad (4.26)$$

where MT is the code length, $R_{aa'}(\tau)$ is the cross correlation between the modulation code and delayed (-1,1) code discussed in the previous section. $R_{aa'}(\tau)$ is triangle like and periodic with the period of the pseudo random code. It is obvious to see that the range

resolved signal (profile) is recovered by choosing $t' = 2R/C$. Notice that the limit of the integral of the signal term goes to infinity, but the ambiguity of range resolution induced by periodic property of $R_{aa'}$ is very well taken care of by geometric factor $G(R)$ which decreases very fast when R gets large. The detecting range is defined by the code length for the M-sequence

The signal power expressions for M, A1 and A2-sequences are

$$S = \left(NTP_o \int_0^{\infty} G(R) P_f(R, t) R_{aa'} \left(t' - \frac{2R}{C} \right) dR \right)^2, \quad (4.27)$$

$$S_1 = \left(2NTP_o \int_0^{\infty} G(R) P_f(R, t) R_{a_1a_1'} \left(t' - \frac{2R}{C} \right) dR \right)^2, \quad (4.28)$$

$$S_2 = \left(4NTP_o \int_0^{\infty} G(R) P_f(R, t) R_{a_2a_2'} \left(t' - \frac{2R}{C} \right) dR \right)^2 \quad (4.29)$$

Since it is assumed that the background shot noise dominates, the mean value and variance of the background shot noise at the output of the receiver can be described using Campbell's theorem,⁵⁹

$$\eta = \langle N \rangle = \lambda \int_{-\infty}^{\infty} h(t) dt, \quad \sigma^2 = \lambda \int_{-\infty}^{\infty} h(t)^2 dt \quad (4.30)$$

where λ is the mean value of the background shot noise, $h(t)$ is the system impulse response function. In our case it is easy to see that $h(t)$ can be expressed as

$$h(t) = \begin{cases} a'(MT-t) & 0 < t < MT \\ 0 & \text{otherwise} \end{cases} \quad (4.31)$$

For the three different modulation codes, the mean values and variances are

$$\eta = \lambda \int_{-\infty}^{\infty} a'(MT-t) dt = T\lambda \quad (4.32)$$

$$\sigma^2 = \lambda \int_{-\infty}^{\infty} a'(MT-t)^2 dt = NT\lambda \quad (4.33)$$

$$\eta_1 = \lambda \int_{-\infty}^{\infty} a_1'(MT-t) dt = 0 \quad (4.34)$$

$$\sigma_1^2 = \lambda \int_{-\infty}^{\infty} a_1'(MT-t) dt = 2NT\lambda \quad (4.35)$$

$$\eta_2 = \lambda \int_{-\infty}^{\infty} a_2'(MT-t) dt = 0 \quad (4.36)$$

$$\sigma_2^2 = \lambda \int_{-\infty}^{\infty} a_2'(MT-t)^2 dt = 4NT\lambda \quad (4.37)$$

The signal to noise ratios are:

$$\frac{S}{\sigma^2} = \frac{NTP_0^2}{\lambda} \left(\int_0^{\infty} G(R) P_f(R, t) R_{aa'} \left(t' - \frac{2R}{C} \right) dR \right)^2 \quad (4.38)$$

$$\frac{S_1}{\sigma_1^2} = \frac{2NTP_0^2}{\lambda} \left(\int_0^{\infty} G(R) P_f(R, t) R_{a_1a_1'} \left(t' - \frac{2R}{C} \right) dR \right)^2 \quad (4.39)$$

$$\frac{S_2}{\sigma_2^2} = \frac{4NTP_0^2}{\lambda} \left(\int_0^{\infty} G(R) P_f(R, t) R_{a_2a_2'} \left(t' - \frac{2R}{C} \right) dR \right)^2 \quad (4.40)$$

From the cross correlation functions in Fig.4.7, it is easy to see that $R_{a_1a_1'}$ and $R_{a_2a_2'}$ are not exactly triangle, there are ripples evenly distributed along x axis (time lag). Because of the nonuniform distribution of the geometric function and aerosol profile, these ripples don't cancel out when integrations are performed. Cross talk between different ranges occurs and will give substantial noise when the code length is short. This can be seen from the simulation results in Fig.(4.8). For moderate or long code length and severe background noise the values inside the brackets of Eq.(4.38)-Eq(4.40) are almost the same. Therefore, a factor of 2 increase of signal to noise ratio is seen for the A1-sequence over the M-sequence and A2 over the A1-sequence. This SNR improvement

makes sense because a factor of 2 of code length is introduced to get new sequences from M-sequence.

The factor of code length increase results in a factor of sampling rate decrease. Therefore, the number of samples decrease by the same factor for a given data collection time. This factor will cancel out with the increase factor of SNR the new sequences introduced. When we average over samples collected within the same time frame, eventually the same (or close if cross talk is considered) SNR's for the recovered profiles would be expected and this is verified by the simulation results.

Simulations are conducted using the technique introduced in the previous section to generate the coding sequences with different lengths. Cross correlations between modulation (0,1) code and demodulation (-1,1) code are calculated and found to be consistent with the theory derived. The Nag library random number generator subroutines are used to simulate a Poisson distributed signal and white background noise. The signal from a target is simulated by delaying the modulation code to the equivalent distance, and then multiplied by poisson numbers with an appropriate mean value. Signals from different targets are simulated and added up to examine the ability of recovering the signals from different ranges. The geometric factor is set to be constant for simplicity. In the following results, each range is an average over 200 samples for the M-sequence, 100 samples for the A1-sequence, 50 samples for the A2-sequence, so that the total accumulation times are the same. The same input signal to noise ratio is chosen for three different modulations.

In Fig.4.8, range resolved profiles are recovered for three different coding schemes. No background noise is included, only the signal shot noise is considered here. As can be

seen from figure (4.8), scattering objects with different scattering coefficients from different ranges are recovered, but for the A1 and A2 sequences, cross talk between different ranges is introduced. There is no cross talk when the M-sequence is used.

Fig.4.9 shows that when severe background noise is present, the three modulation schemes have almost the same signal to noise ratio; no improvement of the A1 or A2-sequence over the M-sequence is observed. A carefully chosen signal level indicates that when the signal is just above the threshold of background noise, the immunity to the cross talk of M-sequence modulation gives a better result. At the same time, there is a DC offset due to background noise as we predicted. This is one of the disadvantage of the M-sequence which must be considered when designing receiver electronics.

the A1 and A2- sequences are generated based on the M-sequence and they are used in RM-CW lidar applications to improve the SNR when severe background noise is presented. Theoretic analysis shows that the same signal to noise ratio is expected when the same accumulation time is used for all three sequences. The improvement of SNR of the A1 and A2-sequence over the M-sequence as claimed in reference 3 has not been observed in these simulations. There could be a confusion in the analysis when the same number of samples or same accumulation times are used.

It should also be aware that even though the A1 and A2-sequence are two and four times longer than the M-sequence, the detection distance does not increase for the A1-sequence and increase by a factor of 2 for the A2-sequence over the M-sequence. This property can be seen from the cross correlations in Fig.4.7.

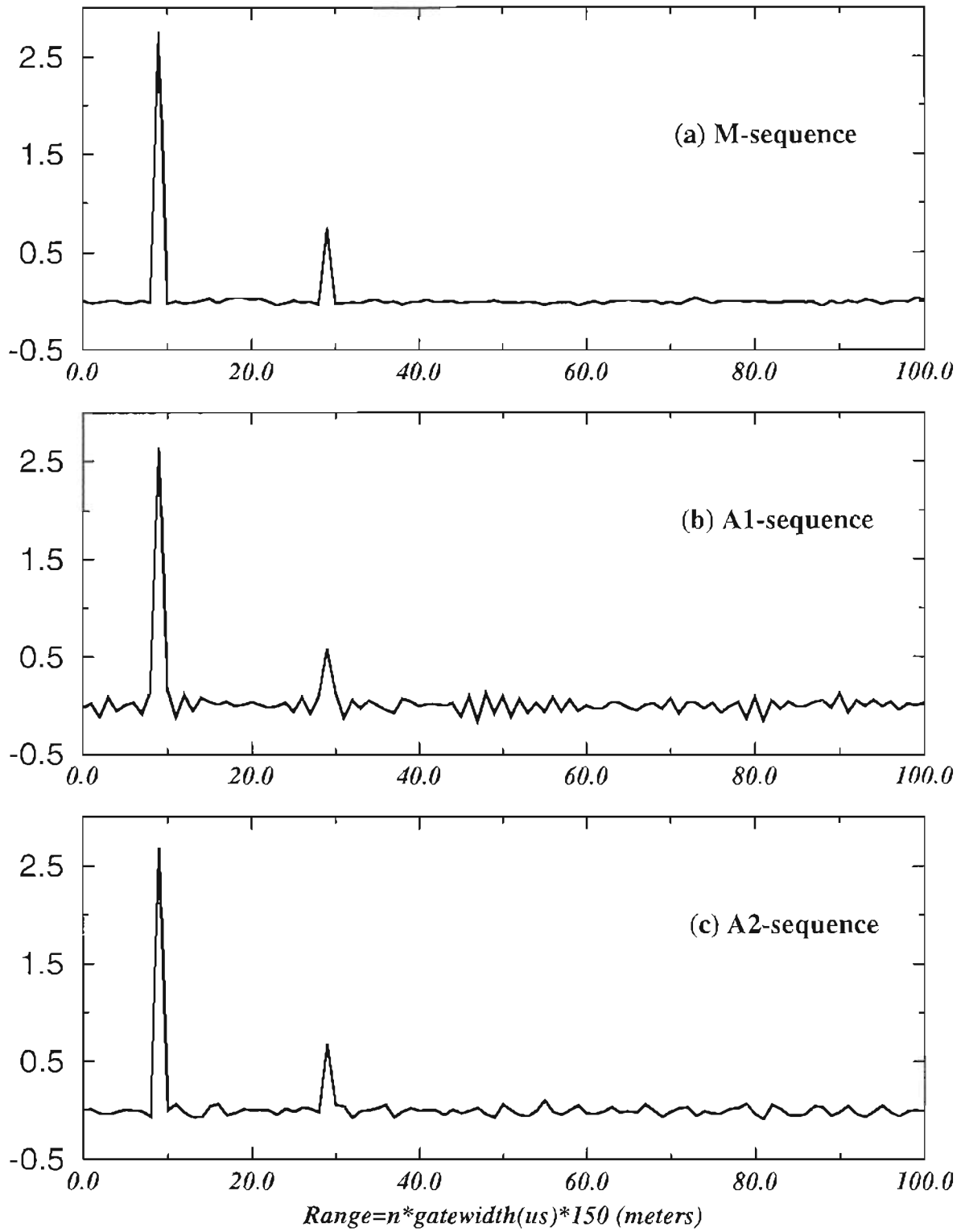


Figure 4.8 Recovered signal for different modulation codes, no background noise.

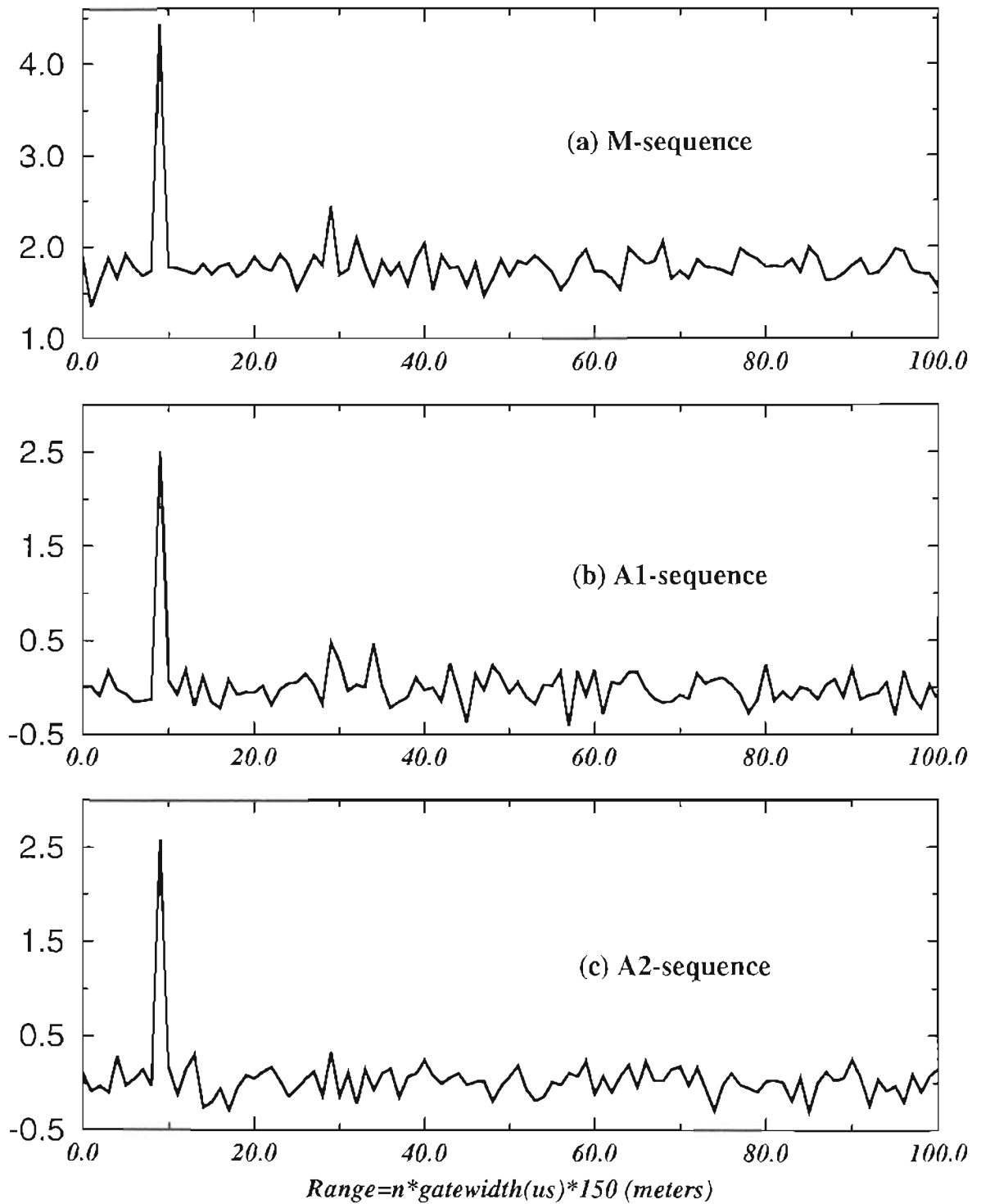


Figure 4.9 Recovered signal for different modulation codes. severe background noise is presented.

4.3 Signal to Noise Ratio for the “White Light” System

It is very difficult to calculate the signal to noise ratio of a lidar system exactly because the atmospheric parameters change for different seasons and different times during the day. Other environmental conditions, such as room light, street light, moon and stars also have random contributions to the noise power. But it is very important to estimate the signal and noise level under some reasonable assumptions, so it will guide the design of receiver electronics and appropriate use of the signal sampling and data processing schemes. For direct detection during the day, the detector noise and electronic noise is negligible. The main contribution is the signal and background shot noise. The shot noise is introduced by the quantum property of photons, and it obeys Poisson distribution statistics.

Signal to noise ratios are estimated for the “White Light” system with hard targets and aerosols and for day times and nights respectively. The transmitted power, target reflection coefficient, aerosol backscattering coefficient and detecting distance are carefully chosen to be close to the real situation. The integrator approach is used. The received power due to the background can be written as⁶⁰

$$P_b = \frac{\pi}{16} R_b \cdot T_r (FOV \cdot D_r)^2 BW_0 \quad (4.41)$$

where $R_b = 300m$ is the range bin size, $T_r = 0.25$ is the hard target reflection coefficient, $FOV = 100 \times 10^{-6}$ is the field of view of the receiver, $D_r = 0.203m$ is the diame-

ter of the receiving telescope, and $BW_0 = 10nm$ is the bandwidth of the optical filter.

The received power becomes

$$P_{bh} = \frac{300\pi}{2 \times 16} (0.25) \left(100 \times 10^{-6} \times 0.203 \right)^2 \times 10^{-8} = 3.03 \times 10^{-11} W \quad (4.42)$$

during the day and with a hard target. A factor of 2 is added because the receiving telescope is divided into two channels. For aerosols, T_r can be written as

$$T_{ra} = \pi\beta \cdot R_b' = \pi \times 5 \times 10^{-8} \times 3.6 \times 10^5 = 5.65 \times 10^{-2} \quad (4.43)$$

where β is the aerosol back-scattering coefficient. Then the noise power from aerosols is

$$P_{ba} = 6.85 \times 10^{-12} W \quad (4.44)$$

Received laser power can be calculated using a similar equation. For a hard target

$$P_{rh} = \frac{P_r T_r}{2 \times 4} \times \left(\frac{D_r}{R} \right)^2 = \frac{0.1 \times 0.25}{2 \times 4} \left(\frac{0.203}{1000} \right)^2 = 1.288 \times 10^{-10} W \quad (4.45)$$

where R is the distance to the target, a distance of 1000 meters is chosen for this calculation. The received power form aerosols is

$$P_{ra} = \frac{P_r \cdot \beta \cdot A \cdot R_b}{R^2} = 4.86 \times 10^{-14} W \quad (4.46)$$

where A is the area of receiver.

The optical signal is converted to an electrical signal by the photo-multiplier tubes (PMT), multiplied by delayed PRC, and integrated for a code length of 511us to recover the signal from a specific range bin. The signal is sampled at the output of the integrators. The signal to noise ratio can be written as

$$\frac{S}{N} = \frac{\rho P_r^2 \left(\frac{m+1}{2}\right)^2 T}{em \left(P_r \left(\left(\frac{m+1}{2}\right) \cdot \frac{1}{m} + P_b \right) \right)} \quad (4.47)$$

where $\rho = 0.07$ is the quantum efficiency of the detector, e is charge of an electron, m is the code length, T is the pulse width of the code, which is 1us. For a hard target,

$$\frac{S}{N} = \frac{0.07 \times \left(1.228 \times 10^{-10} \right)^2 (512)^2 \times 10^{-6}}{1.6 \times 10^{-19} \times 2048 \times \left(1.228 \times 10^{-10} \times \frac{512}{1023} + 3.03 \times 10^{-11} \right)} = 9209 \quad (4.48)$$

which is more than adequate. In order not to saturate the receiver, the gain of the PMT can be turned lower for hard target operation. For aerosols,

$$\frac{S}{N} = \frac{0.07 \times \left(4.86 \times 10^{-14}\right)^2 \times (512)^2 \times 10^{-6}}{1.6 \times 10^{-19} \times 2048 \times \left(4.48 \times 10^{-14} \times \frac{512}{1023} + 6.85 \times 10^{-12}\right)} = 1.9 \times 10^{-2} \quad (4.49)$$

Cross-correlation is performed to the samples from both channels to get the wind speed.

Because the weak signal from aerosols, more samples are needed to get a good correlation function. The signal to noise ratio at the output of the auto-correlation can be written as

$$\left. \frac{S}{N} \right|_{cor} = \frac{n}{n_a} \quad (4.50)$$

where n_a is related to the signal to noise ratio at the input of the correlator given as

$$n_a = 2\frac{N}{S} + \left(\frac{N}{S}\right)^2 \quad (4.51)$$

The signal to noise ratio for hard target is high enough to get good correlation with a reasonable amount of samples. If it measures aerosols during the day,

$$n_a = 2\left(\frac{1}{1.9 \times 10^{-2}}\right) + \left(\frac{1}{1.9 \times 10^{-2}}\right)^2 = 2875.3 \quad (4.52)$$

The number of samples needed if an output S/N of 50 is expected is

$$n = 2875.3 \times 50 = 143,750 \quad (4.53)$$

which is equivalent to 143 seconds. The same procedure can be applied to aerosols at night. It takes too many samples for aerosols during the day, and also means a long sampling time and a big storage device and a very long processing time. To reduce these numbers, some other processing scheme could be used. The Fast Fourier Transform (FFT) is one approach which will work better than the correlation approach.

4.4 Electronics

Following the guidelines of the previous sections, the electronics can be designed and built. It includes digital and analog parts. On the digital board, a 10MHz crystal oscillator is used, a 1MHz clock is generated by dividing the crystal output by 10. A pseudo random code is generated and delivered to diode laser controller using a 1 MHz clock. The PRC code repeats every 511us, so a 9-bit counter is used to produce a sync signal. Other outputs from the counter are also used for producing control logic for the integrator and A/D trigger. A local delayed version of the PRC is generated using shift registers and different clocks (1Mhz and 5Mhz). The 5Mhz clock is the intermediate output of the divide-by-10 function. With these two clocks, the delay time resolution of the PRC is 0.2 us which corresponds to a 30 meters range resolution. Different values of delay time is obtained by different combinations of shifted values of two shift registers. The minimum delay is limited by the minimum propagation delay through the delay circuit. To compensate this, another MC14557B is added to the path of the PRC code which drives the laser diode. Two channel selectors (multiplexer) are used and the selection pins of the selectors are

connected to the parallel I/O port of the A/D board. So the delay time can be controlled by computer through the A/D program. Logic control functions such as reset, hold signals for the integrators and the sampling signal are also generated on the digital board. the last signal from the digital board is a synchronization signal to trigger the A/D board and synchronize the oscilloscope and other monitoring devices. It can be noticed in Fig.3.13 that the A/D trigger has double pulses. This is because the multi-channel A/D board can not be triggered simultaneously. Each channel is triggered in serial which is very raw.

The analog part includes power supplies for photo-multiplier tubes (PMT), transimpedance amplifiers, three gain stages, multipliers and integrators for demodulation to select the range bin and increase the signal to noise ratio. Several buffers are used to compensate the offsets of the op-amps and the multiplier. An ac coupling capacitor with very low cutoff frequency is placed between these gain stages to filter out the DC background in order not to saturate the receiver.

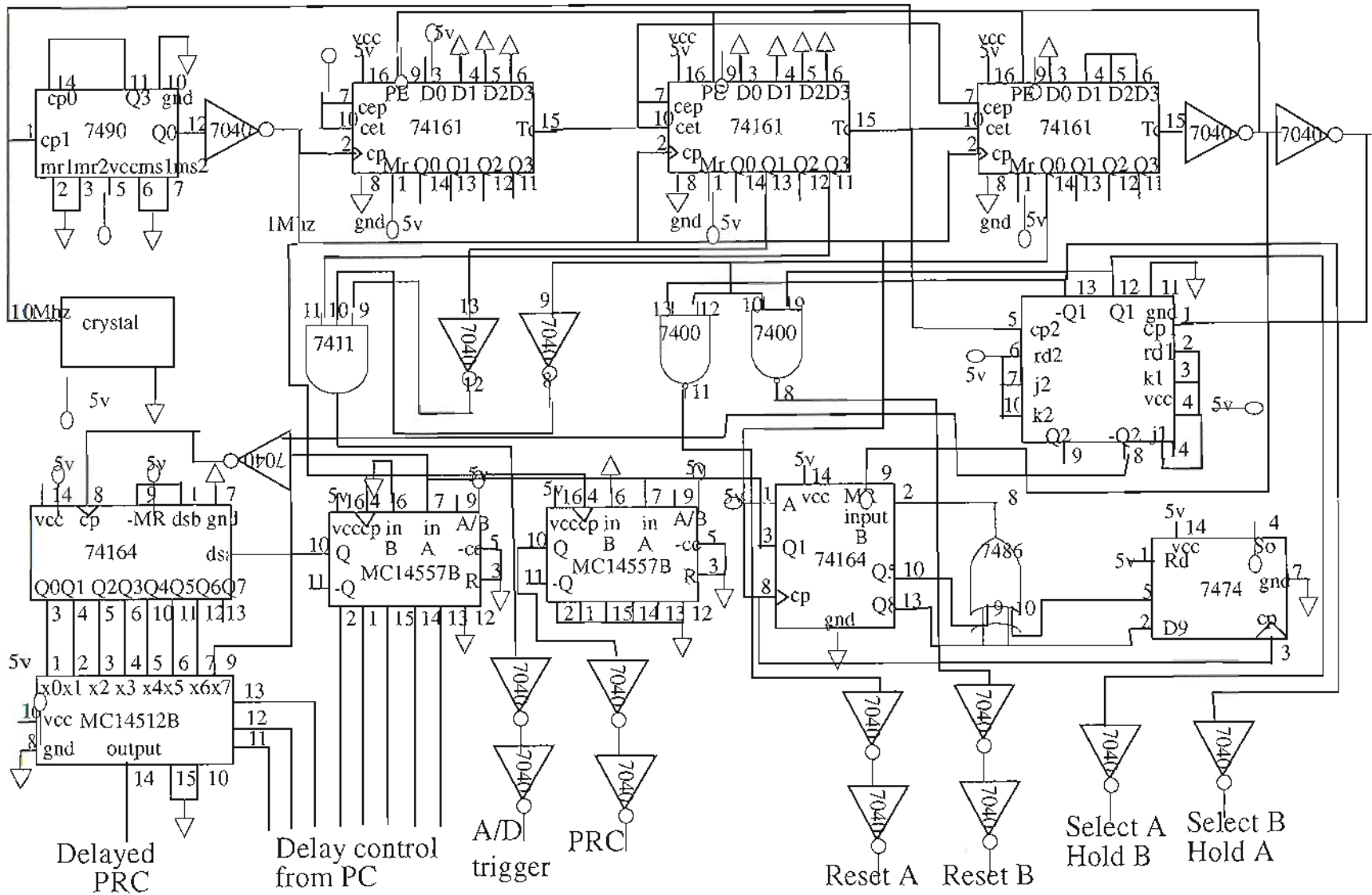


Figure 4.10 Pseudo Random Generator and control logic for the receiver.

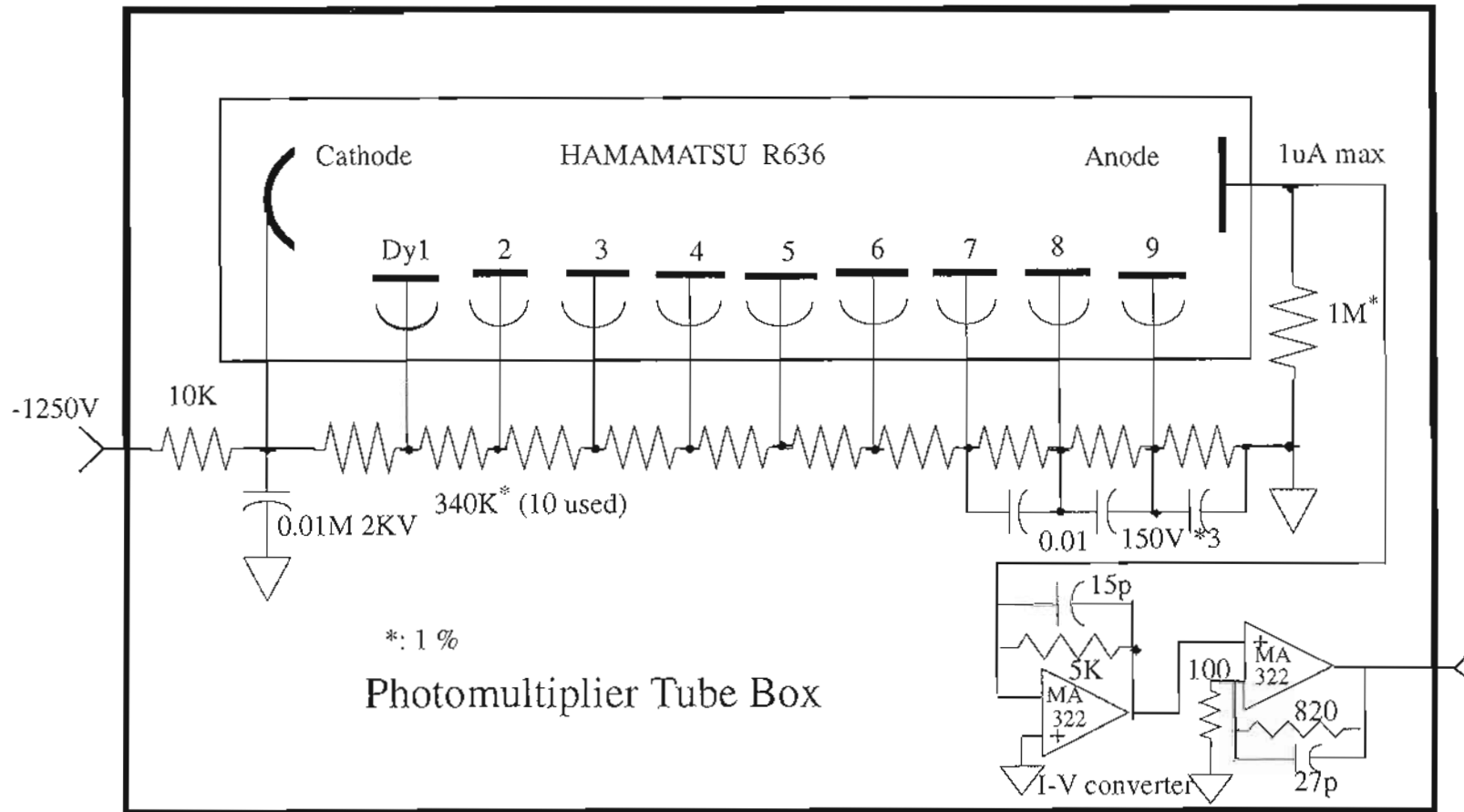


Figure 4.11 Detector and preamplifier.

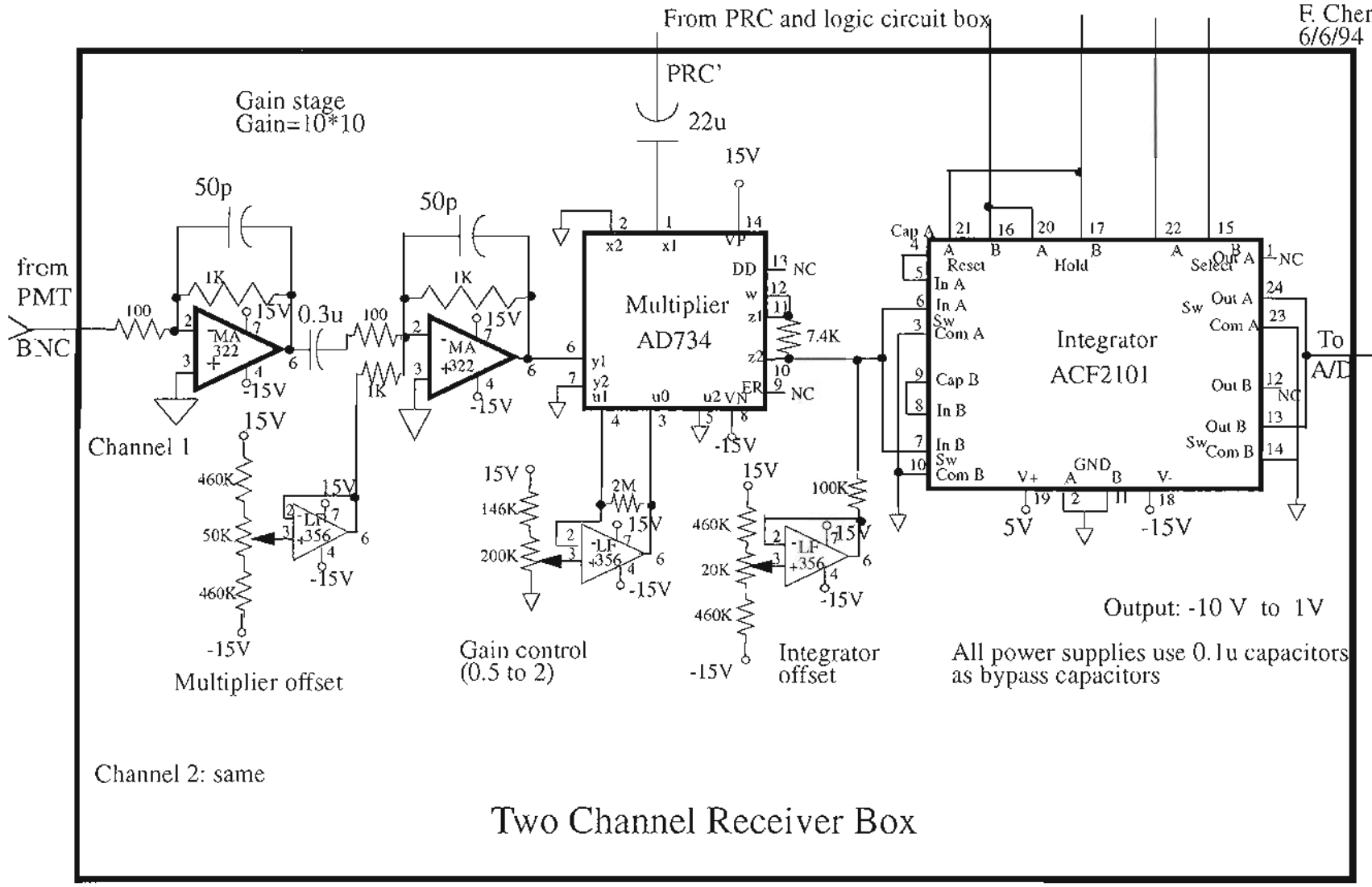


Figure 4.12 Two channel receiver

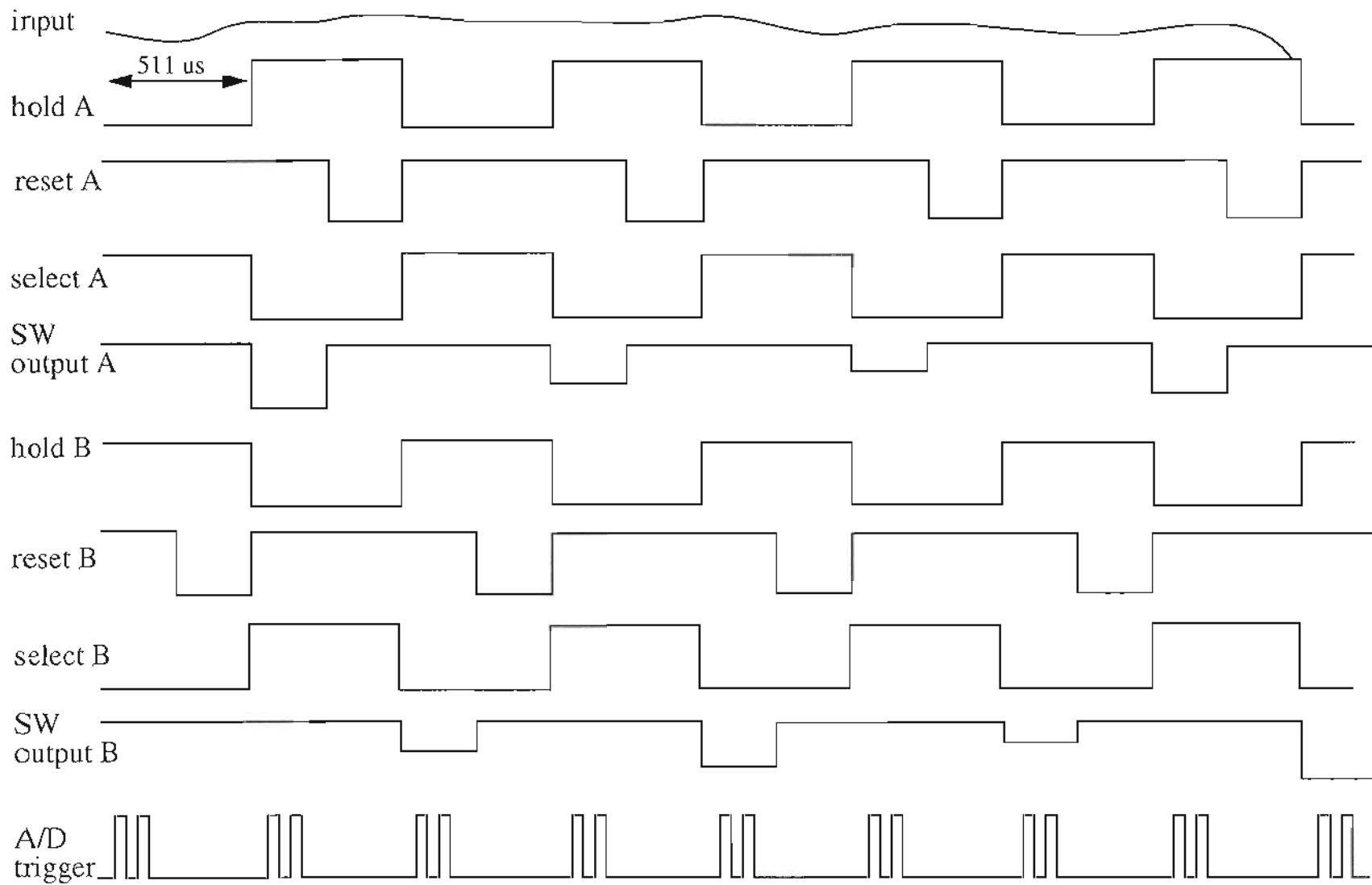


Figure 4.13 Timing diagrams of the "White Light" system.

4.5 Experiment Setup

The ‘White Light’ system is located in a trailer with a window which faces on open field about 1km in length. The telescope, along with the transmitter optics and receiving optics, are placed on a solid table. The diode laser controller, power supply, and all the electronics sit on a table adjacent to the telescope. Optical fibers for both transmitter and receiver run up to the ceiling in order not to be in the way of operation. A PC is used for controlling and data acquisition. The PC is connected to the ether net so recorded data can be transfer to the SUN work station for temporary storage and processing. Another double ended system (CampBell Unit) is put close to the trailer to measure wind and turbulence strength for comparison.

It is very difficult to perform the alignment with an invisible laser beam. First stage of alignment of the transmitter and receiver mirrors is done on the optical table in the lab. With a He-Ne laser aligned to the optical axis of the receiving telescope, and by putting the receiver and transmitter optics in a different order, the alignment of the system can be performed fairly accurately. More alignment is done on the site with the visible laser on the telescope and with the help of an IR-viewer.

The parameters of the components for the ‘white Light’ system are listed in the table 1

Table 1: List of components in “White Light” system.

Components	Parameters
Lasers	Transmitter: Seastar Optics Inc., pigtailed single mode laser diode. Model No: PT-450A-830, 5um pigtailed fiber; Tracer beam laser: Power Technology Inc., Model 635-3.
Laser controller, laser power supply	Melles Griot, Precision Diode Laser Controller Model 06DLD103 Self-designed 1 Am, 5V DC power supply for the tracer beam laser.
Detectors	HAMAMATSU R636 photomultiplier tubes.
HV-power supply LV-power supply	Fluke Inc., High Voltage Power supply Model 412A and 412 B Tektronix Inc., PS503A Dual Power Supply.
Telescope	Coulter Optical, Inc., 8-inch telescope, focal length=36 inches.
Lens	Transmitter lens: D=1 inch, f=63.5 mm; Receiver: 1 lens of D=1inch, f=2inches; 2 lens of D=1inch,f=1inch
Mirrors	Melles Griot 02WBK224 mirror coated for 830 nm.
Optical Filters	Acton Research Corporation Model 830-S-ID optical filter with bandwidth=10nm.
Optical Fibers	3M Specialty Optical Fibers: 300 um and 100 um core diameters.
A/D board	Computer Boards Inc., CIO-AD16 board and CIO-SSH16 interface.
Others	

Chapter 5

Experimental Results

The entire “White Light” system described in the previous chapters was designed in the Remote Sensing Group, Department of Electrical Engineering and Applied Physics, Oregon Graduate Institute of Science & Technology. It was first tested over a propagation path of about 200 meters inside the science park. Then the measurements were made over the vicinity farm land where horizontal paths up to 1000 meters is available for which the turbulence is expected to be quite uniform.

Considerable amounts of data were collected over path lengths of 250 m, 500 m, and 800 m at a laser beam height of about two meters above the ground and a variety of atmospheric conditions. The locations of the targets were chosen to be accessible so that the in situ measurement over the same path could be made. To simulate the weak signal from aerosols and demonstrate the range resolve ability of the system, window screens were also used as targets. In the attempt to measure the signal from aerosols, the telescope was raised up with a small angle after being aligned, in order to avoid the large backscattering from trees and houses.

A collimated laser beam was used in order to get the fully range resolved return signal with a coaxial system. Therefore, the theoretical development with collimated beam assumption was used. The peak delay method and Slope method will be both discussed in this chapter. In the following example, the peak delay method is used and the aperture

averaging effect is not taken into account.

The aperture averaging effect is studied and applied to the analysis of the experimental data. An optimum receiver aperture is obtained for direct detection system. Considerable effort was put into the experiment to get good data from aerosols.

It should be noted that in the development and testing of the "White Light" system, many design changes have been made to optimize the system. For example, fiber size was changed from 100 μm to 300 μm because of the unstable room floor where the telescope sits and angle of arrival fluctuations due to refractive index gradient changes for different time of the day and different temperature. In the study of the aperture averaging effect, different shapes and sizes of apertures were used and a 50/50 beam splitter was also used. Because the multiplier in the receiver circuit has an offset which is very sensitive to temperature, more gain has been put in front of the multiplier to suppress the offset effect. An A/D trigger was also changed from single pulse to double pulse because the A/D converter was designed to be triggered in series for each channel.

An example of the cross wind measurements is shown in figure (5.1) where the hard target at 800 meters was used. The cross wind estimates in figure (5.1) were obtained using the peak delay method and the equivalent detector distance was used without considering the aperture averaging effect even though different receiving apertures were used. To get one wind speed estimate, 12k samples average was used which is equivalent to 12 seconds in time for a single pulse A/D trigger. It should also be mentioned that because a hard target was used, only 1 second worth of data average was good enough to get a good TDC. The in-situ data was obtained by using a Campbell Scientific CA-9 path averaging scintillometer and crosswind sensor.

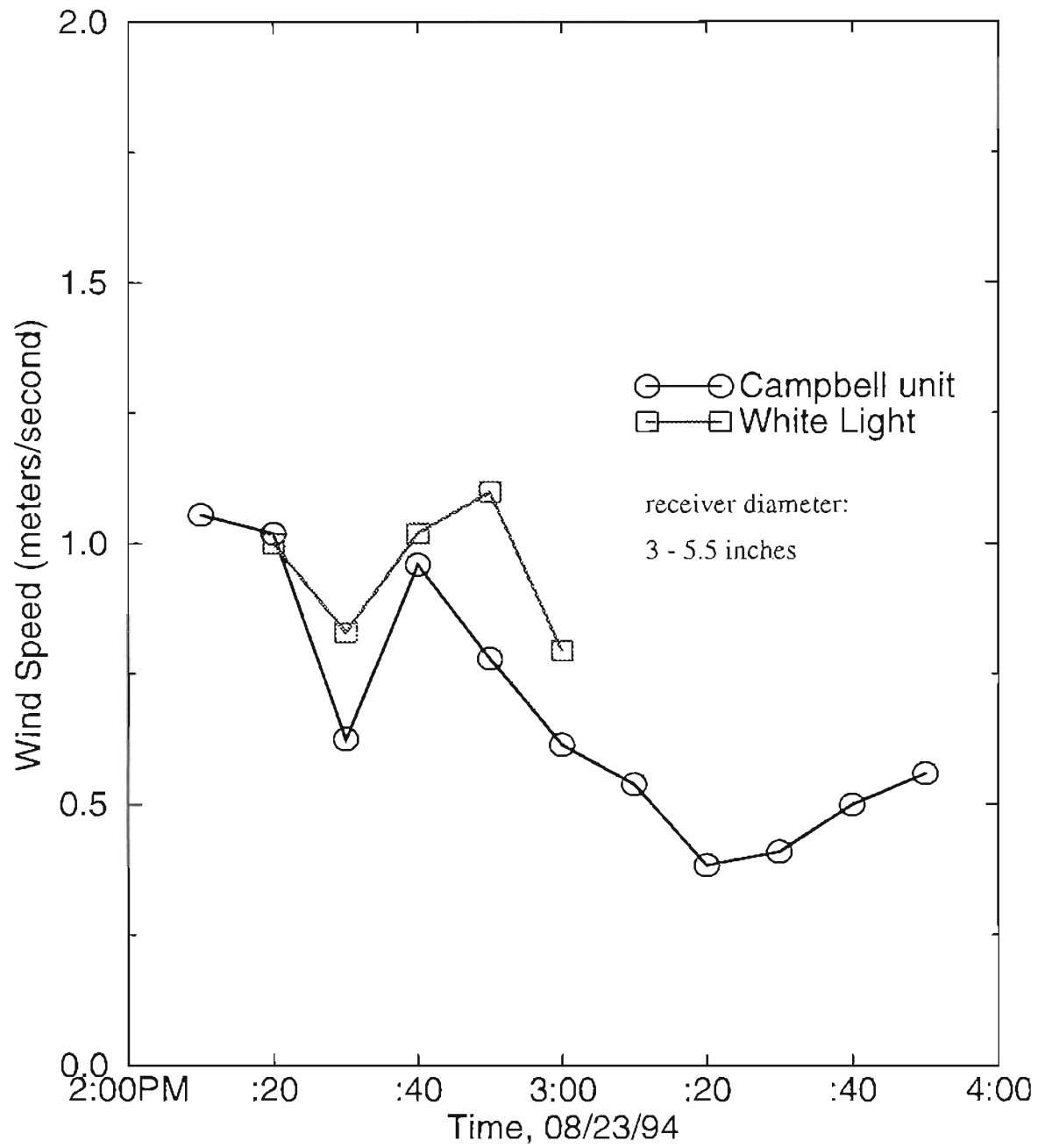


Figure 5.1 Cross wind measurements with both "White Light" and Campbell unit.

The Cambell unit is a double ended instrument which uses a 5 mW He-Ne laser as transmitter at one end and a receiver at the other. The Campbell unit operates on the principle that the slope of the time-delayed covariance function for the log-intensity from a point source in a turbulent atmosphere is proportional to the path averaged crosswind. This type of sensor has been extensively tested using propeller anemometers and found to be accurate to around ± 0.5 m/s. The turbulence level is also measured by the Campbell unit during the experiment so it can be applied to the theoretical formulation for predicting the cross wind speed. The Campbell unit measures σ_χ , which is related to the turbulence level by

$$C_n^2 = \text{const} \cdot L^{-11/6} k^{-7/6} \sigma_\chi^2 \quad (5.1)$$

As was mentioned many times in this dissertation, cross wind remote sensing utilizing the speckle-turbulence interaction requires the measurements of certain statistical parameters. These statistical parameters include the variance, time delayed covariance and autocovariance of the received intensity. In this chapter, experimental measurement of variance, autocovariance, time delayed covariance and cross wind speed are presented. The aperture averaging effect on the autocovariance and TDC for different receiver apertures is also studied and an optimum receiver aperture size is reached for “white Light” system and can be used for other direct detection systems. New methods of measuring the TDC and investigating the aperture averaging effect are proposed and tested. The new processing scheme is found to improve the wind detectability from the TDC using the slope

method. The experimental results show that the system works well with a hard target.

Some of the data from aerosols have also collected but less success is achieved.

5.1 Experiment Procedure and Results of Autocovariance and TDC

The test and experiments of the "White Light" system began in early 1994. The A/D program can be found in Appendix D. The transmitter is a pigtailed diode laser which can put out about 40 mW at the fiber end in CW mode. The high voltage power supply for the PMT can be applied up to -1200 volts. Diffused hard target at about 250 meters was first used. The experiment was conducted only when there was cross wind blowing. Each data file is composed of samples of consecutive ranges where the starting distance and number of ranges are controlled by computer through the A/D program. The number of samples for each range can be 1k to 160 k, or even more. The outputs of the Campbell unit are also sampled before collecting data from each range. The A/D program also calculates the average intensity of each range to help determine the distance to the target. The system can also run in real CW (without modulation) mode, and sampled before the signal is multiplied and integrated in the case of a hard target. The sampling rate is 1 KHz or 2 KHz for a single or double A/D trigger pulse, respectively.

Figure (5.2) is the intensity vs. range off the hard target at about 250 meters with a receiving telescope aperture of 8 inches. A single A/D trigger pulse was used, with an equivalent sampling rate of about 1KHz. Five ranges were chosen in order to find the target. There are 12 K samples in each range. From Fig. (5.2), it can be seen that the target is located at the peak or about 250 m. The resolution of locating the target is ± 15 meters.

Figure (5.3) is the recorded two channel signals used to produce Fig. (5.2). Some similarity with small time shift can be seen in both channels even in the presence of noise. Figure (5.4) is the autocovariance of both channels and figure (5.5) is the time delayed cross-covariance (TDC). Each curve was normalized by the average intensity. The data processing program for getting autocovariance and TDC is listed in Appendix E. The well defined autocovariance and TDC are a result of the significant interaction between laser and turbulence. The small magnitude of autocovariance and TDC is mainly caused by aperture averaging and small path length in which little interaction with turbulence occurs. The significant amplitude difference between the two autocovariances is caused by inaccurate control of equal receiving areas which produces differences of average intensities and variances. Another contribution of error to the average intensity is the offset fluctuation of the electronics which becomes important when the backscattering signal is weak as in the case of using aerosols as target. The time resolution is determined by the sampling rate which is about 1KHZ for the data in figure (5.3). So the time resolution in figure (5.4) and (5.5) is about 1 ms. The time shift of the peak is about 16 ms in figure (5.5) and effective detector distance was chosen as 4 inches. The wind speed can be calculated by the simple equation

$$V_{\perp} = \frac{P}{2\tau} \quad (5.2)$$

which gives 3.2 meters/second. The resolution of wind measurement is determined by sampling rate and detector distance as it will be discussed in section (5.3).

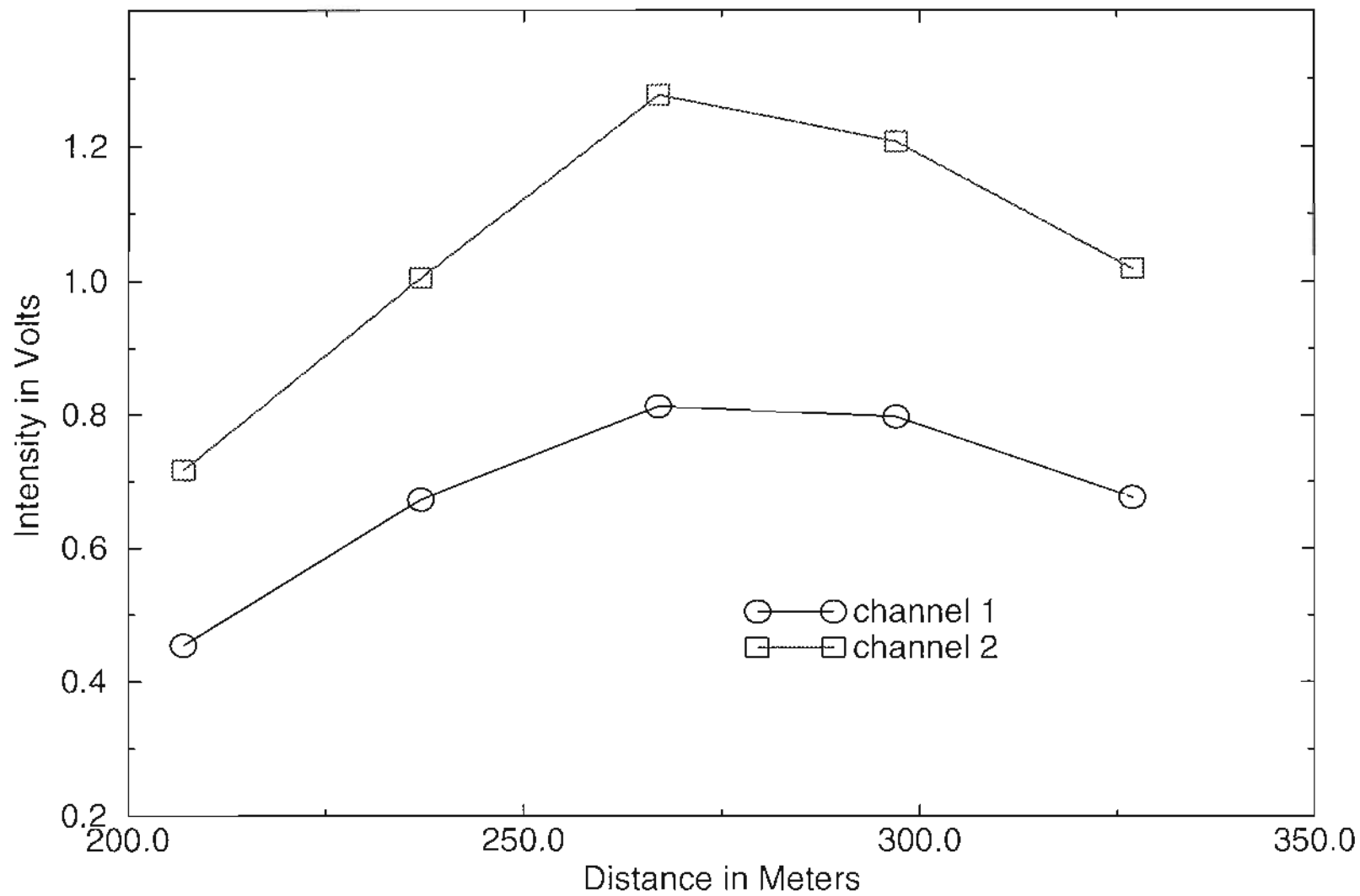


Figure 5.2 Intensity vs. range of the return signal off hard target at 250 meters.

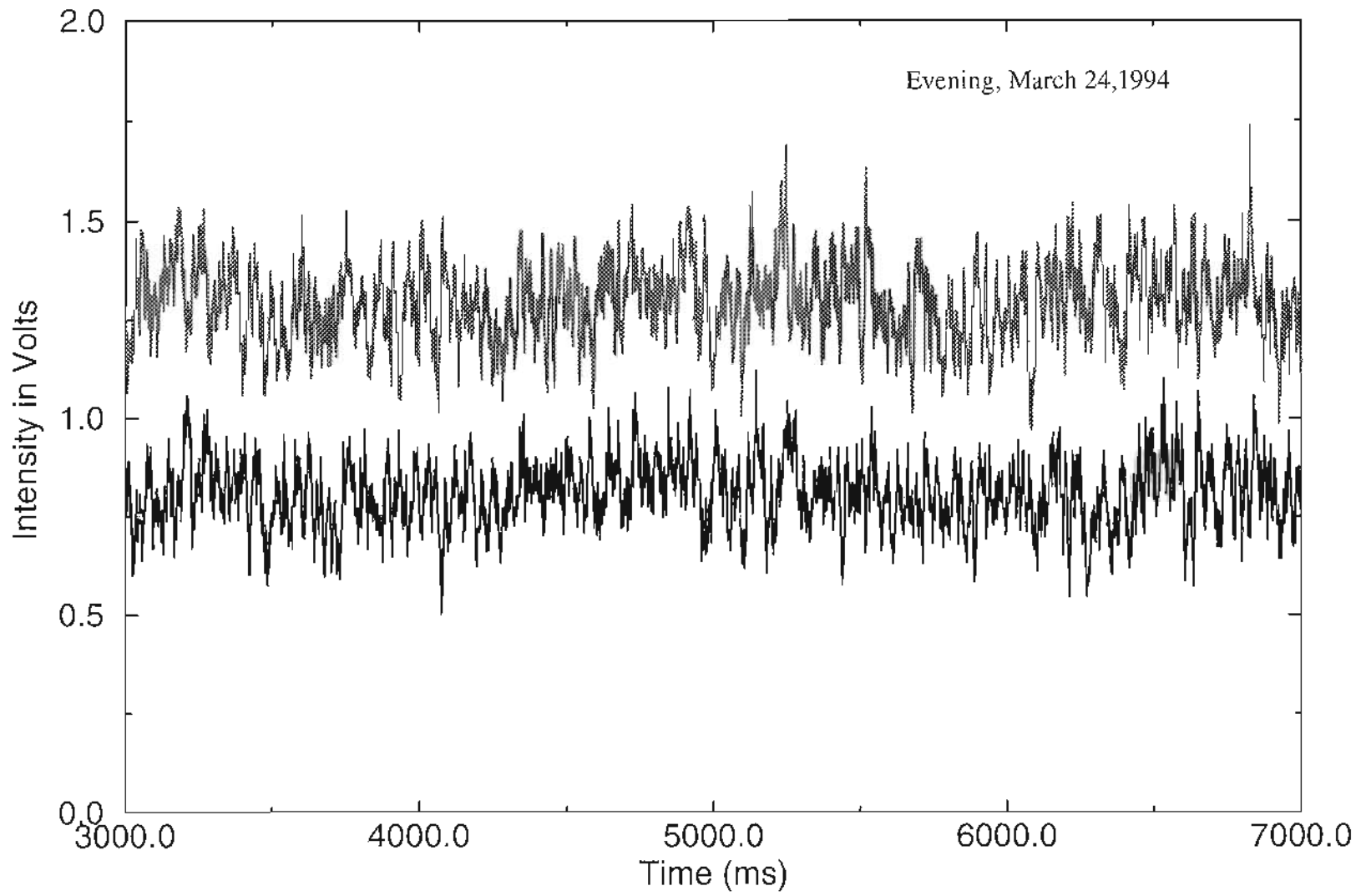


Figure 5.3 Two channel lidar signal from hard target at 250 meters.

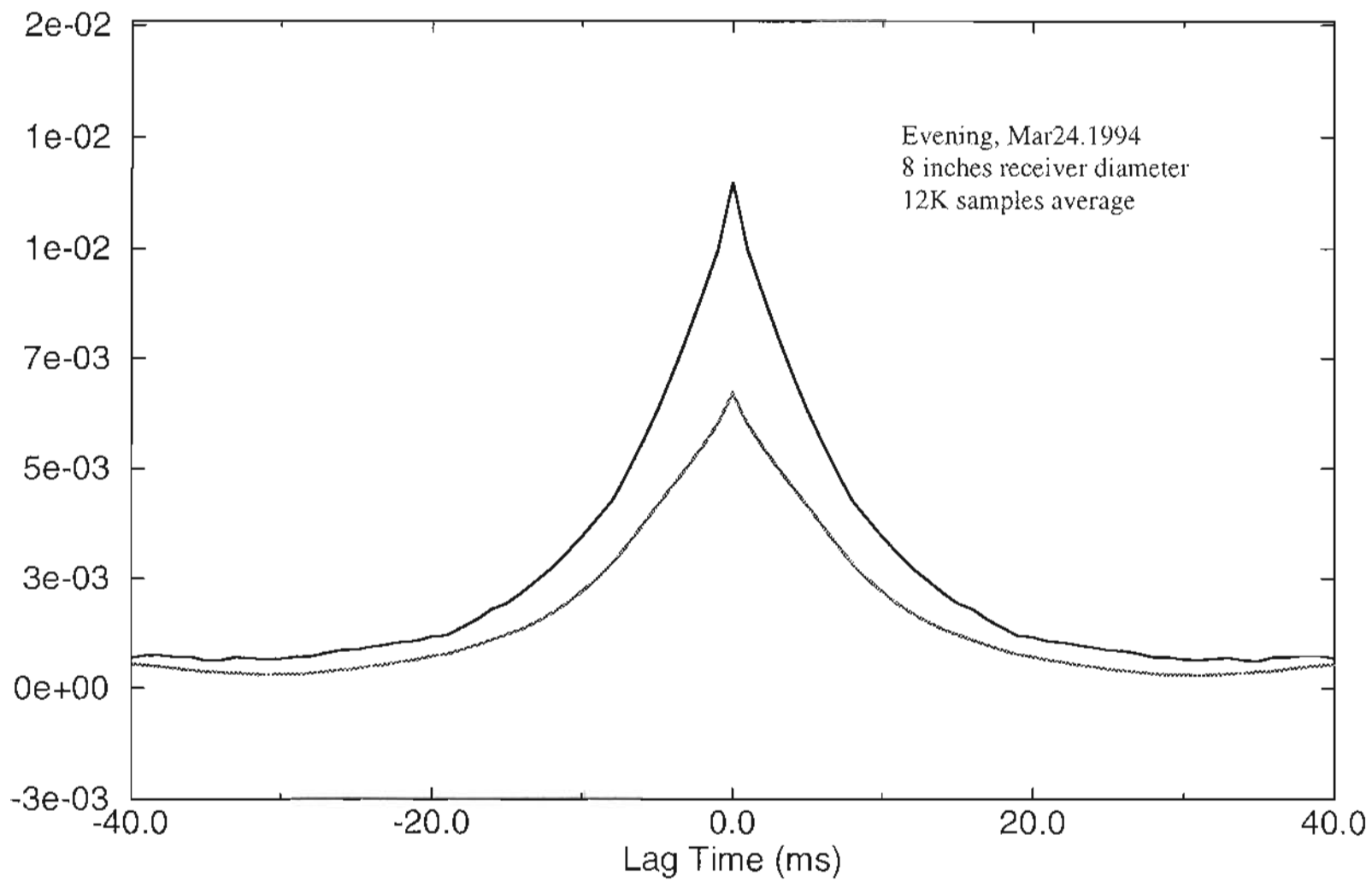


Figure 5.4 Autocovariance of two channel signals from a hard target at 250 meters.

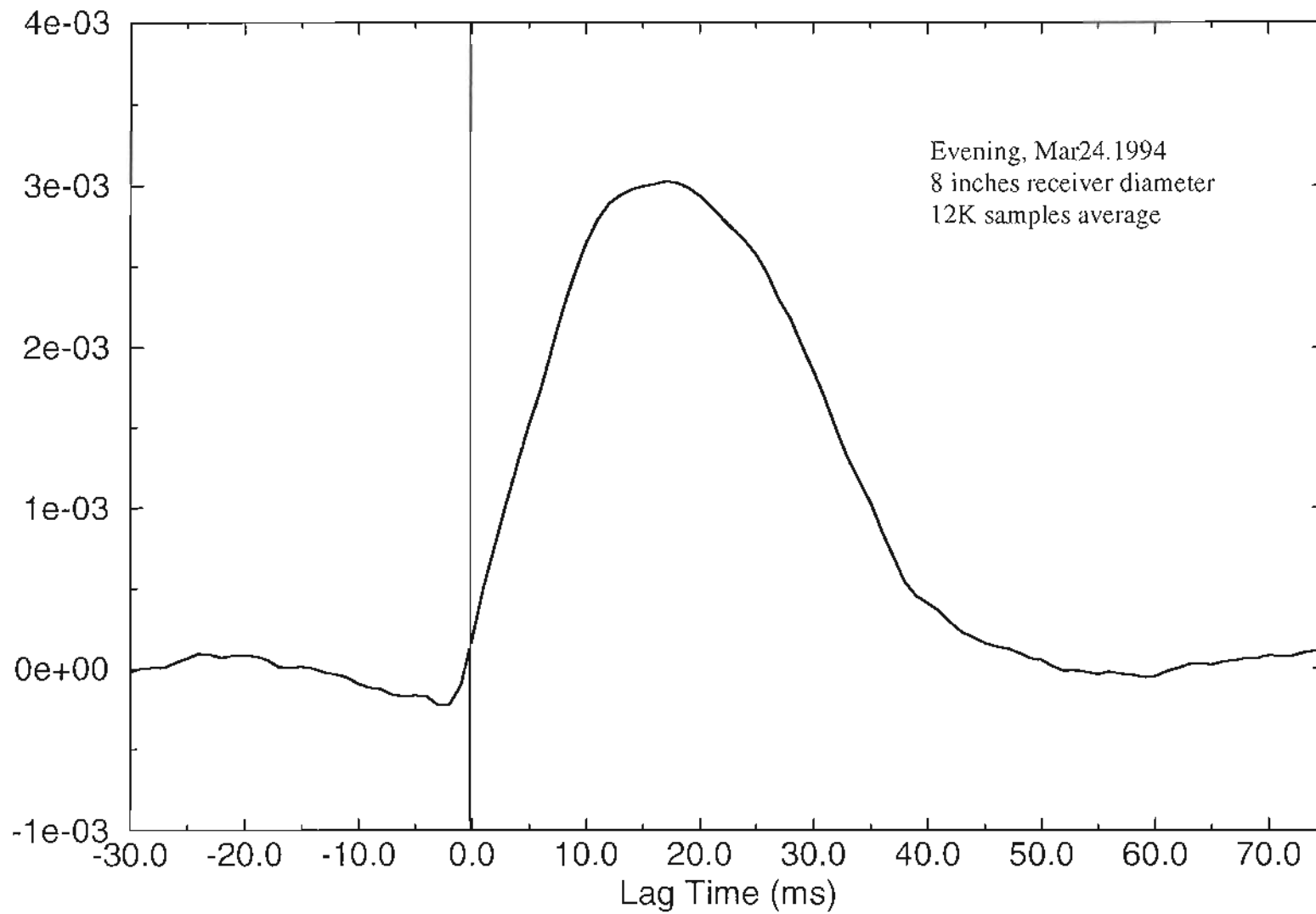


Figure 5.5 Time delayed cross covariance of intensities.

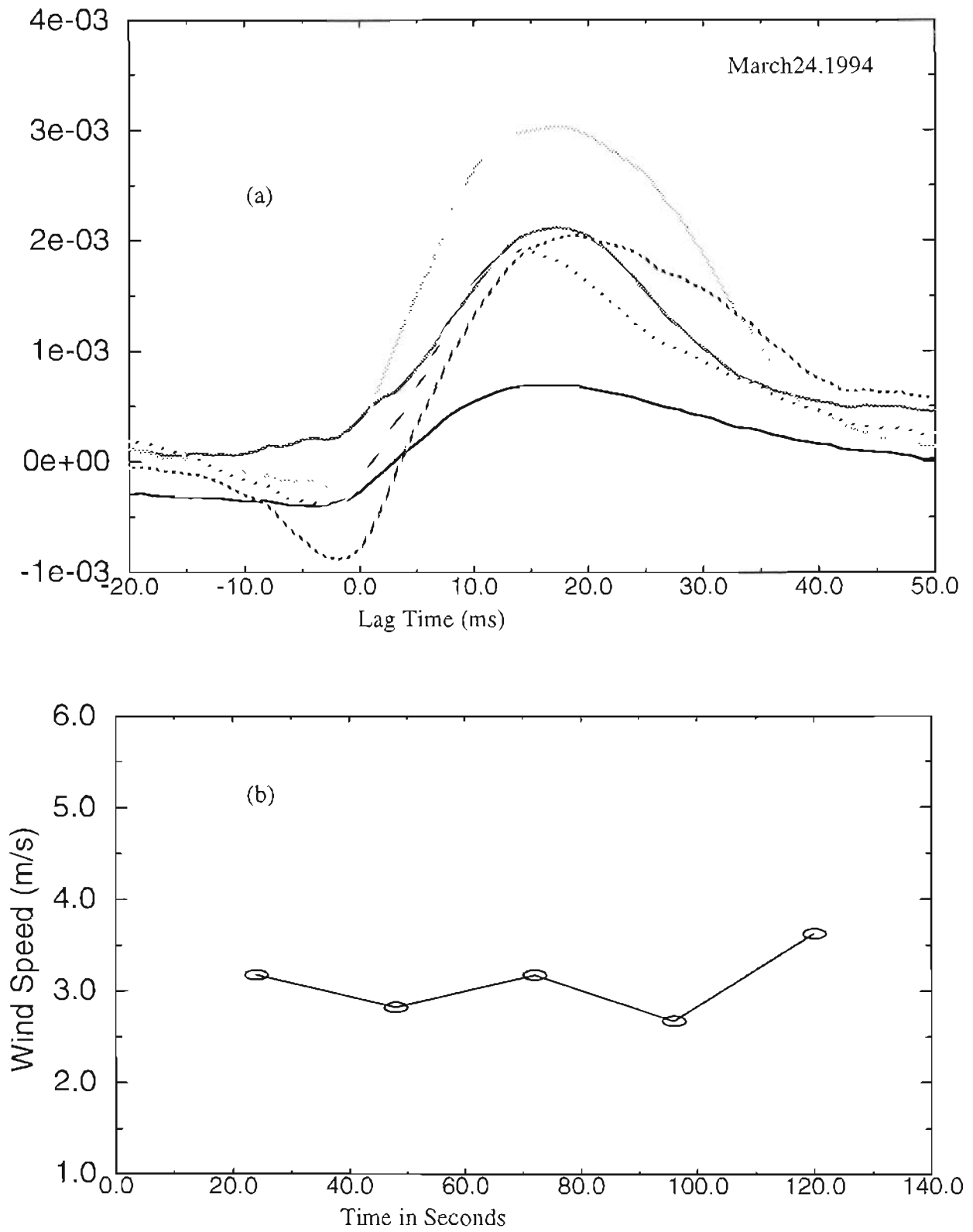


Figure 5.6 Processed results. (a) TDC from different ranges; (b) calculated cross wind speed.

Figure (5.6a) shows plots of the TDC from different ranges corresponding to those in figure (5.2). Since data for different ranges are taken consecutively but actually from the same hard target, by processing data from the different ranges a time series of wind speed can be obtained as in figure (5.6b). Each range represents 12 seconds worth of data, and it takes about the same amount of time to write to the disk after the data for that range is taken, so the total time is about 24 seconds between the wind estimates in figure (5.6b). From figure (4.6), the wind varies between about 2.5 m/s and 3.6 m/s.

It should be stated that proper way to obtain a time series of wind is to keep the range at where the target is, and take consecutive sets of data. Each wind estimate is obtained by processing each data set. The rest of wind time series are obtained this way.

Figure (5.7) is the TDC of received signals from a hard target at 800 meters, using an 8 inch receiving aperture. The single A/D trigger pulse is used which gives a 1 khz sampling rate. Using the peak delay method and an effective receiver distance of 4 inches, the wind speed is calculated to be 1.7 m/s. Figure (5.8) is the autocovariance of the same two channel signals. The TDC and autocovariance in figure (5.7) and (5.8) are normalized by average intensity.

Wind remote sensing using time delayed covariance scheme can give both the magnitude and direction of the wind speed. When cross wind blows turbulent eddies of different sizes cross the laser beam, their effect on the laser signal coming back to the detectors will experience a time lag depending on the wind direction. And this will be shown by the sign of lag time of the peak of the TDC function. Negative lag time is detected as it can be seen in figure (5.9) which means the wind was blowing in the opposite direction compare to the

days of figure (5.5) and (5.7). Figure (5.10) is the autocovariance of the same experiment data as in figure (5.7). The target is at 800 meters, and a smaller receiving aperture (5.5 inches) is used. Again the sampling rate is about 1 khz and wind speed is calculated about 5 m/s. The feature of the TDC function with the peak shifts according to the wind direction is very important and useful. With two detectors, the vector wind's (magnitude and direction) projection along the detector's axis can be measured. If three or more detectors are used, the real wind vector can be defined on the receiver plan. Of course, the wind along the radial direction can not be measured by this scheme, but if it is combined with the well known Doppler method, the complete three dimensional wind speed can be measured.

It can be seen that the magnitudes of the TDC and autocovariance of the experiment results are different from experiment to experiment. These differences are due to changes in turbulence, path length and receiver aperture size. For the same atmospheric conditions, the amplitudes of the TDC and autocovariance are only controlled by the receiver aperture. Therefore, it is important to study the aperture averaging effect because the wind detection is directly related to the time shift to the peak and slope of TDC function.

Autocovariances were plotted to investigate the potential of determining the cross wind using the scheme introduced in chapter 2. Because the Campbell unit was not running during the experiments so far, no comparison can be made. But as the author observed in the experiments, "White Light" works well for hard target. It gives the correct trend of wind amplitude and correct wind direction.

In the following sections, aperture averaging effect was studied experimentally and the Campbell unit was used to compare with “White Light”. Independent information of turbulence strength and wind speed can be obtained so comparison can be made. Different shapes and sizes of receiving aperture were used to find the optimum selection. With practically optimized aperture, several time series of data were taken and time series of wind speed were produced. Very good agreement was found between “White Light” system and Campbell unit.

Attempts have also been made to measure the signal from aerosols both during the day and night. It is very noisy during the day because the system is working in the near infrared. Background noise is huge because of the leakage and finite bandwidth of the optical filter. A big background signal can also saturate the receiver electronics and the detector if the gain of the detector is set too high. Therefore, aerosol detection can be only made during the night. But in this area of the country, there is very little wind during the night, so not many good opportunities for aerosol detection were available. Because of the low signal to noise ratio, covariances measured are very noisy. In addition, huge number of samples are needed to resolve the peak of the TDC function. A few to tens of minutes average is necessary to get a good TDC curve. This time long enough that the atmospheric conditions change and large scale fluctuations of the receiver electronics make the signal nonstationary which eventually produces wrong results. Some fairly good results for aerosols were seen but higher laser power and a better processing scheme may be needed to improve the performance of the system for aerosol detection.

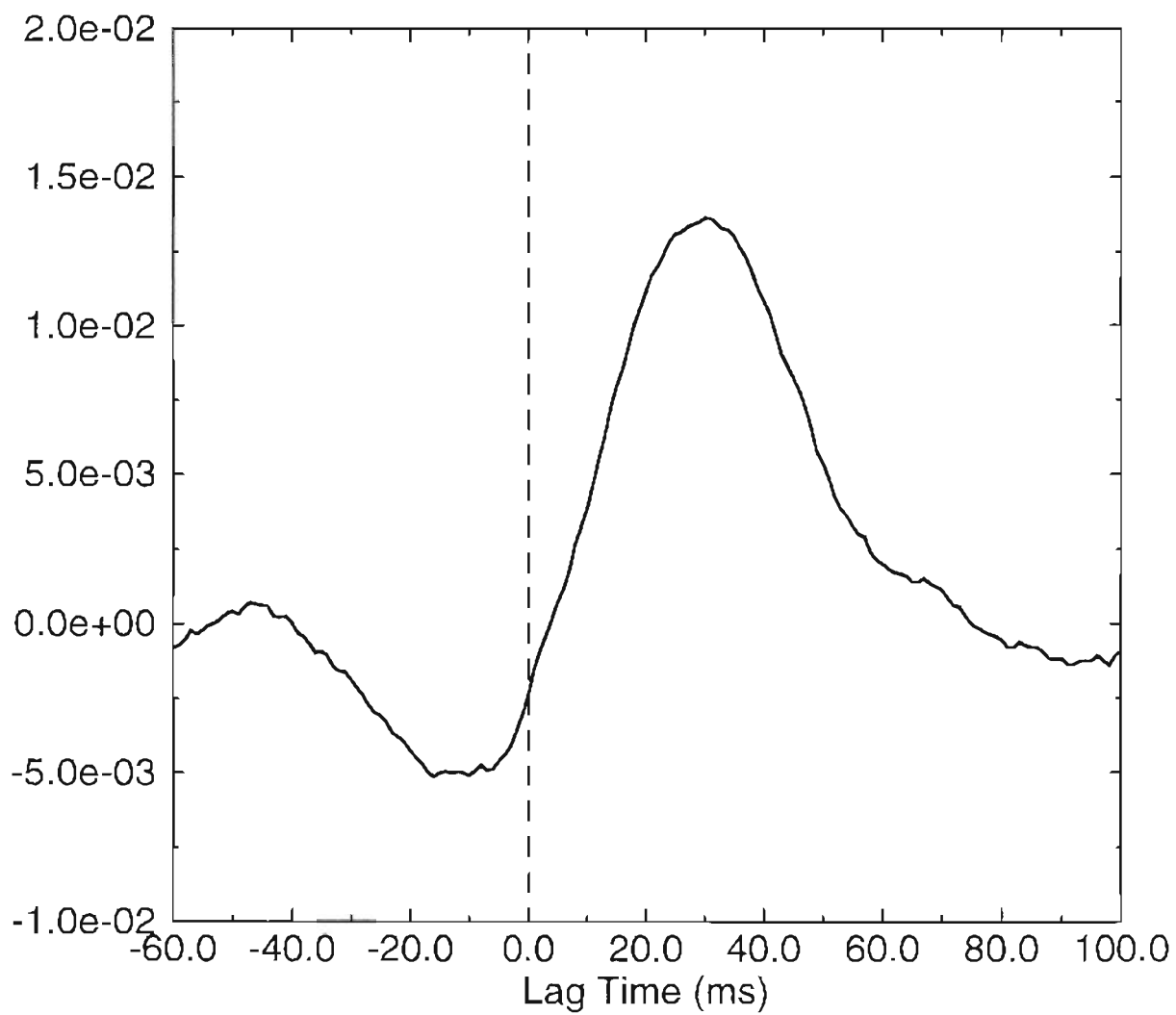


Figure 5.7 TDC off hard target at 800 meters. 3 inches receiver is used.

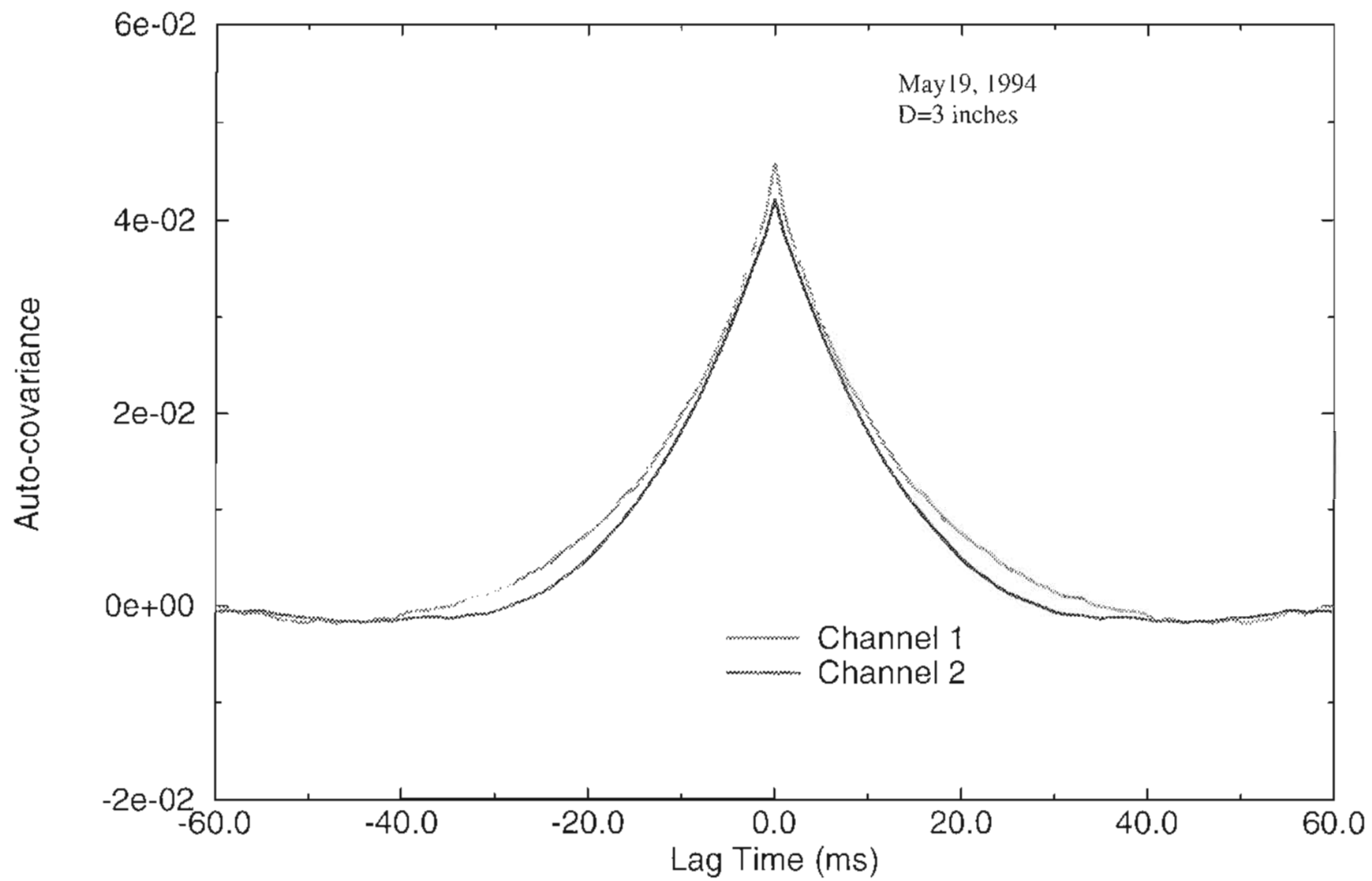


Figure 5.8 Auto-covariances of two channel intensities from hard target at 800 meters.

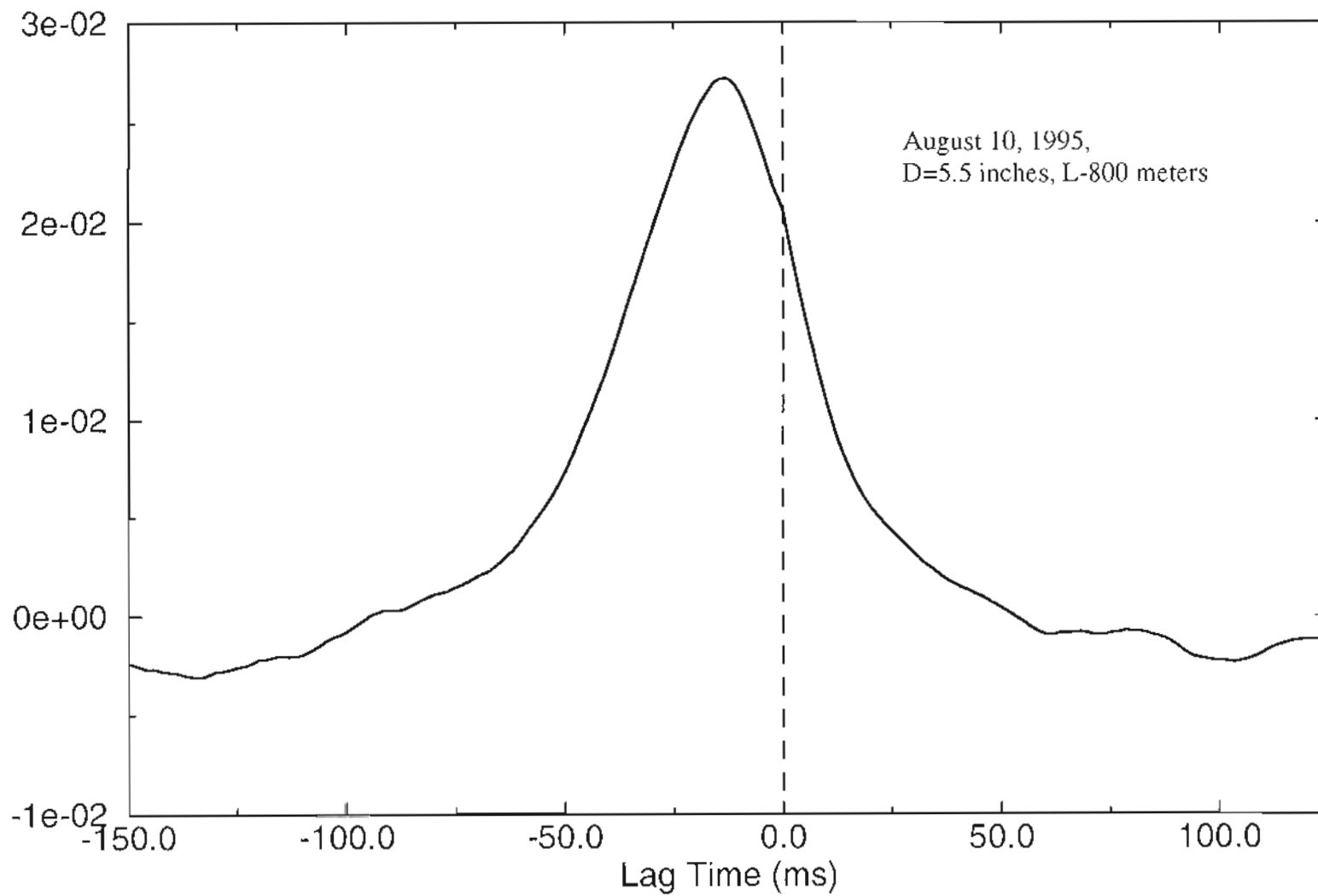


Figure 5.9 TDC with hard target at 800 meters and receiving aperture of 5.5 inches.

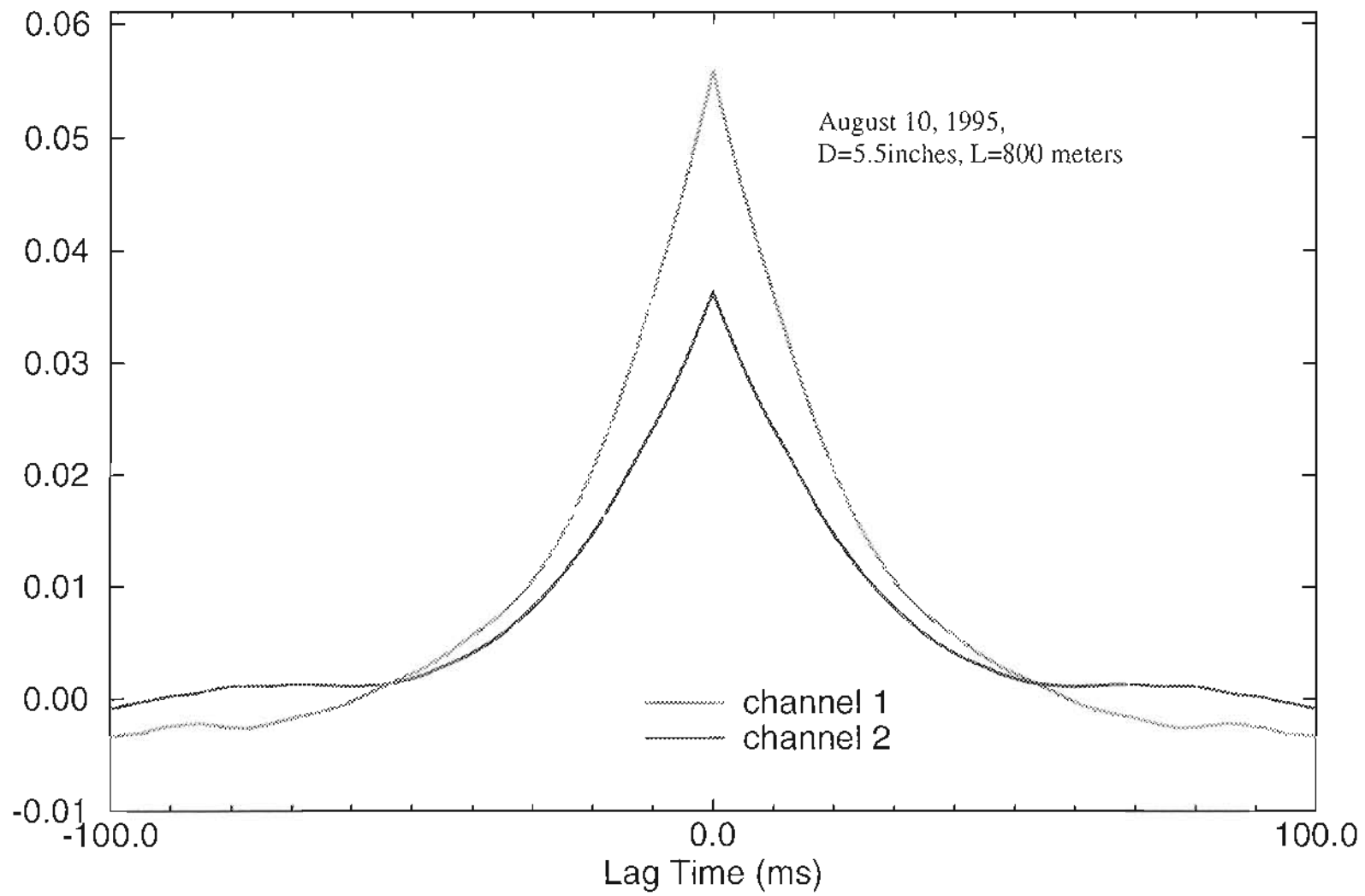


Figure 5.10 Autocovariance with hard target at 800 meters and receiving aperture of 5.5 inches.

5.2 Experiment on Aperture Averaging Effect

When receivers have a finite area, aperture averaging effect starts. The bigger the receiver apertures are, the smaller the covariance because the fluctuating part of the signal is averaged out. Aperture averaging also reduces the width of the autocovariance function. Another factor that effects the covariances is the detector spacing. The bigger the detector spacing, the smaller the covariances are. Both factors exist in the “White Light” system. To study this effect, both two half moons and two rectangular shaped receivers with different sizes are used as shown in figure (5.11).

In figure (5.11 a), the inner circle represents the diagonal mirror inside the telescope which blocks some of the receiving area. This effect is also taken into account in the theoretical analysis. The configuration in figure (5.11 b) is obtained by blocking the aperture of the telescope in

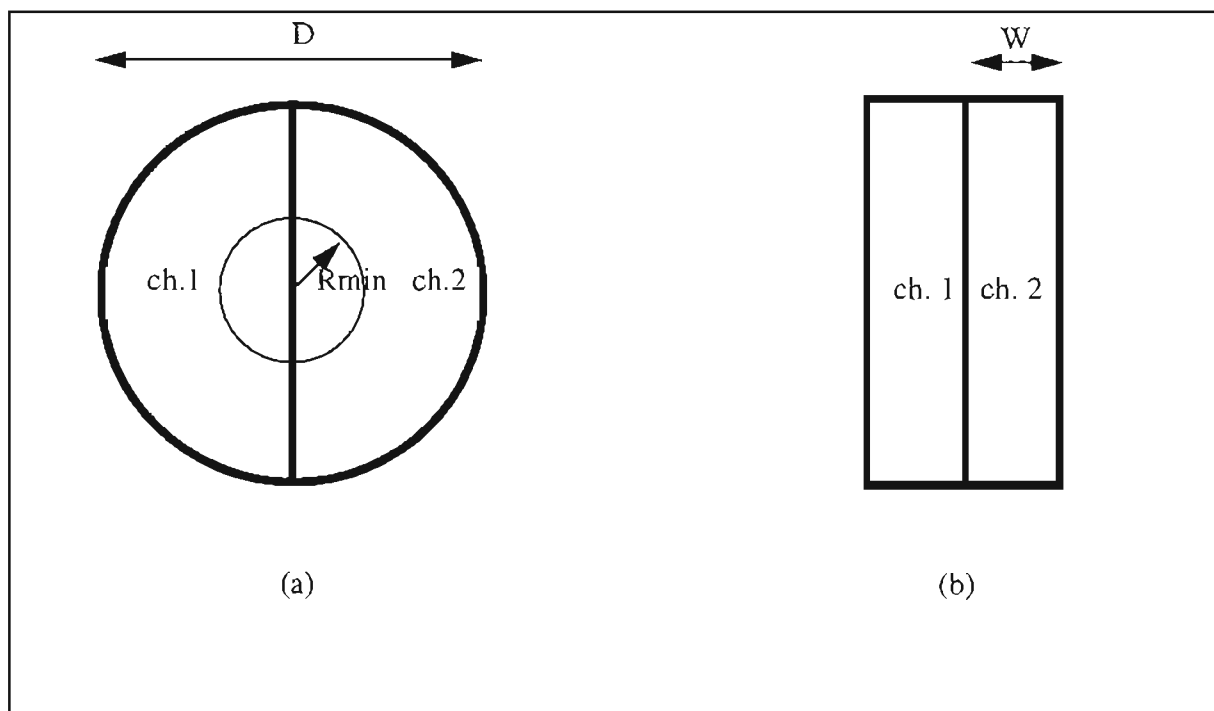


Figure 5.11 Two different receiving apertures: (a) two half-moons; (b) two rectangles.

such a way as to produce a rectangle. The same kind of configurations are used for the theoretical analysis of different sizes at constant wind speed and turbulence strength. The wind speed and turbulence strength are chosen based on the experiment measurements, so comparisons can be made. The experiments were conducted with hard target at 800 meters. Data were taken with different sizes in short enough sampling times in which turbulence doesn't change very much. This is verified by Campbell unit measurements of C_n^2 used for numerical analysis.

Peak values of TDC function of both experiments and numerical simulations for two half-moon configuration is plot in figure (5.12). Wind speed and turbulence are $V = 1$ m/s and $C_n^2 = 2.29e - 14$ from Campbell unit measurement. Very good agreement is found between experiment and numerical analysis of the TDC function. The primary goal is to find an optimum size receiver for the "white Light" system. Figure (5.12) is plotted using log scale on x which is the radius of the telescope. From figure (5.12), the amplitude doesn't change very much as the radius increases. then drops off very fast until a radius is reached at which the TDC becomes stable again. The optimum size can be chosen where the amplitude starts to drop rapidly. In this two-half moon case, a radius smaller than 10 mm should be chosen. But for the coaxial system, it is impossible to implement this aperture because of the size of diagonal mirror which blocks the receiver. Experiment results with relatively bigger apertures were found which agree with the numerical analysis very well. Experimental results of the autocovariance is also found agree with the numerical analysis as it is shown in figure (5.13). A slight difference between ch.1 and ch.2 in figure (5.13) was introduced by inaccurate control of the receiver aperture.

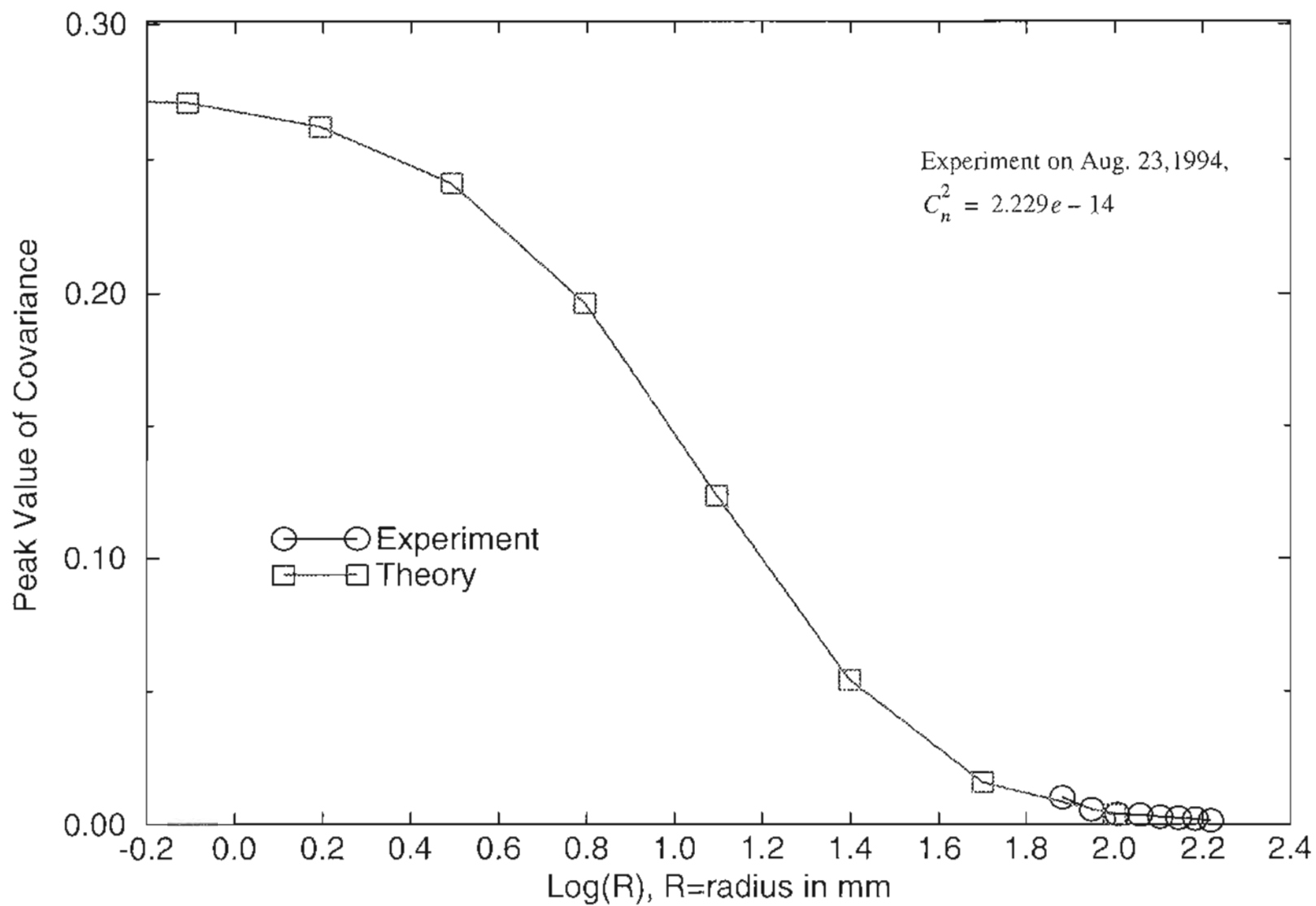


Figure 5.12 Aperture averaging effect on time delayed covariance for two half-moons receiver.

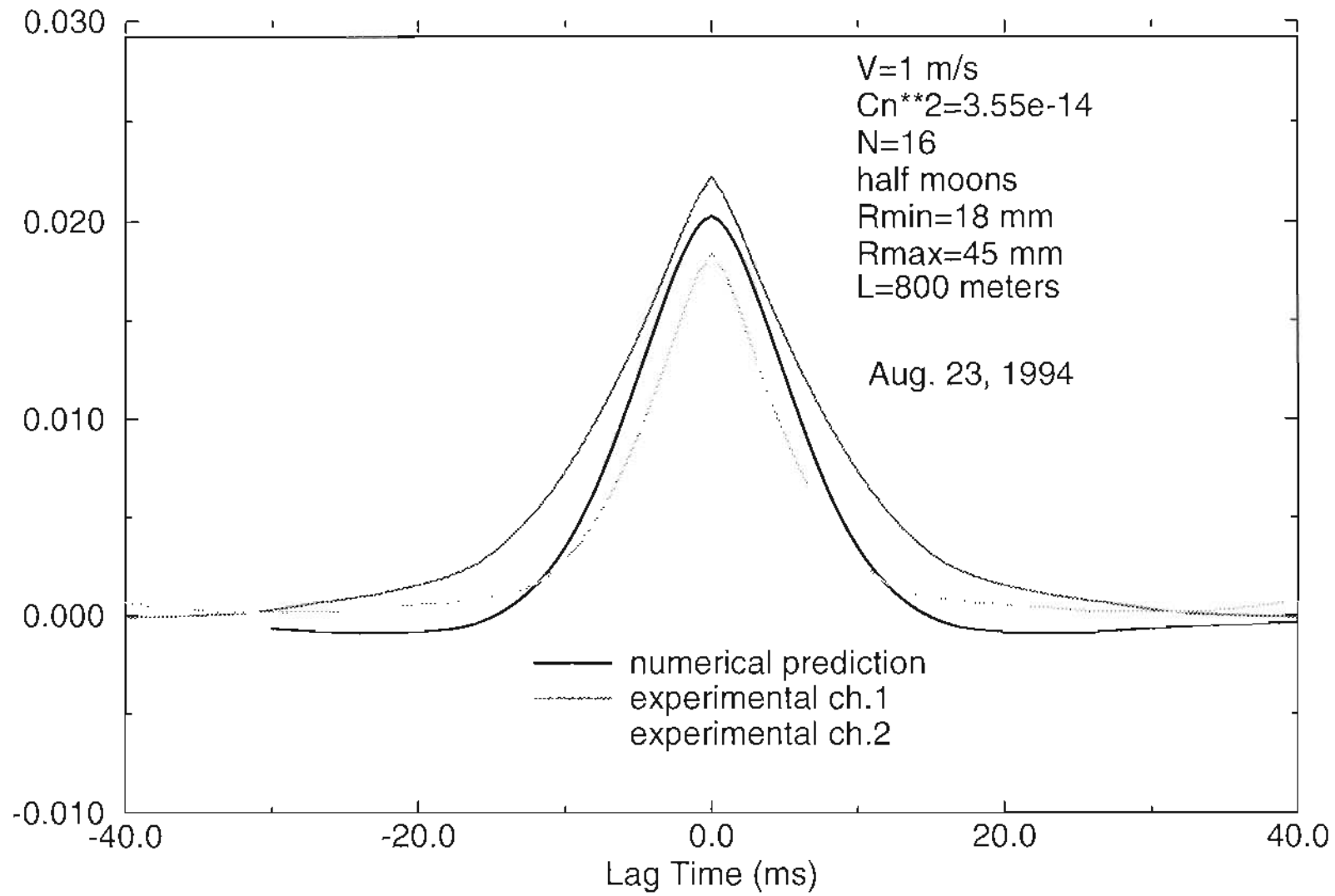


Figure 5.13 Autocovariance of both experiment and numerical analysis of two half-moon receiver.

The rectangular shaped receiver was also used for experiment and numerical analysis. This is more useful practically. The numerical results of peak amplitudes of the TDC with different width of rectangle are plotted in figure (5.14) compared with a few experiment results. The experiment results agree with the numerical predictions very well. The optimum width for rectangle receiver is about 10 mm as it can be seen in figure (5.14). Figure (5.15) and (5.16) are the TDC functions and autocovariance functions of both numerical and experimental results with width of 20 mm of each receiver rectangle, with Campbell unit showed wind speed $V = 2$ m/s and turbulence $C_n^2 = 2.0e - 14$.

Comparisons of experimental results and numerical predictions show that the theoretical development and simplifications are adequate and can be used for future work. The good experimental results demonstrated also show that the “White Light” system is designed following the physics principles. All the concerns in the development and experiment can be used as guideline of a similar system design for future work. It should be pointed out that the parameters chosen for numerical analysis are specific for “White Light”. More generalize analysis should have the formulation normalized by Fresnel zone scale size and for rectangular receiver, the variable height of the rectangular case should also be studied. But it was found from simulations of different heights that the results are similar to figure (5.14) except for a scale factor.

Practically optimum sizes based on the aperture averaging effect in this section were used for further experiments of wind measurements. Very good TDC functions with relatively higher magnitude are obtained for every single set of data. The time series of wind speed were obtained from the TDC function using the peak shift method. The Campbell unit was also set up at a very close path to “White Light” to collect cross wind speed and turbulence data for comparison.

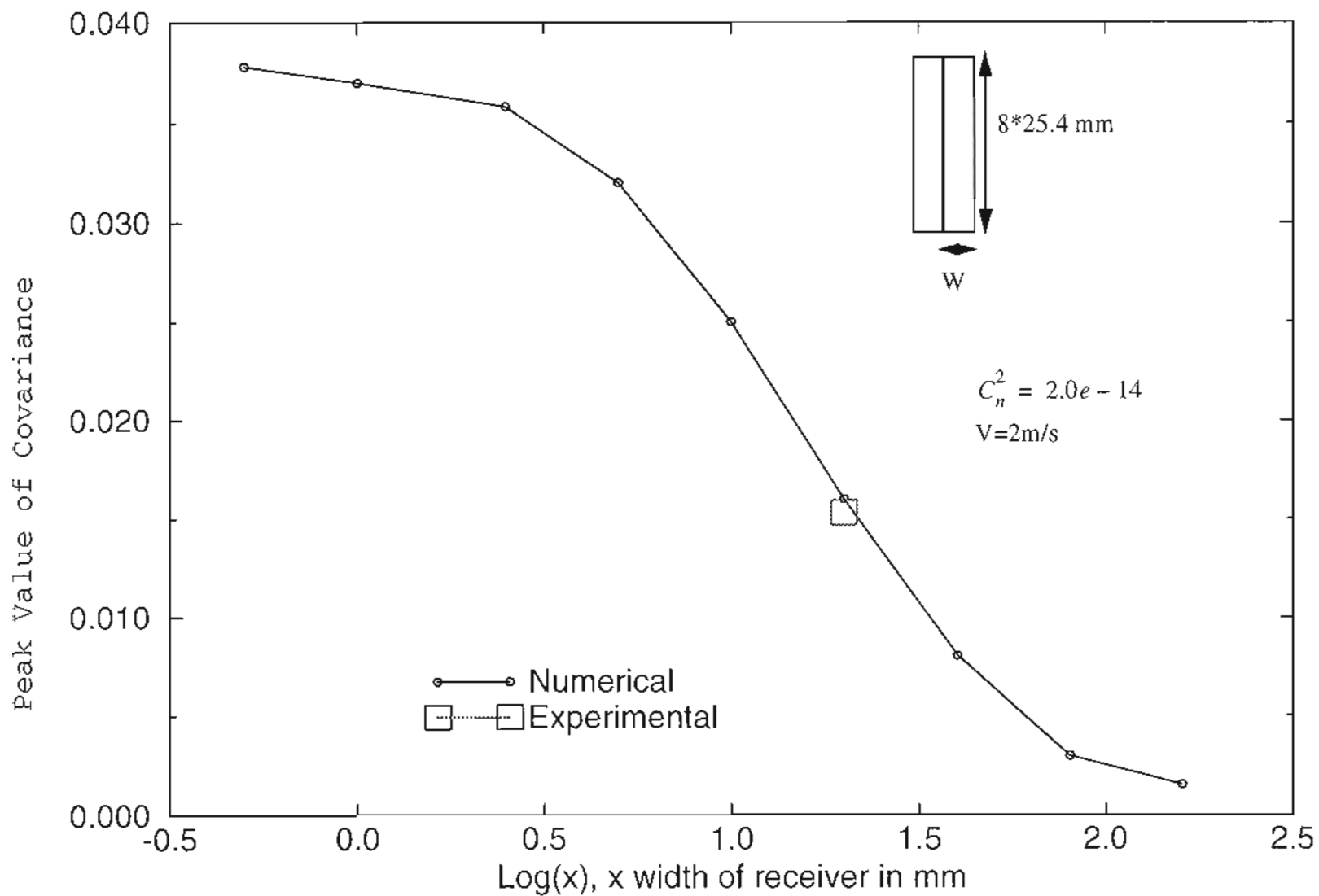


Figure 5.14 Aperture averaging effect on time delayed covariance for two rectangular receivers.

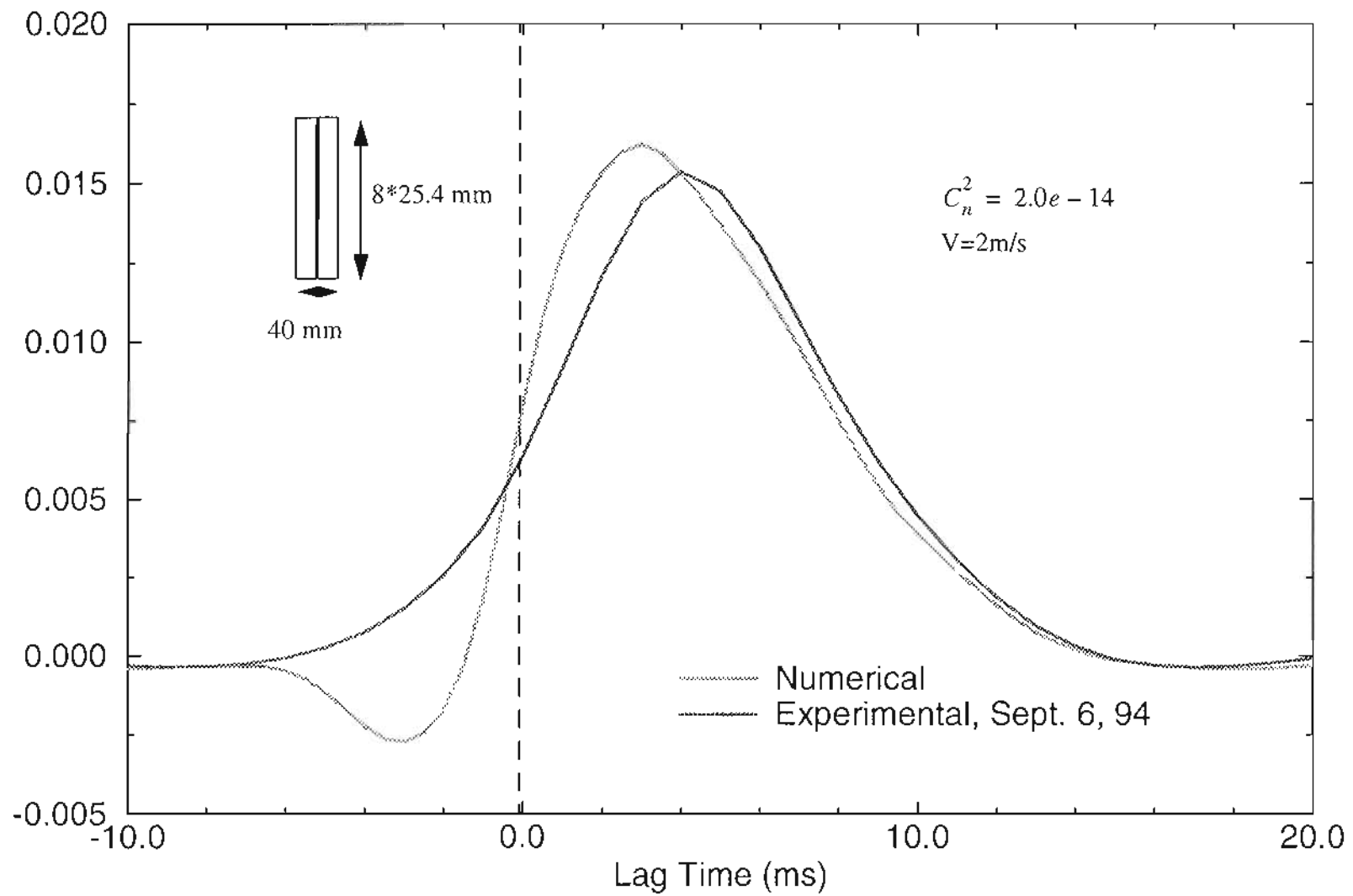


Figure 5.15 TDC's of both numerical analysis and experiment of two rectangular receivers.

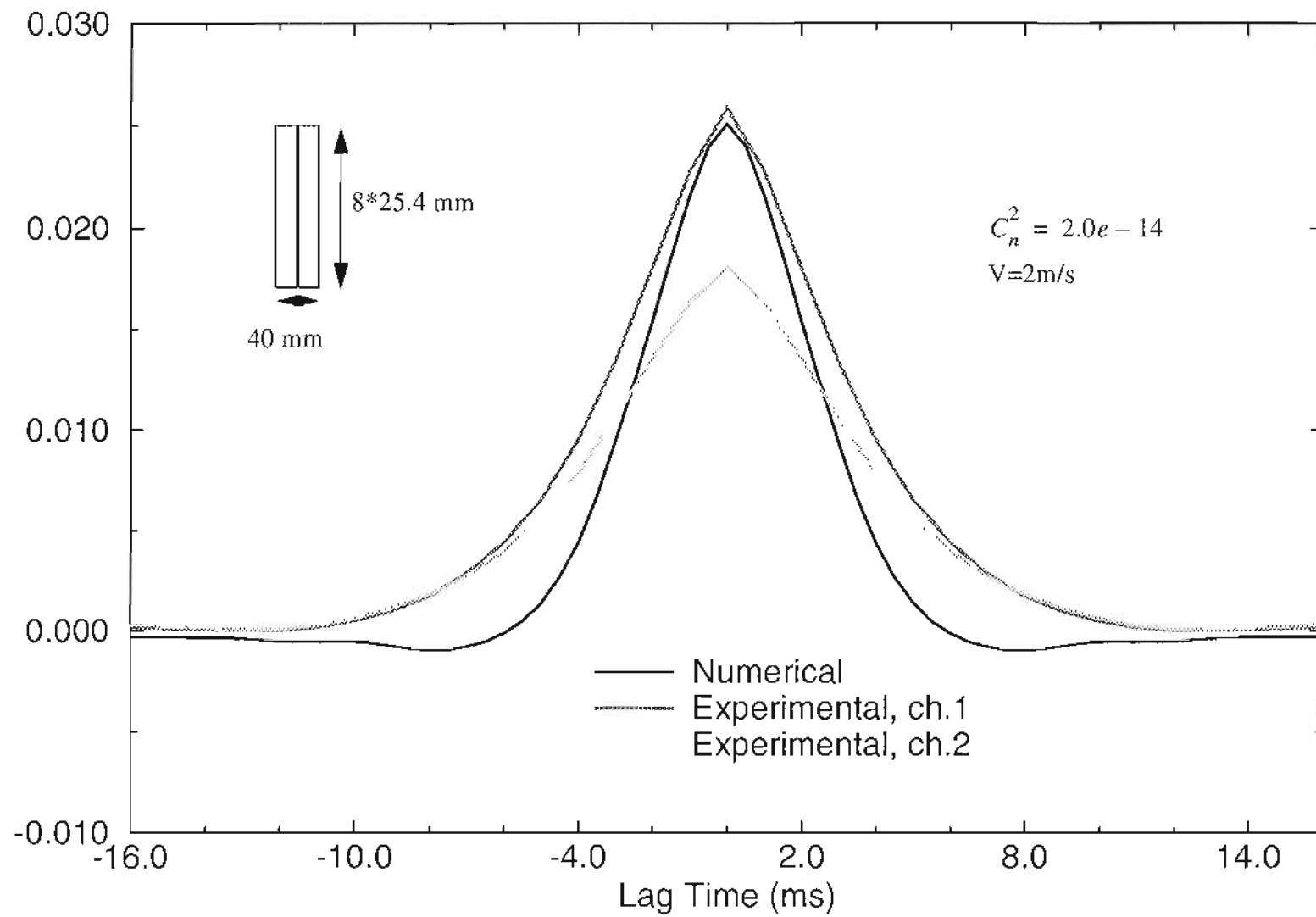


Figure 5.16 Autocovariance of both experiment and numerical analysis with rectangular receivers.

5.3 More Wind Measurements

In the previous section, the aperture averaging effect was discussed and tested to reach an optimum aperture size for the “White Light” system. The criteria of an optimum aperture is that the aperture be big enough so that received signals have good signal to noise ratio, but at the same time be small enough that aperture averaging effect is not too severe that the peak value of the TDC function is above the threshold of the noise. This is especially important for aerosol detection because of the bad signal to noise ratio.

More experiments were conducted under various atmospheric conditions with a hard target at 800 meters with smaller two-half moons and rectangular receiver apertures. The Cambell unit was set on a parallel path less than 0.5 meter from the optical axis of the “White Light” system. A set of independent cross wind speed and turbulence data were collected from the Cambell unit just prior to each data set was taken from “White Light” system. Only about 10 seconds of time delay is introduced for each data set of 12 k samples. Consecutive data sets were taken to develop a time series of cross wind speeds using peak delay method. Comparison are made with Campbell unit measurements.

Figure (5.17) is the TDC function of one data set obtained on September 6, 1994. Rectangular shaped receivers with width of 20 mm were used. Ten consecutive sets of data were taken, each with 24 k samples for each channel. An average of 12 k samples was used to get the TDC curve, and peak shift method is used to get wind speed. The time series of the wind speed is plotted in figure (5.18) and corresponding Campbell unit readings are also plotted in figure (5.18). As it can be seen, “White Light” system can follow the trend of the Campbell unit fairly well. The error of the last two points may be caused

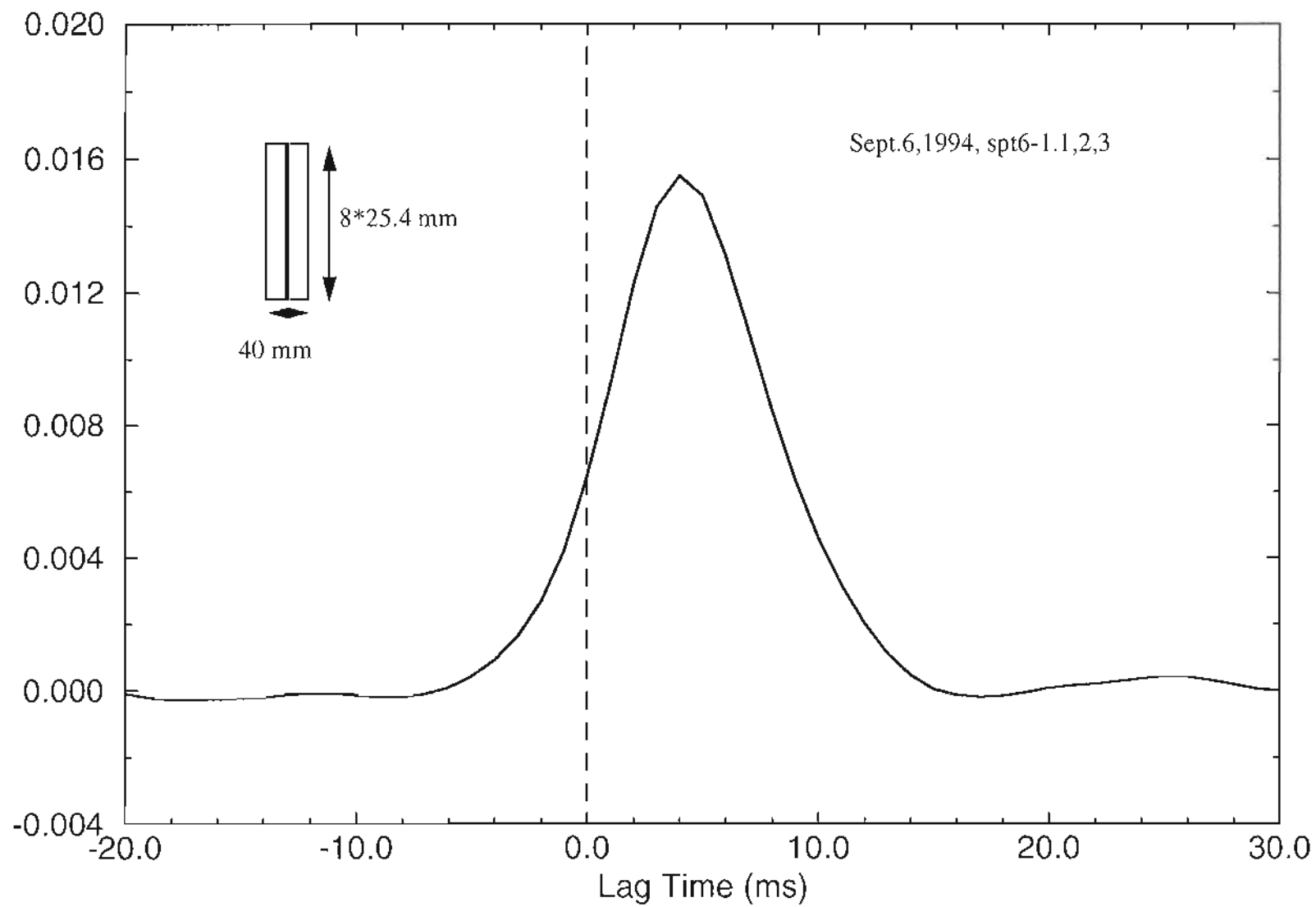


Figure 5.17 The TDC of experiment with two rectangular receivers of width=20 mm.

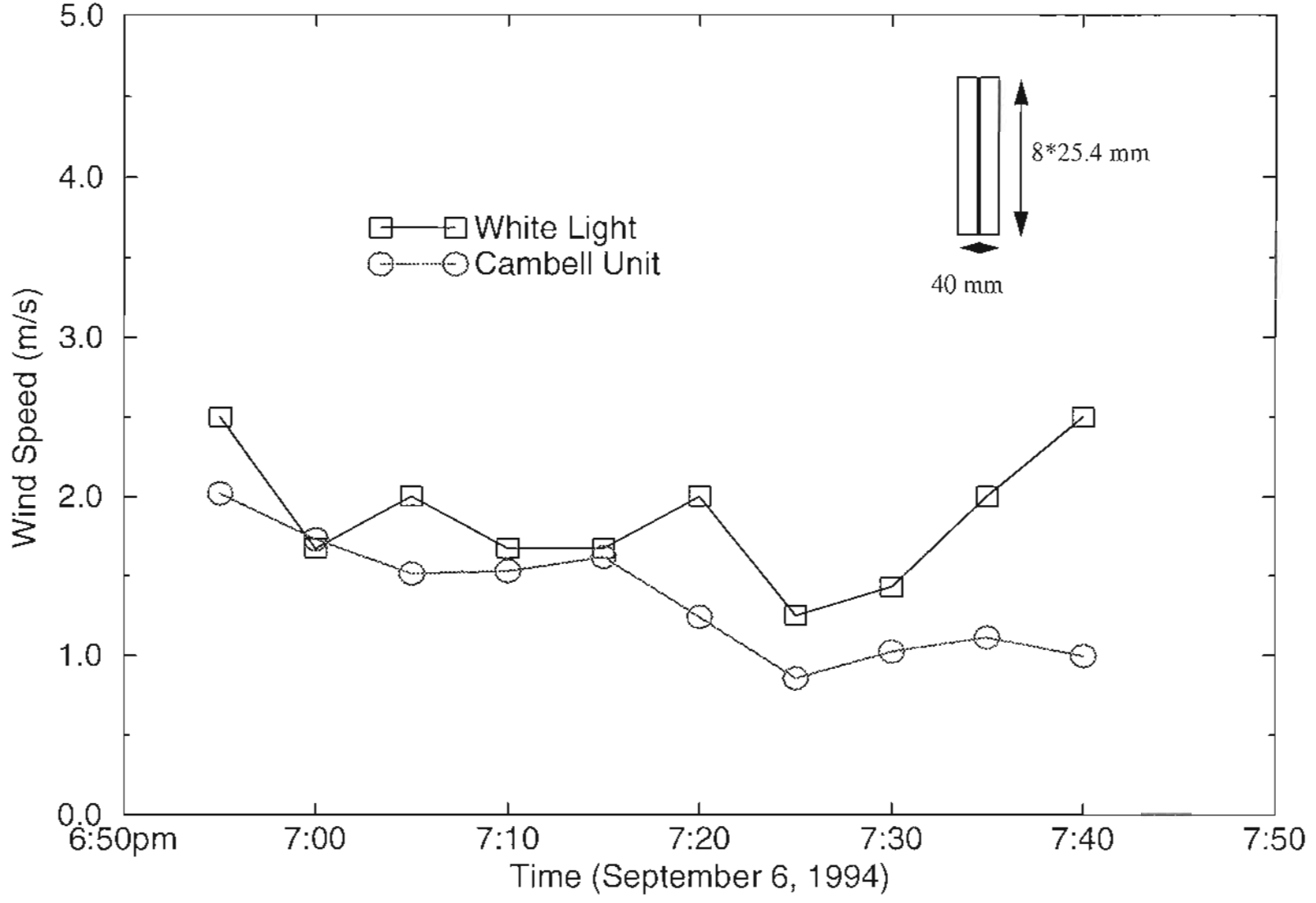


Figure 5.18 Cross wind measurements by both "White Light" and Campbell unit.

by the lag time between the two systems. A low time resolution of the TDC also introduces some error in the measurement. Taking the derivative to the simple equation

$$V = D / (2\tau) \quad (5.3)$$

The error of speed caused by misreading of the peak delay time τ is

$$\Delta V = \frac{D}{2\tau^2} \Delta\tau = \frac{V}{\tau} \Delta\tau \quad (5.4)$$

It is obvious that if wind is bigger, the error introduced by the finite time resolution is bigger. For example, if 3 m/s wind is measured, $D=20\text{mm}$, the correspond time delay measured is about 3 ms. That gives $\Delta V = 1.1 \text{ m/s}$.

Figure (5.19) is the TDC function of one data set obtained on September 20, 1994. The same rectangular receiver was used as in figure (5.17). The A/D trigger signal was changed to double pulses to trigger the two channel signals. The equivalent sampling rate is 2 khz as it was expected when the system was originally designed. The time resolution of TDC function is about 0.5 ms. The error of wind speed measurement introduced by the finite time resolution should reduce by a factor of 2 compared to figure (5.17). Ten consecutive sets of data were taken. Each has 24 k samples for each channel. The time series of wind speed measurements from both “White Light” and Campbell unit are obtained and plotted in figure (5.20). A very good match is found between the “White Light” system and the Campbell unit. The better performance is due to the higher sampling rate which increases the time resolution of the TDC function.

The information introduced by turbulence has frequency spectrum less than 1 khz. Increase sampling rate would result in over sampling. In addition, more data samples

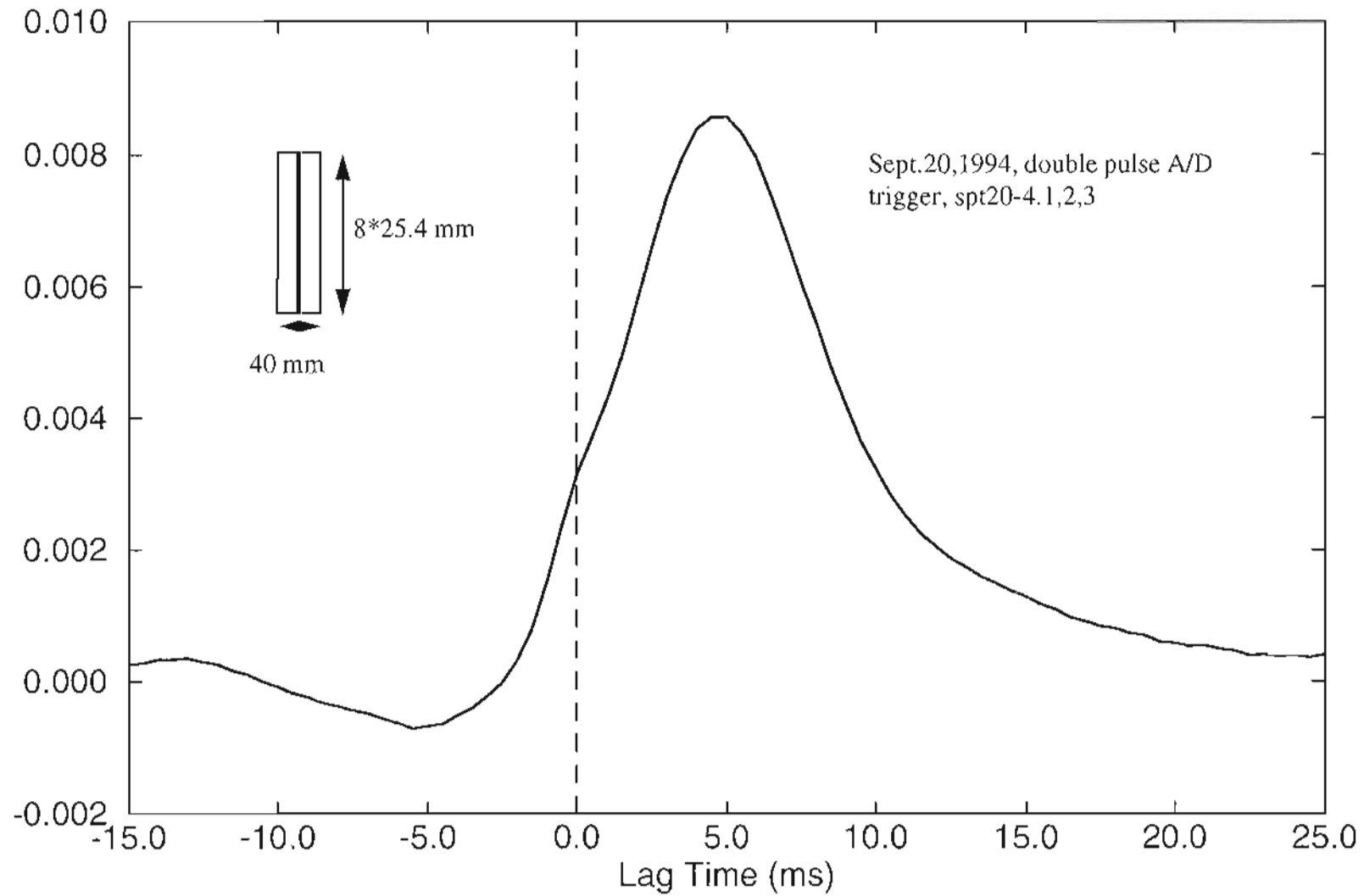


Figure 5.19 The TDC of experiment with rectangular receiver of width=20 mm, double pulse A/D trigger was used.

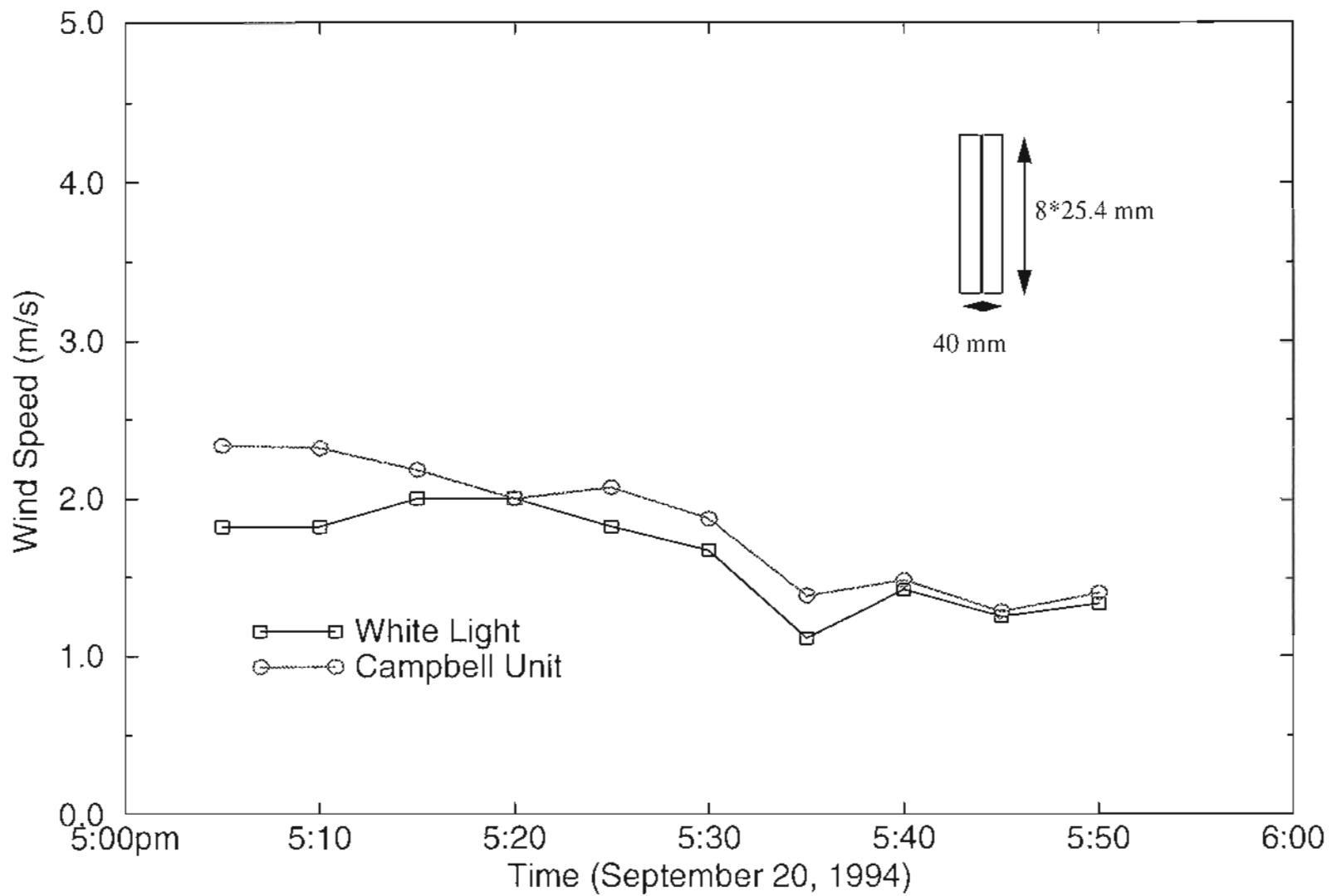


Figure 5.20 Cross wind measurements by both "White Light" and Campbell unit, double pulse A/D trigger was used.

would be needed to be processed and it would take a longer time to get enough information. More storage space would also be needed to store the data. There is a trade-off between precision of measurement and storage space and process time.

The final goal of this project was to measure wind speed using aerosols. A lot of time was spent trying to measure the cross wind speed using aerosols instead of hard target. It was found that during the day, the background noise from the sun is too big for the "White Light" system, due to the finite bandwidth of the optical filter. The background noise was much larger than expected and can saturate the photomultiplier tubes and the receiver electronics. Therefore, experiments can only be done during the night to measure signal off of aerosols. The intensity vs. range plot of figure (5.21) was produced by processing a set of recorded data. Each data point represents 24 k samples, 24 seconds worth of data average. The signal is very noisy, as it can be seen in figure (5.22), even at night. Many data sets were taken and intensity vs. range profile similar to figure (5.21) were obtained. The TDC function of the two channel signals from aerosols is very noisy, and no obvious peak can be seen for 24 seconds even for a 1-minute average.

There are several reasons which make it difficult to detect the cross wind speed at night using aerosols. The turbulence is low at night, so the correlation is low. There is barely any cross wind in the evening in the local area. The road lights make the background level high so the signal to noise ratio is bad. More samples may be needed to do the average so an adequate TDC can be obtained for calculating the cross wind speed. But nonstationary properties of the turbulence and electronics may effect the results if the averaging time is too long. Other better data processing schemes may be used in order to

get good results in a shorter averaging time. Small area detector arrays can also be designed, so higher correlation can be obtained between the adjacent detectors and then a spatial average can be applied to the TDC's of all the detector pairs.

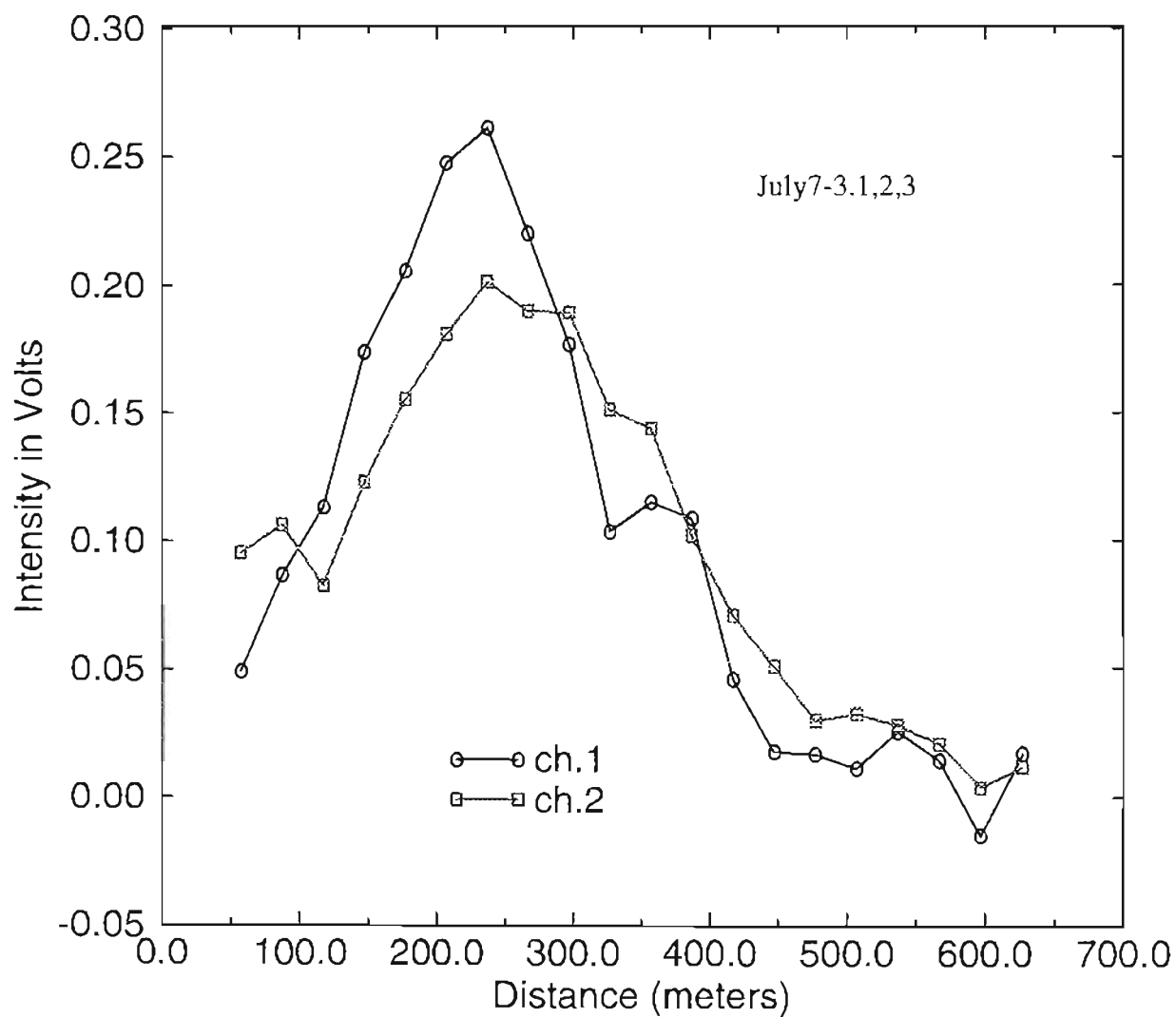


Figure S.21 Intensity vs. range profiles from aerosols produced by “White Light” system.

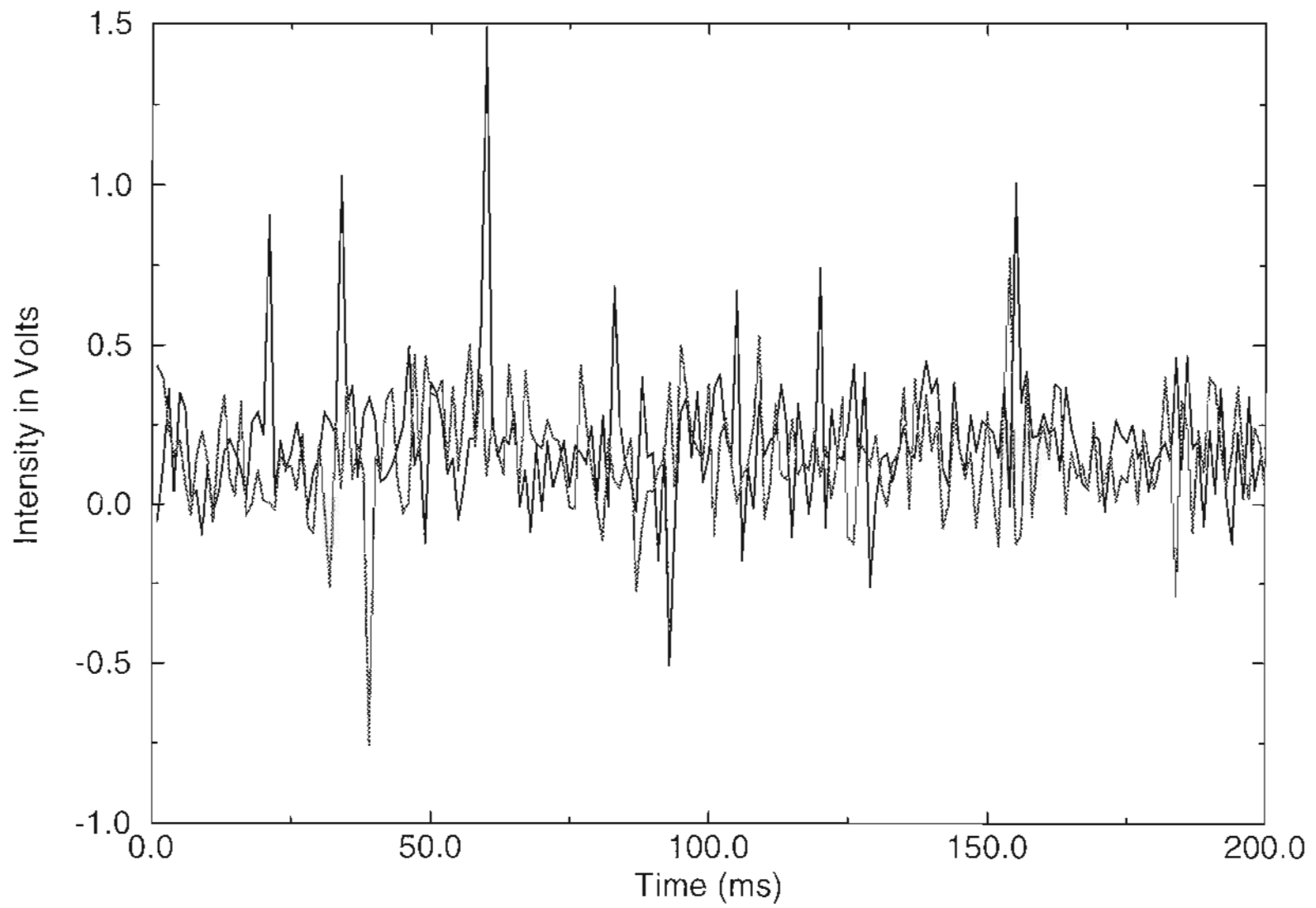


Figure 5.22 Two channels signals from aerosols at about 300 meters.

5.4 New Receiver and Processing Design

A 50/50 beam splitter was used to split the receiver area in two. Two knife edges are used for better control of the receiver area as shown in figure (5.23). More experiments have been conducted to investigate the aperture averaging and to find a better receiver design. By adjusting the positions of the two knife edges, two receiver areas are obtained as explained in figure (5.24). The common area is the overlapped part between the two receivers. The size of the common area is controlled by the two knife edges. The signals from both channels can be expressed as

$$S_1 = S_1' + S_c, \quad S_2 = S_2' + S_c \quad (5.5)$$

where S_1' and S_2' are signals from unoverlapped area, S_c is the signal from the common area. Cross correlating the two signals gives

$$\begin{aligned} C(\tau) &= \langle S_1 S_2 \rangle - \langle S_1 \rangle \langle S_2 \rangle = \\ &\langle S_1' S_2' \rangle - \langle S_1' \rangle^2 + 2(\langle S_1' S_c \rangle - \langle S_1' \rangle \langle S_c \rangle) + \langle S_c^2 \rangle - \langle S_c \rangle^2 \\ &= C'(\tau) + 2C_{sc}(\tau) + C_c(\tau) \end{aligned} \quad (5.6)$$

where $C_{sc}(\tau)$ is the covariance between the unoverlapped area and common area, C_c is the autocovariance of the common area. From Eq. (5.6), it is easy to see that the cross-

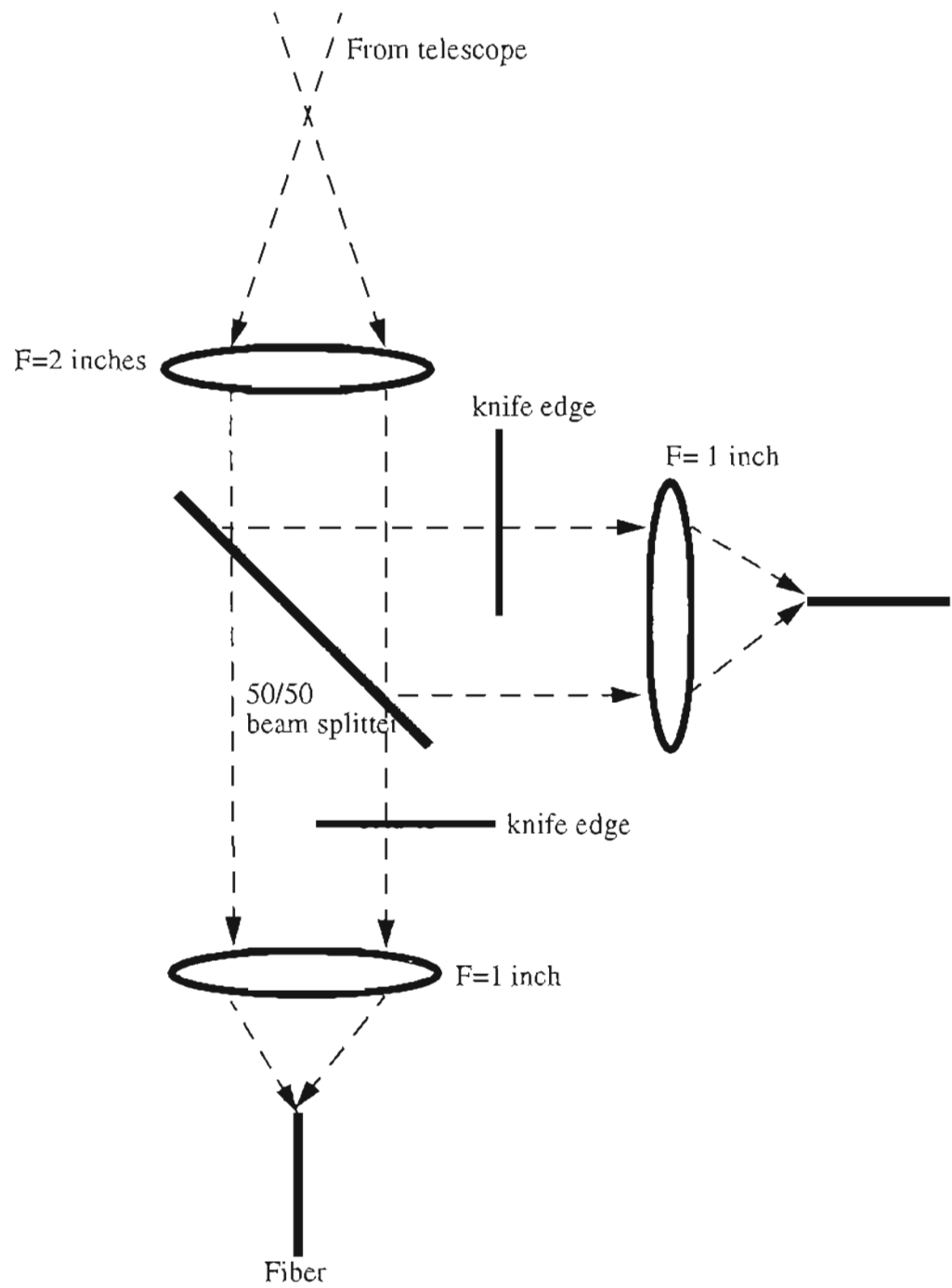


Figure 5.23 Diagram of receiver optics, where a 50/50 beam splitter and two knife edges are used.

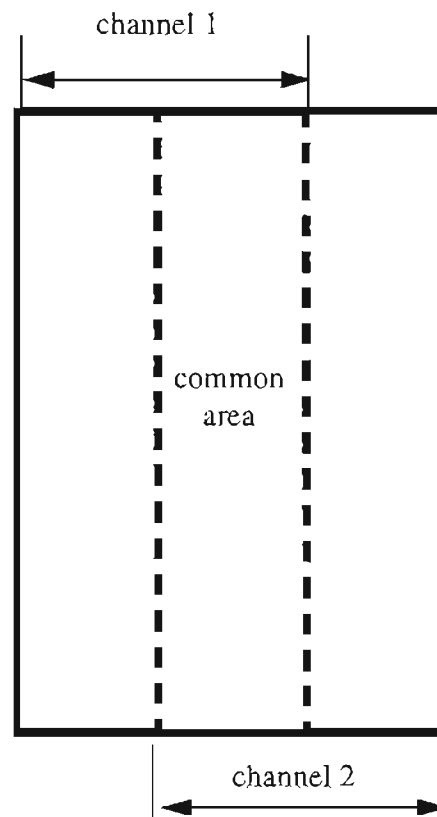


Figure 5.24 Equivalent receiver area for the receiver system shown in figure (5.23).

covariance of this receiver system is higher than the two simple rectangles without overlap. But the final term in Eq. (5.5) is the autocovariance which is not wanted. Some processing scheme is needed to remove the autocovariance part. Using the symmetrical property of autocovariance, one can generate a new function which keeps all the cross-covariance information without the autocovariance term.

$$c(\tau) = C(\tau) - C(-\tau) \quad (5.7)$$

Figures (5.25)-(5.29) are the experiment results of TDC with different sizes. The autocovariance are also subtracted and plotted in these figures. It can be seen that Eq. (5.7) can remove the autocovariance perfectly. The new function has a very smooth and clear slope at zero time delay, so it may be a better choice to use slope method to get the wind speed. More detail theoretical work is needed to describe the relationship between the wind speed and slope obtained by this scheme.

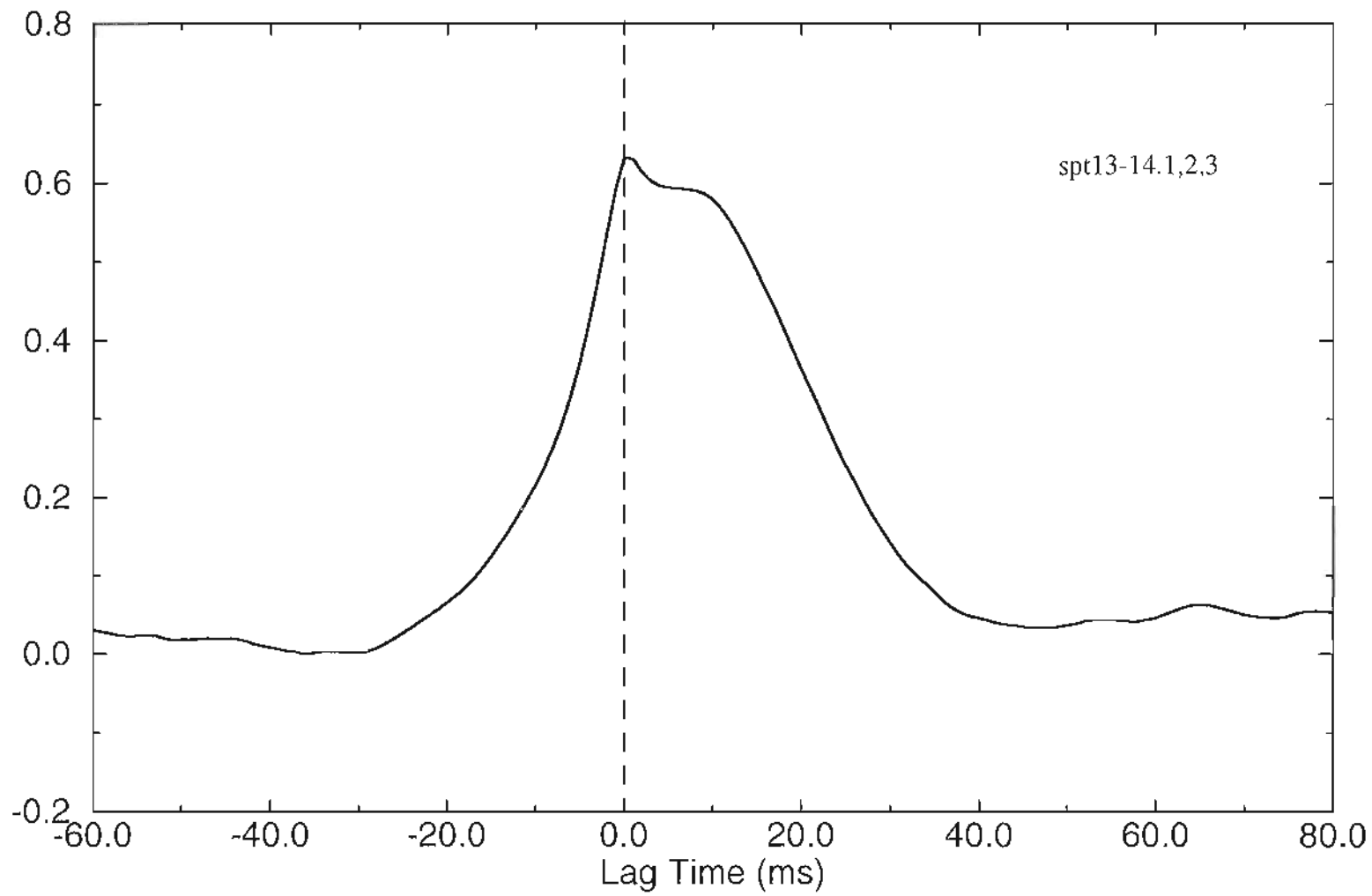


Figure 5.25 Cross covariance with autocovariance, bigger common area was used.

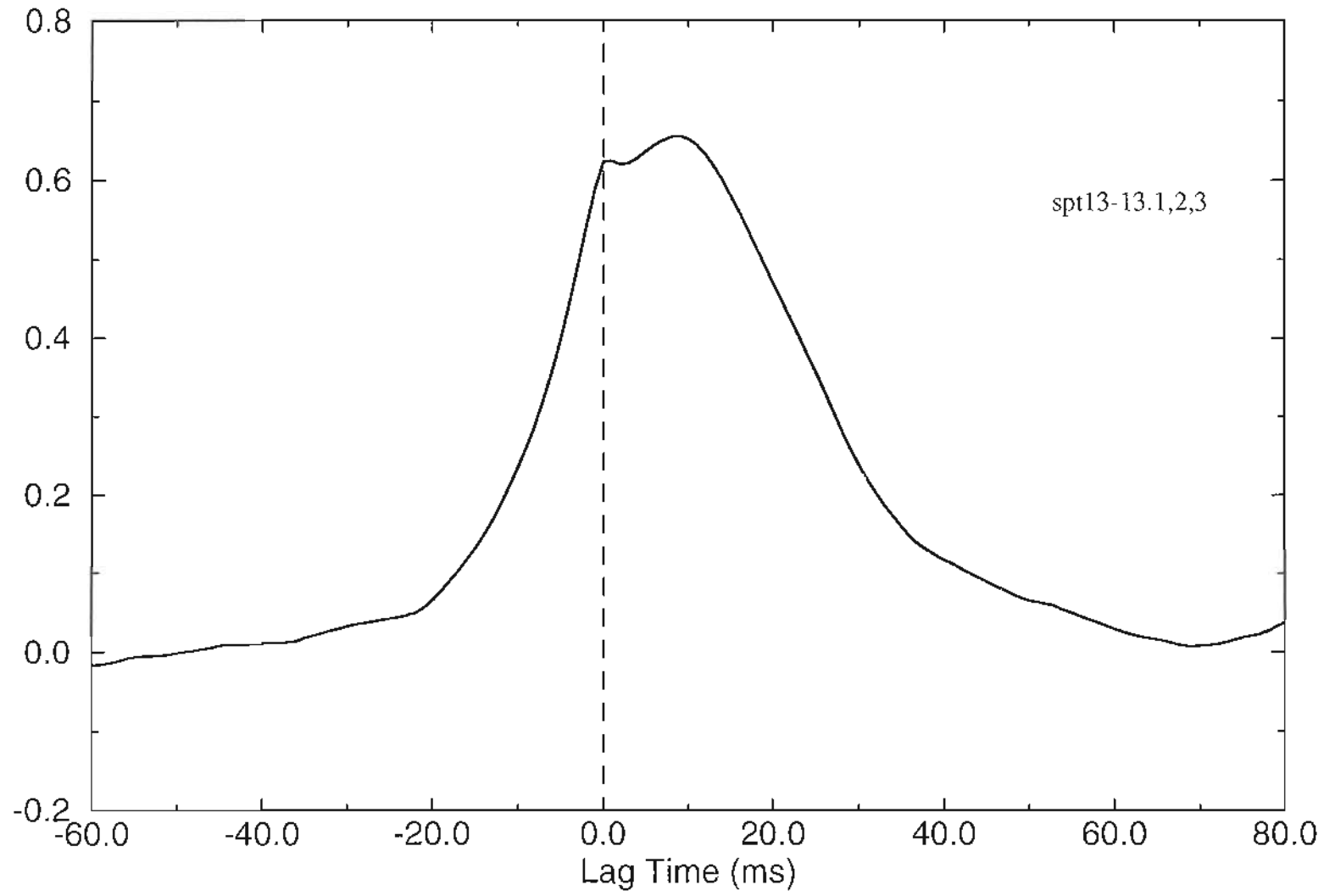


Figure 5.26 Cross covariance with autocovariance, smaller common area was used.

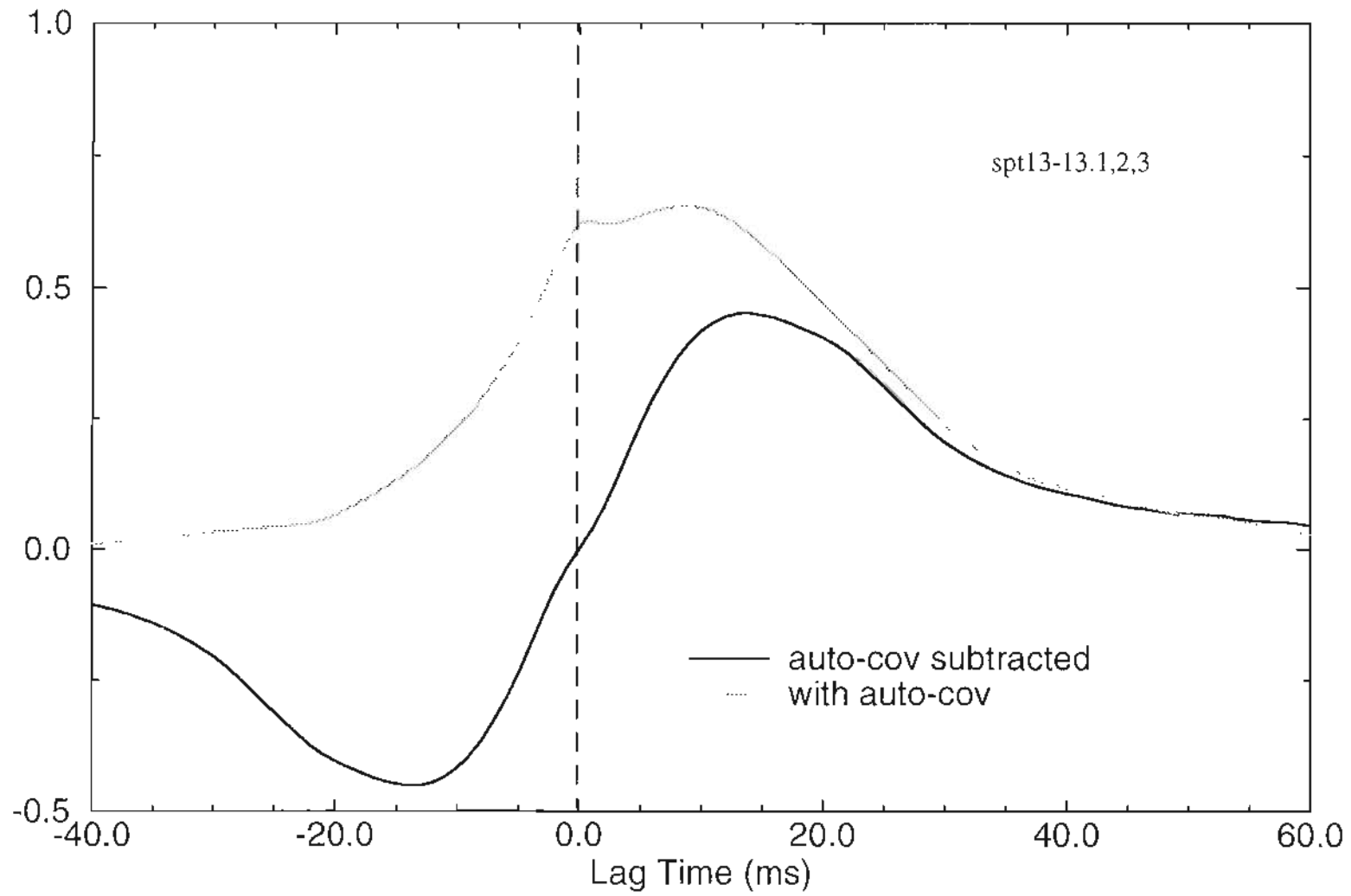


Figure 5.27 Cross covariance with autocovariance subtracted from figure (5.26).

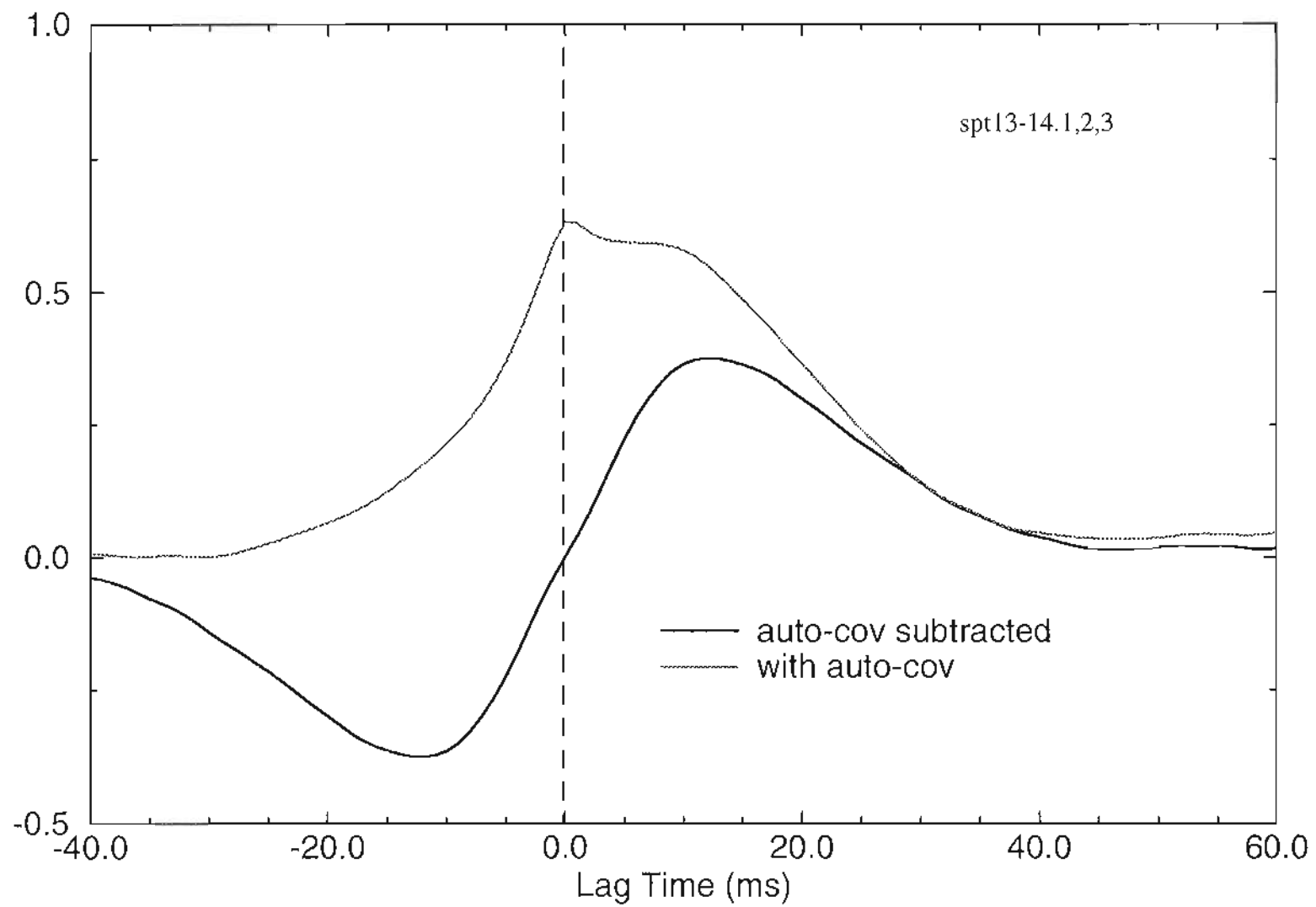


Figure 5.28 Cross covariance with autocovariance subtracted from figure (5.25).

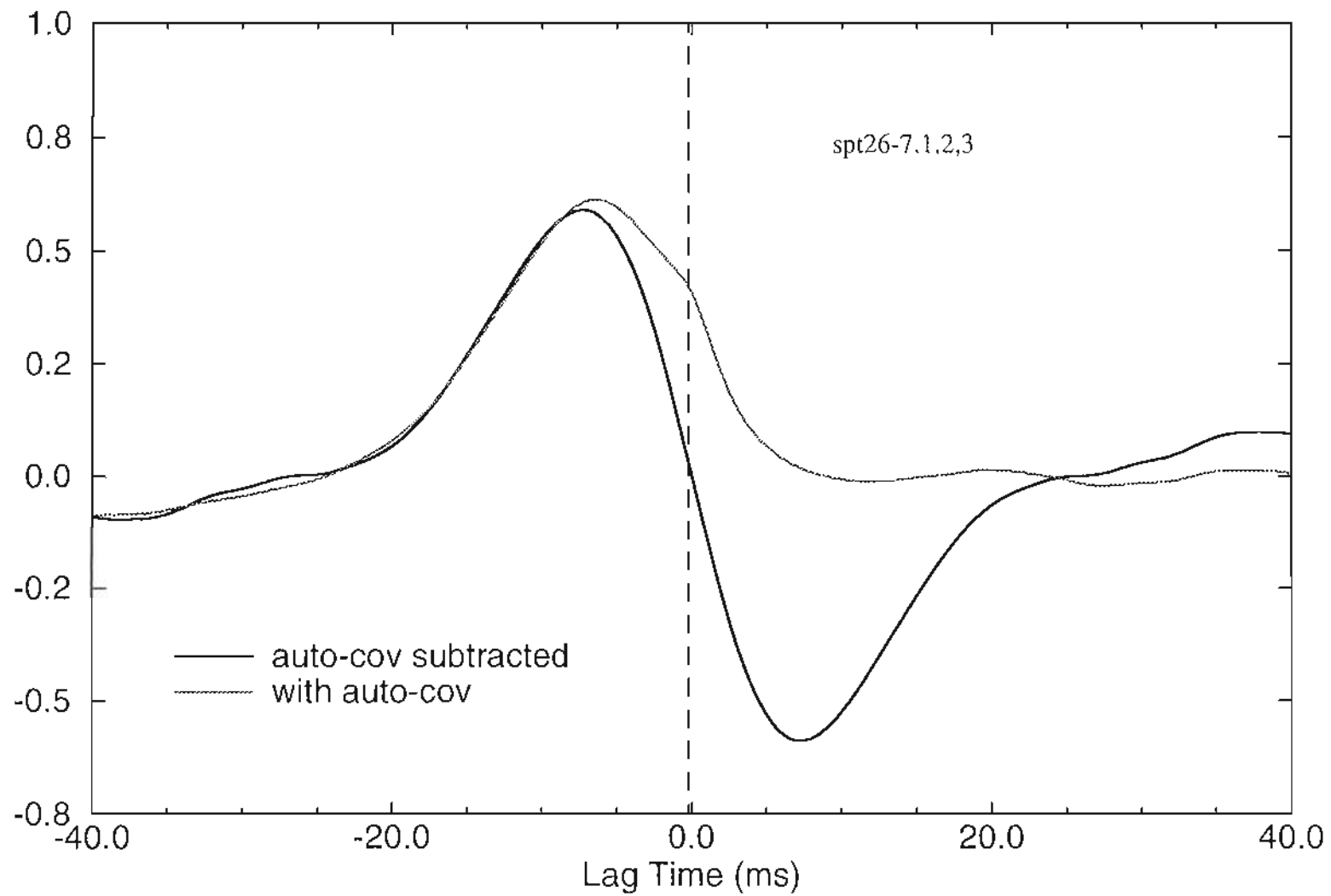


Figure 5.29 Cross covariances before and after autocovariance is subtracted.

Chapter 6

Conclusions and Future Work

The primary goal of this research project was to build a range resolved lidar system for single-ended remote sensing of atmospheric cross wind using speckle turbulence interaction in conjunction with optical direct detection. This was accomplished by using a pseudo random code (PRC) modulated continuous wave (CW) AlGaAs laser as the source, highly sensitive photomultiplier tubes as detectors and an integration detection scheme. A strong interaction between a laser with wavelengths in the near infrared and turbulence was observed as expected. Using the experimental apparatus, cross wind measurements were made in the atmosphere over a flat and featureless terrain. Good agreement between experimental data and the numerical analysis of the theory demonstrated the potential of a portable and reliable wind measurement system for the real world.

The transmitter is a single transverse-mode multi-frequency semiconductor laser. Therefore previously developed wave propagation theory for a polychromatic source must be used. For a laser source with very low vacuum speckle contrast ratio (VSCR), the coherent term of the formulation can be dropped. If these frequencies are very close, a central frequency can be used, so simplified formulations can be obtained. Consequently, the wind sensing processing scheme for the monochromatic case can be adopted. Based on the previous theory, some development and simplifications were made so numerical analysis can be implemented for finite receiving area. Satisfactory numerical calculations

were performed on the SUN work station using the Gauss Quadrature approximation. The autocovariance and TDC functions of fairly good accuracy were obtained in a reasonable amount of computing time. Detailed numerical analysis of the peak amplitude of the TDC function on the specific problem of the "White Light" system showed the aperture averaging effect.

A coaxial system was used for the receiver. One advantage of a coaxial system is that no weighting function is produced as for a biaxial system, so a wider detecting range can be reached. Another is that the spider inside the telescope can block the near field so the dynamic range of the received signal is reduced which makes the design of receiver electronics easier. Semiconductor lasers and fibers made the system very compact and easy to control. Fibers were used to deliver the receiving optical signal and it could also be used for controlling the field-of-view. Intensity vs. range curve were obtained using the Gaussian beam expressions for the laser beam.

Pseudo random code modulation made it possible to run the transmitter as CW and still have range resolving capability. Modulation codes can be directly applied to the semiconductor laser as a driving current. Integration detection has the advantage of demodulating the code to resolve the range and improve the signal to noise ratio, so a high power laser is not needed. Different coding schemes were proposed by other researchers and some were claimed to have better performance than others in terms of signal to noise ratio. Analysis and simulations in chapter 4 did not show the advantage of the A-1 and A-2 sequences over the M-sequence. But they are all easy to generate and work well for CW lidar systems.

A great amount of time was devoted to hardware design and testing. It was found that the multiplier AD734 is very sensitive to temperature. The offset fluctuations associated with environment temperature buried in the signal and can be significant when detecting weak signal from aerosols. Isolation between the digital part and analog part of the electronics is another which requires attention in the design. Usually it is good practice to separate these two parts into two boxes. The modulation input of the diode laser controller has an input impedance of 50 ohms which requires the PRC generator to have a high driving capability. Bipolar parts should be used at the output stage of the PRC instead of MOS devices to avoid interaction of the load to the rest of the circuit. The selection signals for delay time of the local PRC code are connected to the PC through the A/D board. So the selection is done automatically by the A/D program. Since simultaneous sampling is required to record the data, it is important to design the A/D trigger carefully to make sure it fits the specific A/D board.

The aperture averaging effect was studied in detail using numerical analysis. The results of the numerical calculation of the autocovariance and time delayed covariance for the "White Light" system can be generalized to guide the design of similar systems. An optimum receiver size should be chosen from the simulation so a better system can be designed and better measurements can be obtained.

Experiments over a variety of atmospheric conditions showed that the "White Light" system works well for a hard target. The experimental results also demonstrate the range resolve ability of the system. Good matches of experimental results of the autocovariance and TDC with theoretical predictions showed that the theory about statistics of polychro-

matic speckle propagation developed in the past and the new extension on the finite aperture case is correct. The accuracy of the wind measurements depends on the sampling rate and detector distance. There is a trade-off between sampling rate and memory space and processing time. For atmospheric wind measurement using speckle turbulence interaction, the signal bandwidth is less than 1 KHz. So a sampling rate of more than 2 KHz is appropriate. Since in most cases, a finite receiver area is used, the aperture averaging effect must be considered. An effective detector spacing was used for processing the experimental data to get the wind speed using the peak delay method. More accurate results can be obtained using the formulation of a finite receiver. But complex theoretical analysis must be performed to predict the simple solution. Since the aperture averaging is a very complicated process, it may be a better choice using the slope method to process the data. And as it was seen in section 5.4, it is possible to increase the magnitude of the TDC to increase the detectability using the scheme suggested.

Angle of arrival fluctuations were also observed during the experiment. This phenomenon is associated with gradient fluctuations of the refractive index due to temperature gradient changes. It is a severe problem for an optical system with short wavelength. Noticeable displacement of the receiving image was observed that adjustment to the receiver fibers had to be made for very different atmospheric conditions, for example, between noon and evening. This should be a concern of the design and application of the future systems.

Attempts to measure the cross wind speed using aerosols were not successful. Reasons are as discussed as in section 5.3. A longer time average is needed and new process-

ing scheme must be investigated. To make the measurement possible during the day, better control of the frequency of a high quality semiconductor laser is needed, so that a narrower optical filter can be used to filter out the large background light. With the development of more powerful diode lasers, it should be possible to design a wind measurement system for practical applications.

As discussed in chapter 5, detector arrays can be implemented in the system to improve the signal to noise ratio and detectability. Using a detector array can avoid the aperture averaging effect and spatial averaging over all the pairs of detectors will improve the signal to noise ratio of the TDC. The two dimensional wind is also available by using detector array. With modern DSP chips, all the PRC code generator, digital logic and signal and data processing circuits can be integrated in a single chip. Combining the DSP and semiconductor technology, very reliable and compact lidar systems can be achieved.

REFERENCES

1. R. S. Lawrence and J. W. Strohbehn, "A survey of clean-air propagation effect relevant to optical communications," Proc. IEEE **58**, 1523, October 1970.
2. R. L. Fante, "Electromagnetic beam propagation in turbulent media," Proc. IEEE **63**, 1669, December 1975.
3. R. W. Lee and J. C. Harp, "Weak scattering in random media, with applications to remote sensing," Proc. IEEE **57**, 375, April 1969.
4. D. L. Fried, "Remote probing of the optical strength of atmospheric turbulence and wind velocity," Proc. IEEE **57**, 415, April 1969.
5. R. S. Lawrence, G. R. Ochs, and S. F. Clifford, "Use of scintillations to measure average wind across a light beam," Appl. Opt. **11**, 239, February 1972.
6. G. R. Ochs, S. F. Clifford, and Ting-i Wang, "A feasibility study of an optical crosswind monitor," NOAA Technical Memorandum ERLWPL-10, US Department of Commerce, National Oceanic and Atmospheric Administration, Wave Propagation Laboratory, Boulder, Colorado 80302, September 1973.
7. G. R. Ochs and G. F. Miller, "Pattern velocity computers - two types developed for wind velocity measurements by optical means," Rev. of Sci. Instrum., **43**, 879, 1972.
8. T. H. Pries and E. T. Young, "Evaluation of a laser crosswind system," U.S. Army Electronics Command, Research and Development Technical Report ECOM-5546, 1974.
9. G. R. Ochs, S. F. Clifford, and Ting-i Wang, "Laser wind sensing: the effect of saturation of scintillation," Appl. Opt. **15**, 403, February 1976.

10. R. Targ, J. G. Hawley, B. C. Steakley, L. L. Ames and P. Robinson, "Airborne lidar wind detection at 2 μ m," Coherent Laser Radar, 1995 Technical Digest Series, Vol. 19, 178.
11. Timothy J. Dasey and Richard Heinrichs, "An algorithm for recognition and tracking of aircraft wake vortices with a continuous wave coherent laser radar" Coherent Laser Radar, 1995 Technical Digest Series, Vol. 19, 193.
12. R. M. Heinrichs, R. E. Freehart, T. J. Dasey, and R. S. Mandra, "Development and performance of a CW coherent laser radar for detecting vortices," Coherent Laser Radar, 1995 Technical Digest Series, Vol. 19, 186.
13. E. P. Gordov, G. S. Khmel'nitskii and A. Z. Fazliev, "Multi-purpose CW CO₂ auto-dyne lidar," Coherent Laser Radar, 1995 Technical Digest Series, Vol. 19, 172.
14. Wynn L. Eberhard, "Distinguishing ice and water clouds using dual-wavelength CO₂ lidar: theory," Coherent Laser Radar, 1995 Technical Digest Series, Vol. 19, 156.
15. P. Beckmann and A. Spizzichino, The scattering of electromagnetic waves from rough surface, Pergaman/Macmillan, London, New York, 1963.
16. J. W. Goodman, "Statistical properties of laser speckle patterns," in Laser Speckle and Related Phenomena, J. C. Dainty, Springer, Berlin 1975.
17. J. F. Holmes and J. R. Kerr, "Pulsed laser, remote crosswind measurement system--Feasibility study and design," U.S. Army Electronics Command, Research and Development Technical Report ECOM74-0094-1, Atmospheric Sciences Laboratory, White Sand Missile Range, New Mexico 88002, July 1974.
18. J. F. Holmes, J. R. Kerr, M. E. Fossey, R. L. Jacob, and M. H. Lee, "Experimental pulsed laser, remote crosswind measurement system--Feasibility study and design (part II)," U.S. Army Electronics Command, Research and Development Technical Report ECOM75-1, Atmospheric Sciences Laboratory, White Sand Missile Range, New Mexico 88002, July 1975.
19. J. F. Holmes, J. R. Kerr, M. E. Fossey, R. L. Jacob, and M. H. Lee, "Experimental pulsed laser, remote crosswind measurement system--Feasibility study and design (part III)," U.S. Army Electronics Command, Research and Development Technical Report ECOM75-4, Atmospheric Sciences Laboratory, White Sand Missile

Range. New Mexico 88002, July 1975.

20. J. F. Holmes, J. R. Kerr, M. E. Fossey, and M. H. Lee, "Experimental pulsed laser, remote crosswind measurement system--Feasibility study and design (part IV)," U.S. Army Electronics Command, Research and Development Technical Report FA-TR-76065, Frankford Arsenal, Philadelphia, Pennsylvania 19137, November 1976.
21. J. F. Holmes, J. R. Kerr, R. A. Elliott, M. H. Lee, P. A. Pincus and M. E. Fossey, "Experimental pulsed laser, remote crosswind measurement system--Feasibility study and design (part V)," U.S. Army Electronics Command, Research and Development Technical Report ARSCD-CR-79-007, Fire Control and Small Caliber Weapon Systems Laboratory, Dover, New Jersey, June 1978.
22. J. F. Holmes and B. John Rask, "Optimum. optical local oscillator power levels for coherent detection using photodiodes," Appl. Opt., December, 1994.
23. Jeffry Rothermel, Robert M. Hardesty, and Robert T. Menzies, "Airbone scanning pulsed coherent doppler laser radar for atmospheric measurement and satellite doppler lidar simulation." Coherent Laser Radar, 1995 Technical Digest Series, Vol. 19,134.
24. R. T. Menzies, "Doppler lidar atmospheric wind sensors: acomparative performance evaluation for global measurement applications from earth orbit," Appl. Opt. **25**, 2546, August 1986.
25. Farzin Amzajerdian, *Remote sensing of atmospheric winds by utilizing speckle-turbulence interaction and optical heterodyne detection*, Ph. D. thesis at Department of Electrical Engineering & applied Physis. Oregon Graduate Institute of Science & Technology, June, 1988.
26. J. F. Holmes, J. M. Hunt, F. Amzajerdian, and V. S. R. Gudimetla, "An optical system for remote wind sensing using speckle-turbulence interaction," Proc. of the conference on Laser and Electronics, June 9-13, 1986, San Francisco, California.
27. Nobo Takeuchi, Hiroshi Baba, Katsumi Sakurai, and Toshiyuki Ueno, "Diode-laser random-modulation CW lidar," Appl. Opt., Vol. 25, No. 1, January 1986.
28. Badih John Rask, *Range Resolved Optical Remote Sensing Using a Continuous Wave, Pseudo-Random Modulated, Heterodyne Lidar Backscattered from Aero-*

- sols*, Ph.D. thesis, Department of Electrical Engineering & Applied Physics, Oregon Graduate Institute of Science & Technology. June, 1995.
29. Chikao Nagasawa, Makoto Abo, Hideki Yamamoto, and Osamu Uchino, "Random modulation CW lidar using new random sequence." Appl. Opt. Vol. 29, No. 10, April 1990.
 30. Jonathan A. R. Rall, *Differential Absorption Lidar Measurements of Atmospheric Water Vapor Using a Pseudonoise Code Modulated AlGaAs Laser*, NASA Technical Memorandum 104610, Ph.D. thesis at NASA Goddard Space Flight Center, Greenbelt, Maryland.
 31. D. M. Norman and C. S. Gardner, "Satellite laser ranging using pseudonoise code modulation laser diodes," Appl. Opt. **27**, 3650 (1988).
 32. J. B. Abshire, J. A. R. Rall, S. S. Manizade, "Altimetry and lidar using AlGaAs lasers modulated with pseudo-random codes," 16th International Laser Radar Conference, NASA Conference Publication 3158, Part 2, pp 441, Boston, MA July 20-24, 1992.
 33. J. A. R. Rall, J. B. Abshire, S. S. Manizade, "Lidar measurements of clouds and aerosols using AlGaAs lasers modulated with pseudorandom codes," IEEE Lasers and Electro-Optics Society 1992 Annual Meeting Conference Proceedings, Boston MA, November 16-19, 1992.
 34. J. B. Abshire and J. A. R. Rall, "AlGaAs lidar-theory & measurement," in Optical Remote Sensing of the Atmosphere Technical Digest, 1993 (Optical Society of America, Washington D. C., 1993), Vol. 5, postdeadline papers.
 35. N. Takeuchi, N. Sugimoto, H. Baba, and K. Sakurai, "Random modulation CW lidar," Appl. Opt. **22**, 1383 (1983).
 36. M. H. Lee, J. F. Holmes and J. R. Kerr, "Statistics of speckle propagation through the turbulent atmosphere," J. Opt. Soc. Am. **66**, 1164(1976).
 37. J. F. Holmes, M. H. Lee and J. R. Kerr, "Effect of the log-amplitude covariance function on the statistics of speckle propagation through the turbulent atmosphere," J. Opt. Soc. Am. **70**, 355 (1980).

38. V. S. Rao Gudimetla, *Statistics of Polychromatic Speckle Propagation Through the Turbulent Atmosphere*, Ph. D. thesis at Department of Electrical Engineering & Applied Physics, Oregon Graduate Institute of Science & Technology, April 1982.
39. J. L. Lumley and H. A. Panofsky, The structure of the atmospheric turbulence, Wiley-Inter Science, New York, 1964.
40. A. S. Monin and Y. M. Yaglom, Statistical fluid mechanics, MIT Press, Cambridge, Massachusetts 1971.
41. R. J. Hill, "Models of the scalar spectrum for turbulent advection," J. Fluid Mech. **88**, 541 (1978).
42. V. I. Tatarskii, Wave propagation in a turbulent medium (Trans. R. A. Silberman), McGraw Hill, New York, 1961.
43. V. I. Tatarskii, The effect of the turbulent atmosphere on wave propagation, Springfield, U.S. Dept. Commerce, 1971.
44. A. Ishimaru, Wave propagation and scattering in random media, Vols. 1 and 2. Academic Press, New York 1978.
45. J. W. Strohbehn, Ed., Laser beam propagation in the atmosphere (Topics in Applied Physics, Vo. 25) Springer Verlag 1978.
46. H. M. Pedersen, "Second order statistics of light diffracted from Gaussian rough surfaces with applications to the roughness dependence of speckles," Opt. Acta **22**, 523 (1975).
47. G. Parry, "The scattering of polychromatic light from rough surfaces: the first order statistics," Opt. and Quant. Electron. **7**, 311 (1975).
48. H. M. Pedersen, "On the contrast of polychromatic speckle patterns and its dependence on surface roughness," Opt. Acta **22**, 15 (1975).
49. J. W. Goodman, "Statistical properties of laser speckle patterns," Tech. Reprt ,No. 2303-1, System Laboratory, Stanford Electronics Laboratories, Stanford, California (1963).

50. D. L. Fried, "Spectral and angular covariance of scintillation for propagation in randomly homogeneous medium," Appl. Opt. **10**, 721 (1971).
51. P. Pincus and J. R. Kerr, "Spectral covariance of scintillations," Appl. Opt. **15**, 2305 (1976).
52. Larry C. Andrews, "Aperture-averaging factor for optical scintillations of plane and spherical waves in the atmosphere," J. Opt. Soc. Am. A, Vol. 9, No. 4, April 1992.
53. D. L. Fried, "Aperture averaging of scintillation," J. Opt. Soc. Am. **57**, 169-175 (1967).
54. R. F. Lutomirski and H. T. Yura, "Aperture-averaging factor of a fluctuating light signal," J. Opt. Soc. Am. **59**, 1247-1248 (1969).
55. S. J. Wang, Y. Baykal, and M. A. Plonus, "Receiver-aperture averaging effect for the intensity fluctuation of a beam wave in the turbulent atmosphere," J. Opt. Soc. Am. **73**, 831-837 (1983).
56. V. S. Rao Gudimetla, J. F. Holmes, and Richard A. Elliott, "Two-point joint-density function of the intensity for a laser-generated speckle field after propagation through the turbulent atmosphere," J. Opt. Soc. Am. A, Vol. 7, No. 6, June 1990.
57. Joseph C. Palais, Fiber optical communications, Second Edition, 103-105. Prentice Hall Englewood Cliffs, NJ 07632.
58. F. Jessie MacWilliams and Neil J. A. Sloane, "Pseudo-random sequences and arrays," Proceedings of the IEEE, Vol. 64, No. 12, December, 1976.
59. Athanasios Papulis, Probability, random variables and stochastic process, Chapter 10.3, p285.
60. J. F. Holmes, "Further S/N calculation for white light," personal notes, June 25, 1992.
61. M. Abramowitz and I. A. Stegun, Handbook of mathematical functions, AMS 55. NBS, U.S. Dept. of Commerce, 1972.

Appendix A

Use the Confluent Hypergeometric Functions to simplify the term

(1)

$$func = \left\{ \frac{\exp(i(\pi/12))}{2i} F_1\left(-\frac{5}{6}; 1; -\frac{ib^2}{8a_1^2}\right) - \frac{\exp(-i(\pi/12))}{2i} F_1\left(-\frac{5}{6}; 1; \frac{ib^2}{8a_1^2}\right) \right\}$$

For small z , the Confluent Hypergeometric expansions can be used,

$$\begin{aligned} M(a, c, x) &= 1 + \frac{ax}{c1!} + \frac{a(a+1)x^2}{c(c+1)2!} + \dots \\ &= \sum \frac{(a)_n x^n}{(c)_n n!} \quad c \neq 0, -1, -2, -3, \dots \end{aligned} \quad (2)$$

let $k = \pi/12$, $a = -5/6$, $y = b^2/(8a_1^2)$, $c = 1$, then,

$$\begin{aligned} func &= \frac{\cos(k) + i \sin(k)}{2i} \left(1 - i \frac{a}{c} y - \frac{a(a+1)y^2}{c(c+1)2!} + i \frac{a(a+1)(a+2)y^3}{c(c+1)(c+2)3!} + \dots \right) \\ &\quad - \frac{\cos(k) - i \sin(k)}{2i} \left(1 + i \frac{a}{c} y - \frac{a(a+1)y^2}{c(c+1)2!} - i \frac{a(a+1)(a+2)y^3}{c(c+1)(c+2)3!} + \dots \right) \\ &= (\cos(k)) \left[-\frac{a}{c} y + \frac{a(a+1)(a+2)y^3}{c(c+1)(c+2)3!} - \frac{a(a+1)(a+2)(a+3)(a+4)y^5}{c(c+1)(c+2)(c+3)(c+4)5!} + \dots \right] \\ &\quad + (\sin(k)) \left[1 - \frac{a(a+1)y^2}{c(c+1)2} + \frac{a(a+1)(a+2)(a+3)y^4}{c(c+1)(c+2)(c+3)4!} + \dots \right] \end{aligned} \quad (3)$$

When $Z \geq 4\pi$, Asymptotic expansion must be used,

$$M(a, b, Z) = \frac{\Gamma(b)}{\Gamma(b-a)} \exp(\pm i\pi a) Z^{-a} \sum_{n=0}^{R-1} \frac{(a)_n (1+a-b)_n}{n!} (-Z)^{-n} \\ + \frac{\Gamma(b)}{\Gamma(a)} \exp(Z) Z^{a-b} \sum_{n=0}^{S-1} \frac{(b-a)_n (1-a)_n}{n!} Z^{-n} \quad (4)$$

+ sign is used when $-\frac{1}{2}\pi < \arg Z < \frac{3}{2}\pi$, - sign is used when $-\frac{3}{2}\pi < \arg Z \leq -\frac{1}{2}\pi$, so

$$\begin{aligned} \text{func} &= \frac{1}{2i} \left\{ \exp(ik) \left[\frac{\Gamma(b)}{\Gamma(b-a)} \exp(-i\pi a) (-iy)^{-a} \sum_{n=0}^{R-1} \frac{(a)_n (1+a-b)_n}{n!} (iy)^{-n} \right. \right. \\ &\quad \left. \left. + \frac{\Gamma(b)}{\Gamma(a)} \exp(-iy) (-iy)^{(a-b)} \sum_{n=0}^{S-1} \frac{(b-a)_n (1-a)_n}{n!} (-iy)^{-n} \right] \right. \\ &\quad \left. - \exp(-ik) \left[\frac{\Gamma(b)}{\Gamma(b-a)} \exp(i\pi a) (iy)^{-a} \sum_{n=0}^{R-1} \frac{(a)_n (1+a-b)_n}{n!} (-iy)^{-n} \right. \right. \\ &\quad \left. \left. + \frac{\Gamma(b)}{\Gamma(a)} \exp(iy) (iy)^{(a-b)} \sum_{n=0}^{S-1} \frac{(b-a)_n (1-a)_n}{n!} (iy)^{-n} \right] \right\} \\ &= \frac{1}{2i} \left\{ \frac{\Gamma(b)}{\Gamma(b-a)} e^{i(k-\pi a+\pi a/s)} y^{-a} \sum_{n=0}^{R-1} \frac{(a)_n^2}{n!} \exp(-in\pi/2) y^{-n} \right. \\ &\quad \left. + \frac{\Gamma(b)}{\Gamma(a)} e^{i[k-y-\pi(a-b)/2]} y^{(a-b)} \sum_{n=0}^{S-1} \frac{(1-a)_n^2}{n!} \exp\left(in\frac{\pi}{2}\right) y^{-n} \right. \\ &\quad \left. - \frac{\Gamma(b)}{\Gamma(b-a)} e^{i[-k+\pi a-\pi a/2]} y^{-a} \sum_{n=0}^{R-1} \frac{(a)_n^2}{n!} \exp\left(in\frac{\pi}{2}\right) y^{-n} \right. \\ &\quad \left. - \frac{\Gamma(b)}{\Gamma(a)} e^{i[-k+y+\pi(a-b)/2]} y^{(a-b)} \sum_{n=0}^{S-1} \frac{(1-a)_n^2}{n!} \exp\left(-in\frac{\pi}{2}\right) y^{-n} \right\} \end{aligned}$$

$$\begin{aligned}
&= \frac{1}{2i} \left\{ \frac{1}{\Gamma(b-a)} y^{-a} \sum_{n=0}^{R-1} \frac{(a)_n^2}{n!} y^{-n} \left[e^{i[k-\pi a/2-\pi a/2]} - e^{i[-k+\pi a/2+n\pi/2]} \right] \right. \\
&\quad \left. \frac{1}{\Gamma(a)} y^{(a-b)} \sum_{n=0}^{S-1} \frac{(1-a)_n^2}{n!} y^{-n} \left[e^{i[k-y-(a-b)\pi/2+\pi a/2]} - e^{i[-k-y+(a-b)\pi/2+n\pi/2]} \right] \right\} \\
&= \frac{1}{2i} \left\{ \frac{1}{\Gamma(1-a)} y^{-a} \sum_{n=0}^{R-1} \frac{(a)_n^2}{n!} y^{-n} \cdot 2i \sin \left[k - (a+n) \frac{\pi}{2} \right] \right. \\
&\quad \left. + \frac{1}{\Gamma(a)} y^{(a-1)} \sum_{n=0}^{S-1} \frac{(1-a)_n^2}{n!} y^{-n} \cdot 2i \sin \left[k-y - (a-1-n) \frac{\pi}{2} \right] \right\} \\
&= \frac{1}{\Gamma(1-a)} \sum_{n=0}^{R-1} \frac{(a)_n^2}{n!} y^{-(n+a)} \cdot \sin \left[k - (a+n) \frac{\pi}{2} \right] \\
&\quad + \frac{1}{\Gamma(a)} \sum_{n=0}^{S-1} \frac{(1-a)_n^2}{n!} y^{-(n+1-a)} \cdot 2i \sin \left[k-y + (n+1-a) \frac{\pi}{2} \right] \quad (5)
\end{aligned}$$

Appendix B

Programs for numerical analysis of the TDC of point detectors

(A) Newton trapezoidal method

```

c This program is called final.f, which uses Newton's trapezoidal
c rule to do the integration
c This program simulate time delayed covariance for two point
c detector case. the time delayed covariance is normalized by
c average intensity.

c all the parameters are read from a file called "parameters"
c the calculated results are stored in file "tdcpt.1"

    real td(-100:100), term(-100:100)

c a0 is beam size, L is the target distance, F is the focal distance
c Cn is the turbulence strength. V is the wind speed, P is the detector
c distance, k is the wave number
    real a0,L,F,Cn,V,P,k,lamda
    real rol0,rol,const,pi
    real a,a1,b,y,x,rolterm,temp
    real t,thita,H
    real a,co1(20),co2(20),cc1(20),cc2(20)

    double precision gama1,gama2,gama3,gama4
    double precision argu,bsl
    double precision s14aaf, arg1,arg2,arg3,arg4
    double precision s17aef
    external      s14aaf
    external      s17aef
    integer ifail

c print *, 'input beam size in (mm)'
c read(5,*) a0
c print *, 'input distance of the target in (m)'
c read(5,*) L
c print *, 'input focal distance in (m),10**5 for collimated'
c read(5,*) F
c print *, 'input trbulence strength'
c read(5,*) Cn

```

```

c   print *, 'input wind speed in (m/s)'
c   read(5,*) V
c   print *, 'input the detector distance in (mm)'
c   read(5,*) P
c   print *, 'input wavelength in (nm)'
c   read(5,*) lamda

      open(9,file='parameters')
      open(10,file='tdcpt.1')
      read(9,*)a0,L,F,Cn,V,P,lamda
c   print *, a0,L,F
c   print *, Cn,V,P,lamda
      pi=4.0*atan(1.0)
      a0=a0*0.001
      P=P*0.001
      k=2*pi*1.0e9/lamda
      a=-5./6.0
      rol0=(0.545625*Cn*L*k*k)**(-3./5.0)
      const=L*L/(2.*a0*a0*k**2)+2*(L/(k*rol0))**2
*      +a0*a0*(1-L/F)**2/2.
c   print *, k,rol0
c get gamma fuctions for the numbers in the calculation
      ifail=1
      arg1=11./6.
      arg2=-5.0/6.
      arg3=1.0/3.0
      arg4=1.0/6.0
      gama1=s14aaf(arg1,ifail)
      gama2=s14aaf(arg2,ifail)
      gama3=s14aaf(arg3,ifail)
      gama4=s14aaf(arg4,ifail)
      print *, gama1,gama2,gama3,gama4
c First loop is for different time delay td(i1), to get different
c covariance.

c small loop to get coefficients for regular expansion
      a=-5.0/6
      cc1(1)=-cos(pi/12)*a
      cc2(1)=sin(pi/12)
      do i=2,18
      cc1(i)=-cc1(i-1)*(a+2*i-2)*(a+2*i-3)/((2*i-1)*(2*i-2))**2
      cc2(i)=-cc2(i-1)*(a+2*i-4)*(a+2*i-3)/((2*i-2)*(2*i-3))**2
      end do

```

c another small loop to get coefficients of the expansion

```

    col(0)=1
    co2(0)=1
    do i=1,18
    col(i)=(a+i-1)**2*col(i-1)/i
    co2(i)=(i-a)**2*co2(i-1)/i
c    print *, col(i),co2(i)
    end do

```

```

do 100 i1=-60,60    ! should be 100
    td(i1)=i1*.5e-3

```

c the forth loop is for different t, which is normalized

c distance

```

    H=0
    do 400 i4=1,1000 ! should be 1000
    t=i4*0.0009999
    a1=sqrt(t*(1-t)*L/(2*k))
    b=sqrt((P*t-V*td(i1))**2)
    y=(b**2)/(8.*a1**2)
    if(y.gt.12.56) goto 500    ! to use asymptotic expansion
    x=0
    do i=1,18
    x=x+(cc1(i)*y**(2*i-1)+cc2(i)*y**(2*i-2))
    end do
    goto 600

```

c when $y > 4\pi$ use asymptotic expansion

```

500    x=0.
    do i=0,18
    x=x+col(i)*y**(-i-a)*sin(pi/12.-(a+i)*pi/2.)/gama1+
    * co2(i)*y**(-i-1+a)*sin(pi/12.-y+(i+1-a)*pi/2)/gama2
    end do

```

```

600 H=H+(-3.*b**(5./3)*gama3**2*cos(pi/6)/(20*pi**(1./2)
    * *gama1)+3.*aa**(5./3)*gama4*x/(5*2**(1./6)))

```

c print *, y

c print *, H

```
400 continue

c end of the forth loop

    H=H*0.001
    term(i1)=exp(5.206*k*k*L*Cn*H)
c    print *,Cn,sterm

c to write the final result
    write(10,99)td(i1)*1.0e3,term(i1)
99    format(1x,f12.5,f20.10)
100 continue
c the end of the first loop
    close(10)

    stop
    end
```

(B) Use Gauss Quadrature intergration subroutines

```

c   This program is called final2.f
c   Gauss Quadrature intergration subroutines are used here to
c   calculate time delayed covariance for point detector case.
c   *** the result is normalized by average intensity ***

c   all the parameters are read from a file called "parameters"
c   the calulated results are stored in file "tdc.pt"

c   a0 is beam size, L is the target distance, F is the focal distance
c   Cn is the turbulence strength, V is the wind speed, P is the detector
c   distance, k is the wave number
real a0,L,F,Cn,V,P,k,lamda
real rol0,rol,pi
real a,aa,b,y,x
real t,H
real col(24),co2(24),cc1(24),cc2(24)
real td(-500:500),term(-500:500)
double precision gama1,gama2,gama3,gama4
double precision argu,bsl
double precision s14aaf, arg1,arg2,arg3,arg4
double precision s17aef
external    s14aaf
external    s17aef
integer ifail,N,itYPE

double precision var4(64)
double precision wt4(64)
double precision A4,B4
external d01bbf,d01bax,d01bay,d01baz,d01baw

c   print *, 'input beam size in (mm)'
c   read(5,*) a0
c   print *, 'input distance of the target in (m)'
c   read(5,*) L
c   print *, 'input focal distance in (m),10**5 for collimated'
c   read(5,*) F
c   print *, 'input trbulence strength'
c   read(5,*) Cn

```

```

c   print *, 'input wind speed in (m/s)'
c   read(5,*) V
c   print *, 'input the detector distance in (mm)'
c   read(5,*) P
c   print *, 'input wavelength in (nm)'
c   read(5,*) lamda
c   print *, 'what is number N'
c   read(5,*) N
c   print *, 'input itype'
c   read(5,*) itype

open(9,file='parameters')
open(10,file='tdc.pt')
read(9,*)a0,L,F,Cn,V,P,lamda,N,itype
pi=4.0*atan(1.0)
a0=a0*0.001
P=P*0.001
k=2*pi*1e9/lamda
a=-5.0/6.0
rol0=0.545625*Cn*L*k*k
c   print *, k,rol0
   ifail=0

   A4=0.0
   B4=1.0
c to get abscis and weights
   call d01bbf(d01baz,A4,B4,itype,N,wt4,var4,ifail)

c get gamma fuctions for the numbers in the calculation
   arg1=11./6.
   arg2=-5.0/6.
   arg3=1.0/3.0
   arg4=1.0/6.0
   gama1=s14aaf(arg1,ifail)
   gama2=s14aaf(arg2,ifail)
   gama3=s14aaf(arg3,ifail)
   gama4=s14aaf(arg4,ifail)
c   print *, gama1,gama2,gama3,gama4
c First loop is for different time delay td(i1), to get different
c covariance.

c small loop to get coefficients for regular expansion
   a=-5.0/6

```



```

cc1(1)=-cos(pi/12)*a
cc2(1)=sin(pi/12)
do i=2,20
cc1(i)=-cc1(i-1)*(a+2*i-2)*(a+2*i-3)/((2*i-1)*(2*i-2))**2
cc2(i)=-cc2(i-1)*(a+2*i-4)*(a+2*i-3)/((2*i-2)*(2*i-3))**2
end do

```

c another small loop to get coefficients of the expansion

```

col(0)=1.0
co2(0)=1.0
do i=1,20
col(i)=(a+i-1)**2*col(i-1)/i
co2(i)=(i-a)**2*co2(i-1)/i
end do
do 100 i1=-60,60 ! should be 100
td(i1)=i1*.5e-3

```

c the forth loop is for different t, which is normalized

c distance

```

H=0.0
do 400 i4=1,N ! should be 1000
t=var4(i4)
aa=sqrt(t*(1-t)*L/(2*k))
b=sqrt((P*t-V*td(i1))**2)
y=(b**2)/(8.*aa**2)
if(y.gt.12.56) goto 500 ! to use asymptotic expansion
x=0.0

do i=1,18
x=x+(cc1(i)*y**(2*i-1)+cc2(i)*y**(2*i-2))
end do

```

```

c x=0.805*y-y**3*4.347e-3+7.458e-5*y**5-9.1e-7*y**7+
c * 0.2587+0.009*y**2-1.578e-4*y**4+2.312e-6*y**6
goto 600

```

c when $y > 4\pi$ use asymptotic expansion

```

500 x=0.
do i=0,18
x=x+col(i)*y**(-i-a)*sin(pi/12.-(a+i)*pi/2)/gama1+
* co2(i)*y**(-i-1+a)*sin(pi/12.-y+(i+1-a)*pi/2)/gama2
end do

```

```

c  */gama1+(-sin(y)*y**(-11./6)+3.361*sin(4.71-y)*y**(-17./5)
c  * -13.49*sin(y)*y**(-23./6)+66*y**(-29./6)*sin(7.854-y))
c  */gama2
600 H=H+(-3.*b**(5./3)*gama3**2*cos(pi/6)/(20*pi**(1./2)
    * *gama1)+3.*aa**(5./3)*gama4*x/(5*2**(1./6)))*wt4(i4)
c 600 H=H+(x*0.5345*gama4*aa**(5./3)-0.07335*b**(5./3)*gama3**2
c  * /gama1)*wt4(i4)
c  print *, y
c  print *, H
400 continue

```

```

c  end of the forth loop

```

```

    term(i1)=exp(5.206*k*k*L*Cn*H)-1

```

```

c  to write the final result

```

```

    write(10,99)td(i1)*1.0e3,term(i1)
99  format(1x,f12.5,f20.10)
100 continue
c  the end of the first loop
close(10)

```

```

stop
end

```

Appendix C

Programs for numerical analysis of aperture averaging effect on TDC functions

(A) Two half-moon receivers

```

c   This program is called start1.f
c   Gauss Quadrature intergration subroutines are used here to
c   calculate time delayed covariance for two half-moon case.
c   *** the result is normalized by average intensity ***

c   all the parameters are read from a file called "parameters"
c   the calculated results are stored in a file called "tdc.pt"

c   a0 is beam size, L is the target distance, F is the focal distance
c   Cn is the turbulence strength, V is the wind speed, P is the detector
c   distance, k is the wave number
    real a0,L,F,Cn,V,P1,P2,k,lamda
    real rol0,rol
    real a,aa,b,y,x,thita1,thita2
    real t,H,out_term
    real term1,term2,term3_1,term3_2
    real co1(24),co2(24),cc1(24),cc2(24)
    real td(-500:500)
    double precision gama1,gama2,gama3,gama4
    double precision s14aaf, arg1,arg2,arg3,arg4
    double precision s17aef
    external    s14aaf
    external    s17aef
    integer ifail,N,N1,itpe

    double precision var1(64),var2(64),var3(64),var4(64)
    double precision wt1(64),wt2(64),wt3(64),wt4(64)
    double precision A1,B1,A2,B2,A3,B3,A4,B4,pi
    external d01bbf,d01bax,d01bay,d01baz,d01baw

c   print *, 'input beam size in (mm)'
c   read(5,*) a0
c   print *, 'input distance of the target in (m)'
c   read(5,*) L

```

```

c   print *, 'input focal distance in (m).10**5 for collimated'
c   read(5,*) F
c   print *, 'input trbulence strength'
c   read(5,*) Cn
c   print *, 'input wind speed in (m/s)'
c   read(5,*) V
c   print *, 'input the receiver inner radius in (mm)'
c   read(5,*) A1
c   print *, 'input the receiver outer radius in (mm)'
c   read(5,*) B1
c   print *, 'input wavelength in (nm)'
c   read(5,*) lamda
c   print *, 'what is number N'
c   read(5,*) N
c   print *, 'what is number N1'
c   read(5,*) N1
c   print *, 'input itype'
c   read(5,*) itype

open(9,file='parameters')
open(10,file='tdc.pt')
read(9,*)a0,L,F,Cn,V,A1,B1,lamda,N,N1,itype
pi=4.0*atan(1.0)
a0=a0*0.001
c   P=P*0.001
k=2*pi*1e9/lamda
a=-5.0/6.0
rol0=0.545625*Cn*L*k*k
c   print *, k,rol0
ifail=0

A1=A1*0.001
B1=B1*0.001
A2=-pi/2.
B2=pi/2.
A3=pi/2.
B3=3*pi/2.
A4=0.0
B4=1.0
c to get abscis and weights
call d01bbf(d01baz,A4,B4,itype,N,wt4,var4,ifail)
call d01bbf(d01baz,A1,B1,itype,N1,wt1,var1,ifail)
call d01bbf(d01baz,A2,B2,itype,N,wt2,var2,ifail)

```

```

call d01bbf(d01baz,A3,B3,itpe,N,wt3,var3,ifail)

c get gamma fuctions for the numbers in the calculation
  arg1=11./6.
  arg2=-5.0/6.
  arg3=1.0/3.0
  arg4=1.0/6.0
  gama1=s14aaf(arg1,ifail)
  gama2=s14aaf(arg2,ifail)
  gama3=s14aaf(arg3,ifail)
  gama4=s14aaf(arg4,ifail)
c   print *, gama1,gama2,gama3,gama4
c First loop is for different time delay td(i1). to get different
c covariance.

c small loop to get coefficients for regular expansion
  a=-5.0/6
  cc1(1)=-cos(pi/12)*a
  cc2(1)=sin(pi/12)
  do i=2,20
cc1(i)=-cc1(i-1)*(a+2*i-2)*(a+2*i-3)/((2*i-1)*(2*i-2))**2
cc2(i)=-cc2(i-1)*(a+2*i-4)*(a+2*i-3)/((2*i-2)*(2*i-3))**2
  end do

c another small loop to get coefficients of the expansion
  col(0)=1.0
  co2(0)=1.0
  do i=1,20
  col(i)=(a+i-1)**2*col(i-1)/i
  co2(i)=(i-a)**2*co2(i-1)/i
  end do
c   do 100 i1=-60,100   ! should be 100
  do 100 i1=-5,30
    td(i1)=i1*.5e-3

c first loop of the integration is P1
  term1=0
  do 110 j1=1,N1
    P1=var1(j1)
c second loop of the intergration is P2
  term2=0
  do 200 j2=1,N1
    P2=var1(j2)

```

```

c the third loop of integration is thita1
  term3_1=0
  do 310 i3=1,N
    thita1=var2(i3)
c the third II loop of integration is thita2
  term3_2=0
  do 320 j3=1,N
    thita2=var3(j3)

c the forth loop is for different t, which is normalized
c distance
  H=0.0
  do 400 i4=1,N ! should be 1000
    t=var4(i4)
    aa=sqrt(t*(1-t)*L/(2*k))
    b=sqrt(((P1*cos(thita1)-P2*cos(thita2))*t-V*td(i1))**2
*   +((P1*sin(thita1)-P2*sin(thita2))*t)**2)
    y=(b**2)/(8.*aa**2)
    if(y.gt.4*pi) goto 500 ! to use asymptotic expansion
    x=0.0

    do i=1,18
      x=x+(cc1(i)*y**(2*i-1)+cc2(i)*y**(2*i-2))
    end do

c   x=0.805*y-y**3*4.347e-3+7.458e-5*y**5-9.1e-7*y**7+
c * 0.2587+0.009*y**2-1.578e-4*y**4+2.312e-6*y**6
    goto 600

c when y>4pi use asymptotic expansion
500   x=0.
      do i=0,18
        x=x+co1(i)*y**(-i-a)*sin(pi/12.-(a+i)*pi/2)/gama1+
*      co2(i)*y**(-i-1+a)*sin(pi/12.-y+(i+1-a)*pi/2)/gama2
      end do

c * /gama1+(-sin(y)*y**(-11./6)+3.361*sin(4.71-y)*y**(-17./5)
c * -13.49*sin(y)*y**(-23./6)+66*y**(-29./6)*sin(7.854-y))
c * /gama2
600 H=H+(-3.*b**(5./3)*gama3**2*cos(pi/6)/(20*pi**(1./2)
* *gama1)+3.*aa**(5./3)*gama4*x/(5*2**(1./6)))*wt4(i4)
c 600 H=H+(x*0.5345*gama4*aa**(5./3)-0.07335*b**(5./3)*gama3**2
c * /gama1)*wt4(i4)

```

```

c    print *, y
c    print *, H
400  continue

c  end of the forth loop

      term3_2=exp(5.206*k*k*L*Cn*H)*wt3(j3)+term3_2
320  continue
c end of third II loop

      term3_1=term3_1+term3_2*wt2(i3)
310  continue
c end of third I loop

      term2=var1(j2)*term3_1*wt1(j2)+term2
200  continue
c end of the second loop

      term1=term1+var1(j1)*term2*wt1(j1)
110  continue
c end of the first loop

c  to write the final result

      out_term=4.*term1/(pi*(B1**2-A1**2))**2-1.0

      write(10,99)td(i1)*1.0e3,out_term
99   format(1x,f12.5,f20.10)
100  continue
c  the end of the first loop
      close(10)

      stop
      end

```

(B) Two rectangular shaped receivers

```

c   This program is called start2.f
c   Gauss Quadrature intergration subroutines are used here to
c   calculate time delayed covariance for two-half rectangle case.
c   *** the result is normalized by average intensity ***

c   all the parameters are read form a file called "parameters.2"
c   the results are stored in a file called "tdc2.pt"

c   a0 is beam size, L is the target distance, F is the focal distance
c   Cn is the turbulence strength, V is the wind speed, P is the detector
c   distance, k is the wave number
  real a0,L,F,Cn,V,P1,P2,k,lamda
  real rol0,rol
  real a,aa,b,y,x,thita1,thita2
  real t,H,out_term
  real term1,term2,term3_1,term3_2
  real co1(24),co2(24),cc1(24),cc2(24)
  real td(-500:500)
  double precision gama1,gama2,gama3,gama4
  double precision s14aaf, arg1,arg2,arg3,arg4
  double precision s17aef
  external    s14aaf
  external    s17aef
  integer ifail,N,N1,itype

  double precision var1(64),var2(64),var3(64),var4(64)
  double precision wt1(64),wt2(64),wt3(64),wt4(64)
  double precision A1,B1,A2,B2,A3,B3,A4,B4,pi
  external d01bbf,d01bax,d01bay,d01baz,d01baw

c   print *, 'input beam size in (mm)'
c   read(5,*) a0
c   print *, 'input distance of the target in (m)'
c   read(5,*) L
c   print *, 'input focal distance in (m),10**5 for collimated'
c   read(5,*) F
c   print *, 'input trbulence strength'
c   read(5,*) Cn

```



```

c   print *, 'input wind speed in (m/s)'
c   read(5,*) V
c   print *, 'input the receiver inner radius in (mm)'
c   read(5,*) A1
c   print *, 'input the receiver outer limit in (mm)'
c   read(5,*) B1
c   print *, 'input wavelength in (nm)'
c   read(5,*) lamda
c   print *, 'what is number N'
c   read(5,*) N
c   print *, 'what is number N1'
c   read(5,*) N1
c   print *, 'input itype'
c   read(5,*) itype

open(9,file='parameters.2')
open(10,file='tdc2.pt')
read(9,*)a0,L,F,Cn,V,B1,lamda,N,N1,itype
pi=4.0*atan(1.0)
a0=a0*0.001
c   P=P*0.001
k=2*pi*1e9/lamda
a=-5.0/6.0
rol0=0.545625*Cn*L*k*k
c   print *, k,rol0
ifail=0

A1=0.0 ! x1 coordinate
B1=B1*0.001
A2=-B1 ! x2 coordinate
B2=0.0
A3=-0.01562*25.4e-3 ! y coordinate
B3=0.01562*25.4e-3
A4=0.0
B4=1.0
c to get abscis and weights
call d01bbf(d01baz,A4,B4,itype,N,wt4,var4,ifail)
call d01bbf(d01baz,A1,B1,itype,N1,wt1,var1,ifail)
call d01bbf(d01baz,A2,B2,itype,N1,wt2,var2,ifail)
call d01bbf(d01baz,A3,B3,itype,N1,wt3,var3,ifail)

c get gamma fuctions for the numbers in the calculation
arg1=11./6.

```

```

arg2=-5.0/6.
arg3=1.0/3.0
arg4=1.0/6.0
gama1=s14aaf(arg1,ifail)
gama2=s14aaf(arg2,ifail)
gama3=s14aaf(arg3,ifail)
gama4=s14aaf(arg4,ifail)
c   print *, gama1,gama2,gama3,gama4
c   First loop is for different time delay td(i1), to get different
c   covariance.

c   small loop to get coefficients for regular expansion
a=-5.0/6
cc1(1)=-cos(pi/12)*a
cc2(1)=sin(pi/12)
do i=2,20
cc1(i)=-cc1(i-1)*(a+2*i-2)*(a+2*i-3)/((2*i-1)*(2*i-2))**2
cc2(i)=-cc2(i-1)*(a+2*i-4)*(a+2*i-3)/((2*i-2)*(2*i-3))**2
end do

c   another small loop to get coefficients of the expansion
co1(0)=1.0
co2(0)=1.0
do i=1,20
co1(i)=(a+i-1)**2*co1(i-1)/i
co2(i)=(i-a)**2*co2(i-1)/i
end do
do 100 i1=-60,100      ! should be 100
td(i1)=i1*.5e-3

c   first loop of the integration is P1
term1=0
do 110 j1=1,N1
P1=var1(j1)
c   second loop of the intergration is P2
term2=0
do 200 j2=1,N1
P2=var2(j2)
c   the third loop of integration is thita1
term3_1=0
do 310 i3=1,N1
thita1=var3(i3)
c   the third II loop of integration is thita2

```

```

term3_2=0
do 320 j3=1,N1
  thita2=var3(j3)

c the forth loop is for different t, which is normalized
c distance
  H=0.0
  do 400 i4=1,N ! should be 1000
    t=var4(i4)
    aa=sqrt(t*(1-t)*L/(2*k))
    b=sqrt(((P1-P2)*t-V*td(i1))**2
*    +((thita1-thita2)*t)**2)
    y=(b**2)/(8.*aa**2)
    if(y.gt.4*pi) goto 500 ! to use asymptotic expansion
    x=0.0

    do i=1,18
      x=x+(cc1(i)*y**(2*i-1)+cc2(i)*y**(2*i-2))
    end do

c    x=0.805*y-y**3*4.347e-3+7.458e-5*y**5-9.1e-7*y**7+
c    * 0.2587+0.009*y**2-1.578e-4*y**4+2.312e-6*y**6
    goto 600

c when y>4pi use asymptotic expansion
500 x=0.
  do i=0,18
    x=x+co1(i)*y**(-i-a)*sin(pi/12.-(a+i)*pi/2)/gama1+
*    co2(i)*y**(-i-1+a)*sin(pi/12.-y+(i+1-a)*pi/2)/gama2
  end do

c * /gama1+(-sin(y)*y**(-11./6)+3.361*sin(4.71-y)*y**(-17./5)
c * -13.49*sin(y)*y**(-23./6)+66*y**(-29./6)*sin(7.854-y))
c * /gama2
600 H=H+(-3.*b**(5./3)*gama3**2*cos(pi/6)/(20*pi**(1./2)
* *gama1)+3.*aa**(5./3)*gama4*x/(5**2**(1./6)))*wt4(i4)
c 600 H=H+(x*0.5345*gama4*aa**(5./3)-0.07335*b**(5./3)*gama3**2
c * /gama1)*wt4(i4)
c print *, y
c print *, H
400 continue

c end of the forth loop

```

```
    term3_2=exp(5.206*k*k*L*Cn*H)*wt3(j3)+term3_2
320 continue
c end of third II loop

    term3_1=term3_1+term3_2*wt3(i3)
310 continue
c end of third I loop

    term2=term3_1*wt2(j2)+term2
200 continue
c end of the second loop

    term1=term1+term2*wt1(j1)
110 continue
c end of the first loop

c to write the final result

    out_term=term1/(B1*2*B3)**2-1.0

    write(10,99)td(i1)*1.0e3,out_term
99  format(1x,f12.5,f20.10)
100 continue
c the end of the first loop
    close(10)

    stop
end
```

Appendix D

The A/D program

c NEW RECORD.FOR TO RECORD DATA WITH 12KSAMPLES/SET
 c DATA AND BACKGROUND ARE SEPERATE IN TWO FILES
 c FILES ARE IN ASCII
 c CAMBELL UNIT IS CONNECTED TO CH.2 AND CH.3 FOR TURBULENCE
 C AND WIND VELOCITY
 c double-pulse trigger is used to trgger the A/D board, so it can
 c record two channel data at the speed we wanted (about 2kHz)
 c Record.for modified from Record3.for
 c Record3.for to take data with longer length
 c this is modified from record2.for

c record2.for by Feng Chen modified from record1.for
 c based on record.for by Chuyan Zhou

Cwhich is

C based on RECDAT.FTN by Todd L. Cloninger

C and adgr6b.for by John Hunt

C to run on a record data program in CIO-AD16

C begin 11/12/93, finished 11/14/93

CDevelopment version, runs a/d

CA file consists of a header block followed by the information of

C wind and turbulence from the Campbell Unit CA-9

CTwo sets of background data are sampled for both channel and put

Cinto two files

C 2*N sets of data are sampled. each channel has N sets, put it in

C the two files where backgroud data is in according to channels

C Turn the delay switchs to the next range bin record 2*N sets of

C data for this range bin and put the data in the files.

C Follow the same procedure for the next range bin until the signal

C is too low to process.

C Each set of data is 2048 bytes long and has 1024 values.

C N can be chosen less than 16. the default value is 10

CIncorporate file containing parameter and common declarations

c this program can also take the average of the data to get the

- c intensity vs. range data , put them in two files named 'range1'
- c and 'range2', and plot them.
- c the time delay switches are automatically controled by computer

Cinclude 'RECORD.VAR'

implicit integer(A-Z)

```
c integer*4 ovflo
creal*4 bgmen, bgvar, satmen, satvar, tpsd
character*1 YorN, Dumy
character*16 ifile
character*16 date, time
character*70 itext(20)
integer*2 icmd, ilpwr, ica
integer*2 iilpwr,iihv,ihv
integer*2 ia,ib,t1,t2,it(100),icode(100),ipts
integer*2 iport,iout
```

```
integer*4 inum, isize, iseg, ibdata,tem,item
integer*2 ibig[allocatable, huge](:)
integer*2 idata(24576)
real ttime, period
```

```
real xx(100),yy(100)
integer jx(100),jy(100)
common ix,iy,iron
try=1
```

```
write(*,'(/////)' )
print *, '*****'
print *, '* RECORD.FOR Last Modified: Dec.20, 1993 *'
print *, '* *'
print *, '* This program uses an Analog To Digital *'
print *, '* Converter to collect data from the two *' print *, ' * channel
receiver and store it on two *'
print *, '* files. *'
print *, '* *'
print *, '* NOTE: Parentheses enclose default responces *'
print *, '*****'
write(*,'(/////)' )
print *, ' Press <RETURN> to Continue.'
read(*,1003) Dumy
```

```

10inum=0

C*****
CAllocate 64k element array in order to be sure
Cthat some portion will be stored at the start of a new
Cpage in physical memory and that at least 32k elements
Cwill be in that page.

isize = 64*1024

allocate (ibig(isize), stat = ierr)
if (ierr .ne. 0) then
print *,'bad ibig allocate status: ',ierr
goto 980
endif

200write(*, '(///)')
print *,' -----'
print *,' | MAIN MENU |'
print *,' |-----|'
print *,' | 1. record data |'
print *,' | 2. view data |'
print *,' | 3. int. vs. range plot |'
print *,' | 4. load data file |'
print *,' | 5. DMA status |'
print *,' | 6. plot data |'
print *,' | 7. fft to data |'
print *,' | 8. exit |'
print *,' | |'
print *,' -----'
print *

write(*, '(///)')
print 1001,'Enter the number ', of your choice (1) --> '
read(*, 1010, err=200) icmd

if (icmd.eq.0) icmd=1
if(icmd .eq. 1) goto 300
Cif(icmd .eq. 2) goto 400
if(icmd .eq. 3) goto 500
Cif(icmd .eq. 4) goto 600

```

```

if(icmd .eq. 5) goto 800
if(icmd .eq. 6) goto 700
if(icmd .eq. 7) goto 850
if(icmd .eq. 8) goto 900
goto 200

```

```

C -----***** Default Parameters *****-----
300ihv = 1000! abs(default High Voltage Setting for PMT)
ilpwr= 200! laser driving current
idnds = 10! default # of data sets of one range bin in the file
ibdata=24576! # of data per data set for two channels
      tem=20      ! temperature of the laser diode

```

```

Cdetermine and print physical address of ibig.
CThe values "index" and "iseg" are returned by caddr.
Cindex is array index to element that is located at
Cthe start of a physical memory page.
Ciseg is the segment for that page.

```

```

call caddr(ibig(1), index, iseg)
cwrite(*,'(1x,i6,2x,z8,a)' )index, iseg, 'index and seg'

```

```

Cinitialize a/d board

```

```

50call adinit(ierr)
if (ierr .ne. 0) then
print *,'bad init a/d board status: ',ierr
goto 980
endif

```

```

1001format(1x,2a,\)
1002 format(/1x, a)
1003format(a1)
1004format(1x, a)
1005format(1x, a, \)
1006format(1x,2a,i5,a,\)
1010 format(i5)

```

```

C -----***** Main Loop For Creating Entire Files *****-----

```

```

      period=.000511

```

```

40print *

```



```

print 1006, 'Enter the laser driving current(high level)',
* '(in Milliamps) (' , ilpwr ,') --> '
read(*, 1010, err=40) iilpwr
if( iilpwr. eq. 0) iilpwr=ilpwr
ilpwr=iilpwr
43  print *
    print 1006, 'Enter the TEC temperature',
    * '(in centigrade) (' , tem ,') --> '
    read(*,1010,err=40) item
    if(item.eq.0) item=tem
    tem=item
    print *
    print 1006, 'Enter the PMT voltage',
    * '(in volts) (' , ihv ,') --> '
    read(*,1010,err=40) iihv
    if( iihv.eq.0) iihv=ihv
    ihv=iihv

45print *
print 1001, 'Enter the Campbell Unit CA-9 Range ',
* '[5, 10, 20] m/sec (5)--> '
read(*,1010,err=45) i
if (i.eq.0) i = 5
if ((i.ne.5) .and. (i.ne.10) .and. (i.ne.20)) goto 45
ica = 256 * i

60print *
print 1001, 'Enter the CA-9 Time Constant ',
* '[1, 10, 100] seconds (1)--> '
read(*,1010,err=60) i
if (i.eq.0) i = 1
if ((i.ne.1) .and. (i.ne.10) .and. (i.ne.100)) goto 60
ica = ica + i

150print 1002,'How many data sets do you want for each range bin?'
print 1040,'[1 to 16] (' ,idnds,') -->'
1040 format (1x,a,i3,a\
read(*,1045,err=150)inds
1045 format(i3)
    if (inds .eq. 0) inds = idnds
if ((inds .lt. 0).or.(inds .gt. 16)) then

```

```

print 1005, char(7)
print *, 'Your entry may not be < 1 or > 16; please try again!'
goto 150
    endif
    idnds = inds

print *
ttime = inds*1024*511*e-6
1050 format(1x,a,f7.2, ' seconds or ',f6.2, ' minutes')

1055  print *, 'input the minium delay time in ns'
      read(*,*) t1
      print *, 'input the maxmum delay time in ns'
      read(*,*) t2
      open(9,file='table')
      ipts=0
      do 1056 i=1,100
      read(9,*) ia,ib
      if(ia.ge.t1) then
      ipts=ipts+1
      it(ipts)=ia
      icode(ipts)=ib
      endif
      if(ia.ge.t2) goto 1057
1056  continue
1057  print *, 'ipts=',ipts
      close(9)
      iran=ipts
      ttime=inds*1.024*2*ipts*0.000511
      print *
      print 1050, 'Sampleing will require: ',ttime, ttime/60
C-----***** Open Files *****-----
      do 2031 i=1,3
2010 print *
print 1007, 'Enter the Data File Name', i, ' --> '
read(*, '(a16)') ifile
1007  format (1x,a,i2,a,\)
      j=i+17
open (j, file=ifile, err=2030, status='old')
2020 write(*,1005) "The File Exist, Overwrite It? [Y/N] "
read(*,1003) YorN
if ((YorN .eq. 'Y').or.(YorN .eq. 'y')) goto 2031

```

```

if ((YorN .ne. 'N').and.(YorN .ne. 'n')) then
  print *, char(7)! ring beeper
  write(*, '(1x, a/)' 'It should be Y or N! ')
  goto 2020
end if
C   1--Header, 2--Channel1, 3-- channel2

goto 2010

2030open (j, file=ifile, err=2010, status='new')
cwrite(*, '(1x,a,a16)') "ifile= ", ifile
2031 continue

      open(14, file='range1')
      open(15, file='range2')

C   -----***** Read Comments Into ibuf As Part Of Header *****-----
2040print 1002,'Enter text for comment block in file header.'
      print 1002,' But no more than 20 lines'
print *,' (Terminate with a blank line!)'
print *,'-----'
print *

do 2050 n=1, 20
  read(*, '(a)') itext(n)
  if (itext(n).eq.' ') goto 350
  write(18,'(1x, a)') itext(n)
2050continue

C   -----***** Finished Reading Comments *****-----

350print *
print *,'Do you need to change the parameters',
      * ' or reenter the text?'
print 1005,' [Y/N] -->'
read(*,1003) YorN
if ((YorN .eq. 'Y').or.(YorN .eq. 'y')) goto 40
if ((YorN .ne. 'N').and.(YorN .ne. 'n')) then
  print 1005, char(7)
  goto 350
endif

```

```

Cset channel 0,1
call chanset(0, 1, ierr)
if (ierr .ne. 0) then
print *, 'the chanel data is out off range '
print *, 'remodify the program'
goto 980
endif

```

```

C *****

```

```

CWrite the Header File

```

```

    print *, 'month/date/year, hour:minute'
    read(*,582) date
    read(*,582) time
    582  format(1x,16a)
write(18,583)date,time
    583  format(1x,12a,12a)
write(18, '(/1x, a, i5, a)')
    * "laser driving current= ", ilpwr, " mA"
write(18, '(1x, a, i5)') "num. of data per set = ", ibdata
write(18, '(1x, a, i3)') "num. of data sets = ", inds
write(18, '(1x, a, i5, a)')
    * "high voltage of PMT = ", ihv, " Volts"
    write(18,'(1x,a,i3)') "TEC temperature=", tem

write(18, '(/1x, a/)') "***** End of Commends *****"

```

```

c  initialize the i/o
    iport=787
    iout=139
    call outbyt(iport,iout)

```

```

C  -----***** Begin Recording Background*****-----

```

```

print 1002, 'BLOCK LASER '
print *, 'Press <RETURN> to begin recording background'
read(*,1003) Dumy
iport=784
do 1100 i=1,ipts
call outbyt(iport,icode(i))

call takead(ibig(index),2048,idata,iseg,1,ierr)

```

```

        jx(i)=ix
        jy(i)=iy
1100 continue

C-----***** Begin Recording Data *****-----
ibadds = 0! number of bad data sets

        print 1002, ' UNBLOCK LASER!'
        print *, 'Press <RETURN> to begin recording data.'
        read(*,1003) Dumy
        do 5500 i=1,ipts
            xx(i)=0
            yy(i)=0
            iport=784
            call outbyt(iport,icode(i))
            ids=0          ! data set number
6000ids = ids + 1! next data set

C    Executive call to get current time

c    initialize the a/d board again
    call adinit(ierr)
    if(ierr .ne. 0) then
        print *, 'bad init a/d board status: ', ierr
        goto 980
    endif

Cset channel 2 and 3 to get 4 wind and 4 turb readings
call chanset(0, 3, ierr)      ! must initialize from 0
call takead(ibig(index),16,idata,iseg,0,ierr)
c    we use 16 here because we need 8 samples for ch.2,3

inum = ibdata
if (ierr .ne. 0) ibadds = ibadds + 1! count bad data sets

c    initialize the a/d board again
    call adinit(ierr)
    if(ierr .ne. 0) then
        print *, ' bad init a/d board status: ', ierr
        goto 980
    endif
Cset channel 0 and 1 to record data

```

```

call chanset(0, 1, ierr)
call takead(ibig(index),ibdata,idata,iseq,1,ierr)

      xx(i)=xx(i)+(ix/12.-jx(i))*0.0024426/1024
      yy(i)=yy(i)+(iy/12.-jy(i))*0.0024426/1024

C   -----***** End Block Loop For This Data Set *****-----

C   Take next data set unless this was the last one in this file.
if (ids .lt. inds) goto 6000
      xx(i)=-xx(i)/ids
      yy(i)=-yy(i)/ids

      write(14,*) it(i),xx(i)
      write(15,*) it(i),yy(i)
5500 continue
C   -----***** End Data Set Loop For This File *****-----

print 1005, char(7)
print *,'Finished recording data file.'

820print *, 'Would you like to record another file of data?'
print 1005, '[Y/N] -->'
read(*,1003)YorN
if ((YorN .eq. 'Y').or.(YorN .eq. 'y')) then
  goto 1055
elseif ((YorN .ne. 'N').and.(YorN .ne. 'n')) then
  print 1005, char(7)
  goto 820! ask again
endif
print *

      close(14)
      close(15)

      close(9)
      close(18)
      close(19)
close(20)
close(21)
call clearwindow
goto 200

```

```
*****
```

```
c 400call seedat(ibig(index), inum, idata(1) )
c goto 200
```

```
500 call setgr
    call rplot
    call clearwindow
    call closeSEgraphics
    goto 200
```

```
700call setgr
call plot(idata(1), period)
read(*,*)! save screen until key pressed
call clearwindow
call closeSEgraphics
goto 200
```

```
800call statdma
goto 200
```

```
850call setgr
call datfft(idata(1), period)
call clearwindow
call closeSEgraphics
goto 200
```

```
*****
```

```
900deallocate (ibig, stat = ierr)
if (ierr .ne. 0) then
print *,'bad deallocate status: ',ierr
goto 980
endif
```

```
cprint * , 'deallocated ibig'
```

```
*****
```

```
980write(*, '(1x,a,\n)') "Are you sure to quit? [Y/N] --> "
```

```

read(*,1003) YorN
if ((YorN .ne. 'Y').and.(YorN .ne. 'y')) then
    goto 10
endif

```

```

990call closeSEgraphics
end

```

```

C *****
C

```

```

C *****
C

```

```

*      phys subroutine
*****

```

```

*   converts iad from locfar call to physical address
*   ipad16 (lower 16 bits) and ipage (upper 4 bits)

```

```

subroutine phys(iad, ipage, ipad16)

```

```

integer*4 iad, ipage, ipad16
integer*4 iphi, iplo
integer*4 ihi, ilo
integer*4 ihi1, ilo1, ihi2, ilo2

```

```

ilo= iand(iad, #ffff)
*   shift uper 16 bits down to lower 16 bits
ihi = ishft(iad, -16)
ihi = iand(ihi, #ffff)

```

```

ihi1 = iand(ihi, #f)
ihi2 = ishft(ihi, -4)
ihi2 = iand(ihi2, #fff)

```

```

ilo1 = iand(ilo, #ff)
ilo2 = ishft(ilo, -8)
ilo2 = iand(ilo2, #ff)

```

```

iplo = ilo1 + ishft(ihi1, 4)

```

```

iphi = ihi2 + ilo2

```



```

*   check for carry
    if (iplo .gt. #ff) iphi = iphi+1
*   mask any carry
    iplo = iand(iplo, #ff)

*   example of the variables used to hold the 20 bit physical address
*   12345 (hex) :

*   hex address:  123 45
*                   iphi iplo
*
*                   1  2345
*                   ipage ipad16

    ipage = ishft(iphi, -8)
    ipage = iand(ipage, #f)

    ipad16 = ishft(iphi, 8)
    ipad16 = iand(ipad16, #ff00)
    ipad16 = ipad16 + iplo

    return
end

*****
*caddr subroutine
*****
*In order for the DMA controller to store 32k readings,
*the data array must start at the beginning of a
*physical memory data page.
*This routine calculates which element of the array
*ibig is stored at the beginning of the page.
*That element is returned in the value "index".
*
*It also returns the segment value to be passed to the
*a/d driver. This is the equivalent segment value for
*the starting element address. Since this address is
*at the beginning of a physical page, its offset is zero.

subroutine caddr(jjdata, index, iseg)

integer*4 iad

```

```

integer*4 ioffset, index
integer*4 iseg
integer*2 jjdata [huge]
*dummy array, but needs declaration anyway
dimension jjdata(1)

iad = locfar(jjdata(1))
call phys(iad, ipage, ipad16)
*print *, 'locfar page 16 bits'
*write(*,'(1x,z8,6x,z1,1x,z4,a)')
*   liad, ipage, ipad16

ioffset = -ipad16
ioffset = iand(ioffset, #ffff)
index = (ioffset/2) + 1
*write(*,'(1x,z8,2x,z8,a)')
*   lipad16, ioffset, ' ipad16, offset'
*print *, index , ' index for array held at start of page'

iad = locfar(jjdata(index))
call phys(iad, ipage, ipad16)
*print *, 'locfar page 16 bits'
*write(*,'(1x,z8,6x,z1,1x,z4,a)')
*   liad, ipage, ipad16

*Knowing the desired physical address for the start of
*the offset array, we need to determine the equivalent
*segment and offset values of the address.
*These values are passed to the a/d driver which
*recalculates the physical address and loads it into
*the dma register and dma controller.

*This is an easy calculation since we are at the beginning
*of a page, the offset is zero and the lower 12 bits of
*the segment are zero. The upper 4 bits of the segment are
*just the page value.

*shift page up 12 bits

iseg = ishft(ipage, 12)
iseg = iand(iseg, #f000)

```

```
cwrite(*,'(1x,a,z4)') 'Using segment ', iseg
```

```
return
```

```
end
```

```
C*****
```

```
Cadint subroutine
```

```
C*****
```

```
Cinitialize a/d board
```

```
subroutine adinit(istat)
```

```
implicit integer(A-Z)
```

```
integer*2 ic(16), mode, flag
```

```
CInitialize Das-16G using Mode 0...
```

```
mode=0
```

```
ic(1)=768! board address
```

```
ic(2)=2! interrupt level (as set on card)
```

```
ic(3)=1! DMA level (as set on card)
```

```
flag=0! error flag
```

```
call fdasg(mode, ic(1), Flag)
```

```
if (flag .NE. 0) then
```

```
print *, 'Mode = ', mode, ' Error # ', flag
```

```
endif
```

```
istat = flag
```

```
return
```

```
end
```

```
C*****
```

```
Cchanset subroutine
```

```
C*****
```

```
C set the channel scan upper and lower limits
```

```
subroutine chanset(ichlo, ichhi, istat)
```

```
implicit integer(A-Z)
      integer*2 ic(16),mode,flag
integer ichhi,ichlo
```

```
Cset upper and lower scan limits
Cselect channel from ichhi to ichlo
mode=1
ic(1)=ichlo
ic(2)=ichhi
flag=0
```

```
call fdasg(mode, ic(1), Flag)
```

```
      if (flag .NE. 0) then
        print *, 'Mode = ',mode, ' Error # ',flag
      endif
```

```
istat = flag
```

```
return
end
```

```
*****
```

```
C*****
Ctakead subroutine
C*****
Ctake a/d data
```

```
subroutine takead(iraw, inum, idata, iseg,ipri,istat)
```

```
CThe array iraw holds the raw a/d readings.
CNote that iraw is a dummy array that overlays the array
Cibig.
Ciraw(1) is the same as ibig(index). Index is calculated so that
Ciraw starts at the beginning of a physical memory page.
```

```
implicit integer(A-Z)
integer ipri      ! the difference of C-unit and our system
      integer*2 ic(16), mode, flag
      integer*2 ib(16), mode1, flag1
```

```

        integer*4 iseg, istat, inum
integer*2 iraw[huge]
Cdummy arrays, but they need declaration anyway
dimension iraw(inum)
integer*2 idata(24576)
        common ix, iy
Cinitialize raw data set to be zero
do 100, j=1,inum
iraw(j)= 0
idata(j)=0
100continue

irecyc = 0! non-recycle

ic(1) = inum
ic(2) = iseg! segment to stuff data
ic(3) = 0 ! use External A/D trigger for trigger
ic(4) = irecyc
mode=6
flag=0
        write(*,*) ic(2)
        write(*,*) ic(1)

call fdasg(mode, ic(1), Flag)
        if (flag .NE. 0) then
print *, 'Mode = ', mode, ' Error # ', flag
goto 990
endif

Cconvert a/d word to signed integer
Cfirst shift out channel nibble
        print *, 'something'

*get dma status, out if the conversions done

130continue
mode1 = 8
call fdasg(mode1, ib(1), flag1)
        if (flag1 .NE. 0) then
print *, 'Mode = ', mode, ' Error # ', flag
goto 990
endif

```

```

cprint *, ib(1), ' = operation      1 = DMA, 2 = Interrupt'
cprint *, ib(2), ' = status        0 = done, 1 = active '
c  print *, ib(3), ' conversions so far'

if( ib(2). eq. 1) goto 130
  ix=0
  iy=0

  write(18,*) "Even numbers correspond to turb odd --wind"
do 150 i=1, inum

idata(i)=ishft(iraw(i), -4)

if (ipri. eq. 0) then
  write(18,*) i,idata(i)
  goto 150
endif

  if(inum.eq.2048) then
  write(19,99) idata(i)
  if((i/2.).eq.int(i/2.)) then
  iy=iy+idata(i)-2048
  goto 150
  endif
  ix=ix+idata(i)-2048
  goto 150
  endif
  write(20,99) idata(i)
  if((i/2.).eq.int(i/2.)) then
  iy=iy+idata(i)-2048
  goto 150
  endif
  ix=ix+idata(i)-2048
99  format(1x,i4)
150continue

990istat = flag
  write(*,*) ix,iy

return
end

```

```
*****
```

```

*****
*statdma subroutine
*****

*get dma status

subroutine statdma

implicit integer(A-Z)
  integer*2 ic(16),mode,flag
character*1 Dumy

mode = 8
call fdasg(mode, ic(1), Flag)
  if (flag .NE. 0) then
    print *, 'Mode = ', mode, ' Error # ', flag
    goto 990
  endif

print *
print *, ic(1), ' = operation    1 = DMA, 2 = Interrupt'
print *, ic(2), ' = status      0 = done, 1 = active '
print *, ic(3), ' conversions so far'

990print 1020, 'Press <Return> to exit'
1020format( /1x, a)
read( *, '(a1)') Dumy

  return
end

*****

*****
*setgr subroutine
*****

subroutine setgr
*setup for graphics

*font directory for graphs
  CHARACTER * 30 defaultdirect
  PARAMETER (defaultdirect = 'C:\usr\fortran\lib\*.fon')

```

```
* -3 is autodetect graphics board (or use 16 for EGA)
* defaultdirect is font file directory
* 0 is plotmode (crt only)
```

```
CALL InitSEGraphics(16, defaultdirect, 0)
```

```
return
end
```

```
*****
*plot subroutine
*****
```

cGraph is plotted using setools subroutines.

```
subroutine plot(jdata, period)
```

```
    REAL xdata(0:996), ydata(0:996)
    INTEGER i
integer*2 jdata(0:2048)
real period, tpd, xtics
character*25 ctitle
character*7 cfactor
```

```
*transfer jdata array to real array for plotting
*also create x data array
*convert a/d counts to volts 5V/2047 counts = 2.44 mV / count
```

```
    j=1
10    DO i = j, 200,2
        if(j.eq.1) then
            xdata((i+1)/2-1)=(i+1)/2-1
            ydata((i+1)/2-1)=jdata(i)*0.0024426-5.0
            goto 20
        endif
        xdata(i/2-1) = i/2-1
        ydata(i/2-1) =jdata(i)*0.0024426-5.0
20    continue
    END DO
```



```

    period =511.e-6
    xtics=10.0
    call setplot(xtics, 100.0, -5.0, 5.0)

    calculate time/division

    tpd = period*xtics
    if (tpd .ge. 1.0) then
    write(cfactor, '(f6.1)'tpd
    ctitle = cfactor // 'sec/div'

    else if (tpd .ge. 1e-3) then
    tpd = tpd*1000
    write(cfactor, '(f6.1)'tpd
    ctitle = cfactor // 'ms/div'

    else if (tpd .lt. 1e-3) then
    tpd = tpd*1e6
    write(cfactor, '(f7.1)'tpd
    ctitle = cfactor // 'microsec/div'
    endif

    call titlexaxis(ctitle, 0)

    ipoints = 100! points to plot
    CALL LinePlotData(xdata, ydata, ipoints, 10, 0)
    if(j.eq.2) goto 50
    j=2
    read(*,'(a1)') Dummy
    goto 10

    50return

end

*****
*setplot subroutine
*****
subroutine setplot(xttics, xmax, ymin, ymax)

real xttics, xmax, ymin, ymax

call setpercentwindow(0.0, 0.0, 1.0, 1.0, 1)

```

```

call setwin2plotratio(1, 0.1, 0.05, 0.0, 0.05 )

    CALL SetCurrentWindow(1)
    CALL ClearWindow
!CALL BorderCurrentWindow(6)

    CALL SetAxesType(0, 0)! linear-linear scale
    CALL setxyintercepts(0.0, 0.0)
    CALL SelectColor(7) ! 7 = green
*      xmin, ymin, xmax, ymax
    CALL ScalePlotArea( 0.0, ymin, xmax, ymax)

    CALL SetXYIntercepts(0.0,0.0)
    CALL DrawYAxis(1.0, 0)! tic spacing

    CALL LabelYAxis(1, 0)! tics per label
    CALL DrawXAxis(xttics, 0)

    CALL DrawGridX(1)
    CALL DrawGridY(1)

return
end

*****
*datfft subroutine
*****

Cdata is processed by FFT

subroutine datfft( sdata, period)

    REAL xdata(0:1024), ydata(0:1024)
    REAL zdata(0:1024)
    INTEGER i, il, ic, nd, ipoints
integer*2 sdata(0: 2048)
real period, xtics, freq
real tpd
character*25 ctitle
character*7 cfactor

nd=1024
ic=0

```

```

    period=0.511e-3
    j=1

100do 150 i=j, 2048,2
    if(j.eq.1) then
        xdata((i-1)/2) = sdata(i) * 0.0024426-5.0
        ydata((i-1)/2) = 0.0
        goto 150
    endif
cwrite(*,*) i, xdata(i-1), ydata(i-1)
        xdata(i/2-1) =sdata(i)*0.0024426-5.0
        ydata(i/2-1) =0.0
150continue

xtics=100.0
call setplot(xtics, 1024.0, 0.0, 1.0)

CFFT transformation
call FFTCalc(xdata, ydata, nd)

do 350 i=1, 1024
    i1=i-1
    zdata(i1)=sqrt(xdata(i1)*xdata(i1)+ydata(i1)*ydata(i1))/300.0

c find the peak value and freq. of FFT
c ic is peak number counter
    if(zdata(i1).gt.3) then
        freq=i1/(nd*period)
        if ( freq .gt. 0.5/period) then
write(*,300) "peak",ic," frequency=", freq-1.0/period," Hz"
        else
write(*,300) "peak",ic," frequency=", freq, " Hz"
        endif
write(*,'(1x,a,i2,a,f7.3)') "peak",ic," value=", zdata(i1)
        ic=ic+1
    endif
300format(1x, a,i2,a,f13.3, a)
cwrite(*,*) i1, xdata(i1), ydata(i1), zdata(i1)
350continue

do 450 i=1, 1024
    i1=i-1
    xdata(i1)=i1

```

```

450continue

Ccalculate frequency/division

tpd =xtics*1.0/(1024*period)
if (tpd .ge. 1.0e3) then
tpd = tpd/1.0e3
write(cfactor, '(f6.1)') tpd
ctitle = cfactor // 'KHz/div'

else
write(cfactor, '(f6.1)') tpd
ctitle = cfactor // 'Hz/div'
endif

call titlexaxis(ctitle, 0)

ipoints = 1024! points to plot
CALL LinePlotData(xdata, zdata, ipoints, 10, 0)

      if(j.eq.2) goto 200
      read(*,'(a1)') Dummy
      j=2
      goto 100

200read(*,*)

return
      end

*****
*      rplot subroutine
*****

      subroutine rplot

      common iran
      integer i,j,ipoints
      real xdata(0:100),ydata(0:100),zdata(0:100),tdata(0:100)
      real xh,yh
      character*9 ctitle
      open(14,file='range1')

```

```
open(15,file='range2')
xh=0
yh=0
j=1
ipoints=iran
do 100 i=1,ipoints
read(14,*) xdata(i),zdata(i)
if(zdata(i).gt.xh) then
xh=zdata(i)
endif
read(15,*) tdata(i),ydata(i)
if(ydata(i).gt.yh) then
yh=ydata(i)
endif
100 continue
120 xtics=400.0
call setplot(xtics,4000.0,-0.5,(xh+0.5))
ctitle='400ns/div'
call titlexaxis(ctitle,0)
call LinePlotData(xdata,zdata,ipoints,10,0)
j=j+1
read(*,*)
if(j.eq.3) goto 150
do 130 i=1,ipoints
zdata(i)=ydata(i)
130 continue
xh=yh
goto 120

150 close(14)
close(15)
return
end
```

Appendix E

Program for processing the recorded data to get autocovariance and TDC

```

c this program reads two channel data subtracts the background from the
c data and calculate the correlation and covarrance.
c this program reads in two data files
c the computed auto-covariances are stored in file "auto1" and "auto2"
c the TDC function computed is stored in file "correlat"
c background samples are stored in files "bch1" and "bch2"
c signal samples are stored in files "ch.1" and "ch.2"
c correlation function of the background noise is also calculated and stored in file
c "bcorrelat"
integer ich1(-128:122880),ich2(-128:122880)
real id1,id2,ib1,ib2
c dimension filt(258)
real ch1(122880),ch2(122880)
dimension bcor1(-1024:1024),cor1(-1220:1220)
dimension acor1(-1220:1220),acor2(-1220:1220)
real bch1,bch2
integer ileng
character*10 filter,data1,data2
print*, 'input the range number n'
read(5,*) n
print*, 'input the number of data sets m'
read(5,*) m

print*, 'input the number of sets to process (0,5)'
read(5,*) k
print*, 'how many data to average? input ileng(length=1024*ilen)'
read(5,*) ileng
print *, 'input the file name data1'
read(5,*) data1
print *, 'input the file name of data2'
read(5,*) data2
c print*, 'input the file name of the filter'
c read(5,*) filter
c open(18,file=filter,status='unknown')
open(9,file=data1,status='unknown')
open(10,file=data2, status='unknown')
open(11,file='ch.1', status='unknown')

```

```

open(12,file='ch.2', status='unknown')
open(13,file='correlat', status = 'unknown')
open(14,file='auto1')
open(15,file='auto2')
open(17,file='bcorrelat')
open(19,file='bch1')
open(20,file='bch2')

c   do 1 i=1,256
c   read(18,11)i,flt(i)
c 1  continue
11  format(1x,i5,1x,e20.12)
    do 55 j=1,n
      do i=1,1024
        read(9,*)ich1(i)
        read(9,*)ich2(i)
      end do
55  continue
    ib1=0
    ib2=0
    do 50 i=1,1024
      bch1=5.0-ich1(i)*0.0024426
      bch2=5.0-ich2(i)*0.0024426
      ib1=ib1+ich1(i)/1024.
      ib2=ib2+ich2(i)/1024.
c    write(19,*)i,bch1
c    write(20,*)i,bch2
50  continue
    do 400 j=-1024,1024
      bcorl(j)=0
      if(j.gt.0)goto 450
      do 500 i=1,1024+j
        bcorl(j)=(ich1(i)-ib1)*(ich2(-j+i)-ib2)/(ib1*ib2*1024.0)
      *   +bcorl(j)
500  continue
c    write(17,*)j,bcorl(j)
      goto 400
450  do 460 i=1+j,1024
        bcorl(j)=(ich1(i)-ib1)*(ich2(i-j)-ib2)/(ib1*ib2*1024.0)
      *   +bcorl(j)
460  continue
c    write(17,*)j,bcorl(j)
400  continue

```

```

id1=0
id2=0
do 105 j=1,n
do i=1,12288*m
read(10,*)ich1(i)
read(10,*)ich2(i)
end do
105 continue

99 format(1x,i4,1x,i4)
do 100 i=1,12288*m
ich1(i)=ich1(i)-ib1
ich2(i)=ich2(i)-ib2
id1=id1+ich1(i)/(12288.*m)
id2=id2+ich2(i)/(12288.*m)
100 continue
do i=1,12288*m
ch1(i)=-ich1(i)*0.0024426
ch2(i)=-ich2(i)*0.0024426
end do
id1=-id1*0.0024426
id2=-id2*0.0024426
print*,id1,id2
do i=1,12288
write(11,*)i,ch1(i)
write(12,*)i,ch2(i)
end do
do 150 j=-1032,1032
corl(j)=0
acor1(j)=0
acor2(j)=0
c print*,j,corl(j)
if(j.gt.0)goto 250
do 200 i=12288*k+1,1024*ileng*(k+1)+j
corl(j)=(ch1(i)-id1)*(ch2(-j+i)-id2)/(id1*id2*(1024.*ileng
* ))+corl(j)
acor1(j)=(ch1(i)-id1)*(ch1(-j+i)-id1)/(id1*id1*(1024.
* *ileng))+acor1(j)
acor2(j)=(ch2(i)-id2)*(ch2(-j+i)-id2)/(id2*id2*(1024.
* *ileng))+acor2(j)
200 continue
write(13,*)j,corl(j)

```



```
write(14,*)j,acor1(j)
write(15,*)j,acor2(j)
goto 150
250 do 300 i=1+12288*k+j,1024*ileng*(k+1)
    cor1(j)=(ch1(i)-id1)*(ch2(i-j)-id2)/(id1*id2*(1024.
*   *ileng))+cor1(j)
    acor1(j)=(ch1(i)-id1)*(ch1(i-j)-id1)/(id1*id1*(1024.
*   *ileng))+acor1(j)
    acor2(j)=(ch2(i)-id2)*(ch2(i-j)-id2)/(id2*id2*(1024.
*   *ileng))+acor2(j)
300 continue
write(13,*)j,cor1(j)
write(14,*)j,acor1(j)
write(15,*)j,acor2(j)
150 continue
close(9)
close(10)
close(11)
close(12)
close(13)
close(14)
close(15)
close(17)
close(18)
close(19)
close(20)

stop
end
```

Vita

The author was born in Anhui, China, on January 16, 1965. He attended Anhui University in 1981 and received his Bachelor's degree in Physics in 1985. He was then admitted by Anhui Institute of Optics & Fine Mechanics, Academia Sinica. He received his Master's degree in Laser Remote Sensing in 1988.

He worked as an Radar System Engineer in a weather radar design group at East-China Institute of Electrical Engineering & Technology, China, from 1988 to 1991.

In 1991, he began his studies at Oregon Graduate Institute of Science & Technology and received his Master's degree in Electrical Engineering in 1993. He continued his studies in OGI and completed all the requirements for his Ph. D. degree in Electrical Engineering in 1995.

He is now working as a Design Engineer in Intel Corporation.